PolyPublie
Polytechnique Montréal

POLYTECHNIQUE MONTRÉAL
UNIVERSITÉ D'INGÉNIERIE

Titre: Title:	Bacterial Cellulose Supported Sensor for Bacteria and Gas Detection Development
Auteur: Author:	Bentolhoda Heli
Date:	2017
Type:	Mémoire ou thèse / Dissertation or Thesis
Référence: Citation:	Heli, B. (2017). Bacterial Cellulose Supported Sensor for Bacteria and Gas Detection Development [Ph.D. thesis, École Polytechnique de Montréal]. PolyPublie. https://publications.polymtl.ca/2806/

Document en libre accès dans PolyPublie
Open Access document in PolyPublie

URL de PolyPublie: PolyPublie URL:	https://publications.polymtl.ca/2806/
Directeurs de recherche: Advisors:	Abdellah Ajji, & Arben Merkoçi
Programme: Program:	Génie chimique

Ce fichier a été téléchargé à partir de PolyPublie, le dépôt institutionnel de Polytechnique Montréal
This file has been downloaded from PolyPublie, the institutional repository of Polytechnique Montréal

https://publications.polymtl.ca

UNIVERSITÉ DE MONTRÉAL

BACTERIAL CELLULOSE SUPPORTED SENSOR FOR BACTERIA AND GAS DETECTION DEVELOPMENT

BENTOLHODA HELI

DÉPARTEMENT DE GÉNIE CHIMIQUE

ÉCOLE POLYTECHNIQUE DE MONTRÉAL

THÈSE PRÉSENTÉE EN VUE DE L'OBTENTION

DU DIPLÔME DE PHILOSOPHIAE DOCTOR

(GÉNIE CHIMIQUE)

OCTOBRE 2017

© Bentolhoda Heli, 2017.

UNIVERSITÉ DE MONTRÉAL

ÉCOLE POLYTECHNIQUE DE MONTRÉAL

Cette thèse intitulée:

BACTERIAL CELLULOSE SUPPORTED SENSOR FOR BACTERIA AND GAS DETECTION DEVELOPMENT

présentée par : HELI Bentolhoda

en vue de l'obtention du diplôme de : Philosophiae Doctor

a été dûment acceptée par le jury d'examen constitué de:

M. HENRY Olivier, Ph. D., président

M. AJJI Abdellah, Ph. D., membre et directeur de recherche

M. MERKOÇI Arben, Ph. D., membre et codirecteur de recherche

M. VIRGILIO Nick, Ph. D., membre

M. VERES Teodor, Ph. D., membre

DEDICATION

To God,

my beloved parents,

my beloved husband,

my beloved sister.

ACKNOWLEDGEMENTS

I would like to offer my grateful and sincere appreciation to my Ph.D. research supervisor, Professor Abdellah Ajji for his unconditional and solid support to conduct this challenging multidisciplinary project. It was my great honor to have this opportunity to work with him as a Ph.D. candidate at École Polytechnique de Montréal. I will never forget his patience, enthusiasm, motivation and accurate scientific attitude.

I would also like to express my sincere gratitude to Professor Arben Merkoçi. It was my great privilege to work with his research team in Bioelectronics & Biosensors Group at Institut Català de Nanociencia i Nanotecnologia (ICN), Barcelona, Spain and to have him as co-supervisor in some parts of my research. Their innovative approach, encouragement, patience and broad knowledge helped me throughout this study. I wish to thank Dr. Eden Morales and Dr. Hamed Golmohamadi for full support and vast knowledge which gave me a hand to succeed in my research time in Barcelona fully and to publish the first article.

Besides my supervisors, I would like to thank the rest of my thesis committee, namely Professor Nick Virgilio, Doctor Teodor Veres, Professor Olivier Henry and Professor Clara Santato for accepting to evaluate my thesis.

I would like to acknowledge Professor France Daigle in Microbiology department of Université de Montréal and Professor Mike Buschmann who kindly allowed me to have access to their lab equipment. Furthermore, I would like to thank you Mrs. Julie Tremblay and all students and staff of these two laboratories.

Also, my heartful thanks go to other professors and technical staff of chemical engineering department especially Mrs. Claire Cerclé, Mr. Richard Silverwood, Mr. Redouane Boutrouka, Mrs. Martine Lamarche and Mr. Gino Robin.

Special thanks to all my friends and colleague in 3Spack group and École Polytechnique de Montréal for their help, comments and all great moment we share together, Hanan, Hajer, Mounia, Nury, and Ramin. My warm gratitude thanks to Dr. Nasim Salehi-Nik, for all her valuable advice and endless encouragements.

At the end, with all my heart; I would like to express my perpetual gratitude to my beloved parents and sister for their everlasting and unconditional love and support, for their spiritual encouragement

and for keeping hope alive in every single day of my life. I would also like to thank my lovely husband, Alireza, for being with me side by side in both tough and happy moments. His eternal love, patience, and encouragement have had a huge contribution to my success. Without you, this work could not be possible. However, it will never be a right word to reflect my feeling of appreciation about their self-sacrifice and altruism.

And Finally, I am so blessed by God, puts me in such an opportunity to evaluate myself, improve my personality and talent as well as finding so great people in my life.

RÉSUMÉ

Les intoxications dues à la consommation de produits alimentaires contaminés ont conduit à de nombreuses hospitalisations voire de nombreux décès mais ont également contribué à un énorme fardeau économique pour l'industrie alimentaire suite aux nombreux rappels et mise au rebus. Les méthodes traditionnelles (telles que les cultures microbiennes et croissances bactériennes) pour détecter les pathogènes sont relativement coûteuses et prennent beaucoup de temps et d'expertise à développer. De ce fait, il est devenu impératif de développer des approches de détection rapides et efficaces pour identifier la présence de bactérie(s) dans les aliments afin d'endiguer d'éventuelles épidémies rapidement. Le développement d'emballages alimentaires intelligents a considérablement évoluée récemment et génère de plus en plus d'intérêt afin de satisfaire les exigences des consommateurs et de l'industrie alimentaire, notamment dans tout ce qui a trait aux techniques de détection précoce de la présence de pathogènes et de bactéries.

L'émergence de matériaux nanostructurés a eu un impact considérable sur les techniques de détections précises et rapides d'une molécule unique. De plus, la taille et les propriétés spécifiques des nanoparticules, nanofibres et autres en font des outils prometteurs pour améliorer les tests de détection dans de nombreux domaines tels que la médecine, l'environnement et bien sur, le secteur de l'alimentation. Des appareils miniaturisés, connus sous le nom de biosenseurs, facilitent la détection in situ de pathogènes alimentaires, ce qui donne à l'industrie de l'emballage un atout considérable pour la détection de ces bactéries. Ce travail de recherche se concentre sur le développement de senseurs basés sur des techniques de détections optiques (telles que colorimétrique et fluorescence) pour la détection de bactéries de façon directe via une cellule de détection ou de façon indirecte par la détection de ses sous produits, le tout pour des applications dans le domaine de l'alimentaire. Les senseurs optiques suggérés ont été intégrés à la surface d'une plateforme solide afin de l'adapter à la demande et aux exigences de l'industrie de l'emballage alimentaire. Ici, de la cellulose bactérienne ayant des propriétés remarquables comme une structure en nanofibrilles, une transparence optique, de bonnes propriétés mécaniques et une disponibilité des groupements fonctionnels a été considérée comme plateforme pour assurer la synthèse de nanoparticule et l'immobilisation de biomolécules.

La première partie de ce travail se concentre sur la détection de composés organiques volatils qui peuvent être générés suite à la croissance bactérienne. La méthode proposée consiste en l'utilisation de nanoparticules d'argent, dont les propriétés plasmoniques permettent une détection colorimétrique. Les nanoparticules d'argent sont donc synthétisées dans de la cellulose bactérienne via une procédure in situ qui résulte en la fabrication d'un nano-papier plasmonique dont les propriétés peuvent être hautement modulable uniquement par la modification de la distance entre les particules et/ou de leur taille. Les résultats ont démontré que les nanoparticules plasmoniques ainsi préparées sont très sensibles à des concentrations variées de vapeur d'ammoniaque. La détection précise de l'ammoniaque a été mesurée par absorbance UV-visible qui est associée aux propriétés plasmoniques des nanoparticules d'argent. Une réduction de l'intensité du pic plasmonique de l'argent a été observée lors de l'augmentation de la concentration en ammoniaque et de la durée d'exposition à ses vapeurs. Comme l'ammoniaque est un produit indicateur de contamination bactérienne dans la viande et le poisson, la plate-forme proposée permet la détection et le suivi de la contamination. Il a également été découvert que la taille des nanoparticules d'argent au sein de la cellulose bactérienne subit une réduction due à l'exposition à l'ammoniaque. Suite à ce phénomène, le nano-papier montre un changement de couleur, respectivement d'ambre foncé à ambre clair, au cours de l'interaction avec la vapeur d'ammoniaque, ou de gris à taupe en la présence de poisson ou de viande contaminée (dégageant de l'ammoniaque). Ces résultats prometteurs ouvrent toute une fenêtre d'opportunités pour le développement d'une technique de détection de contamination de la viande et du poisson par l'intermédiaire d'emballages intelligents.

Dans la seconde partie de ce travail, nous avons développé un biosenseur pour la détection de bactéries grâce à la méthode basée sur le principe de fluorescence. Ce biosenseur a été développé en utilisant la technique de transfert d'énergie entre molécules fluorescentes (FRET) reposant sur le principe de Förster, une approche de transfert d'énergie non radiative entre un fuorophore photoexcité et une molécule dite accepteur et qui dépend fortement de la distance entre ces molécules. Parmi plusieurs paires de donneur-accepteur, le quantum dot nano-cristal et les nanoparticules d'or sont reconnus comme étant les plus efficaces dans la technique FRET. Au cours de la deuxième partie de ce travail de recherche, le développement d'un biosenseur pour la détection de bactéries a été étudié. Pour développer un biosenseur prometteur, une plate-forme sur une surface solide a été considérée avec les paramètres appropriés pour supporter la bio-reconnaissance des éléments. Il est apparu que la cellulose bactérienne imprégnée avec des

nanoparticules d'or permet d'arriver à un système intéressant, soit d'obtenir des propriétés plasmoniques pour l'or et d'abondants groupes fonctionnels pour la cellulose bactérienne. Les résultats ont montré que la plate-forme peut ainsi absorber l'énergie de transfert d'un matériau fluorescent photo-excité, causant une réduction de leur photoluminescence. Cependant, la haute densité des nanoparticules d'or qui génère une capacité de réduction forte, si réduite, entrainera une réduction de cette capacité. Le nano-papier synthétisé présente une surface solide novatrice avec des capacités de désactivation qui peuvent être utilisées en détection par fluorescence comme le FRET.

Dans la dernière partie de ce travail, un biosenseur pour la détection bactérienne a été développé basé sur les résultats obtenus au cours de la seconde partie de ce travail. Ce biosenseur a été développé en utilisant l'approche FRET. La cellulose bactérienne carboxylée mélangée avec des nanoparticules d'or sert d'accepteur et en même temps permet la liaison croisée avec l'élément de bio-reconnaissance de la plate-forme solide. Un point quantique (Quantum dot, QD) conjugué à l'anti *E. coli* joue le rôle de donneur qui se lie à la protéine A/G immobilisée à la surface de la cellulose bactérienne carboxylée. La photo-luminescence du QD génère une réaction de réduction une fois que l'anti *E. coli* conjugué avec le QD interagit avec la bactérie respective (*E. coli*). De ce fait, la distance entre le QD et la surface de l'accepteur est réduite, ce qui a pour conséquence le changement de conformation inhérent dans la structure de l'anticorps. Grâce à cette stratégie, *E. coli* a été détectée à la limite de la LOD près (Limite de Détection-Limit of Detection) qui se situe autour de 10 $CFM.mL^{-1}$. Cet immuno-senseur identifie la bactérie directement sans autre traitement supplémentaire. Compte tenu de sa simplicité et de sa sélectivité, ce senseur a le potentiel d'être implanté en tant capteur dans un emballage alimentaire.

Finalement, les résultats de ce projet de recherche sont multidisciplinaires et peuvent influencer plusieurs domaines de la science : 1) le secteur environnemental grâce à l'introduction d'une nouvelle génération d'emballages intelligents qui permettraient la reconnaissance précoce des pathogènes et des bactéries permettant de prévenir les infections; 2) la technologie des biosenseurs, en introduisant le nano-papier comme une plate-forme sensible et versatile pour la détection de vapeur; et 3) la simulation des propriétés intrinsèques d'un anticorps pour une détection directe d'antigènes.

ABSTRACT

Foodborne outbreaks due to the consumption of contaminated food products result not only in hospitalization and death, but also place a large economical burden on the food industry due to product recall and disposal. Traditional methods (such as microbial cultures and bacterial growth) for detecting pathogens are relatively costly, time-consuming, and expert related. Therefore, rapid, accurate and in-situ approaches for identifying bacteria in the food industry are urgently needed to overcome the problem that can be widespread easily. Recently, smart food packaging has evolved to meet the demands of customers and food industries, especially in early recognition techniques of pathogens or spoilage bacteria.

The emergence of nanostructured materials has had the greatest impact on the advancement of the most straightforward, quick and accurate detection of a single molecule. On the other hand, the size and unique properties of nanoparticles, nanofibers, nanorods, etc., make them promising tools for the improvement of recognition bioassay in various fields such as medicine, environment and food sectors. In this case, miniaturized devices, known as sensors, facilitate the in-situ detection of foodborne pathogens, benefiting the food packaging industry significantly. This research was addressed the development and demonstration of sensors based on optical techniques (e.g., colorimetric and fluorescent-based methods) for the detection of bacteria, directly through a whole cell or indirectly through its by-product. The suggested optical sensors were integrated to the surface of a solid platform to make it more compatible with demands in the food packaging. Here, bacterial cellulose with remarkable features such as the nanofibrils structures, optical transparency, mechanical properties and, availability of functional groups was considered as the platform, supporting the synthesis of nanoparticles and immobilization of biomolecules.

The first part of this work focused on the detection of volatile organic compounds which may be produced during bacterial growth. The proposed method relied on using silver nanoparticle and its plasmonic properties, allowing a colorimetric technique. As such, the silver nanoparticles were synthesized within bacterial cellulose through an in-situ procedure that resulted in the fabrication of a plasmonic nanopaper, highly tunable by the change of size and interparticle distance. The results demonstrated that the prepared plasmonic nanoparticle is very sensitive to various concentrations of ammonia vapor. Interestingly, the precise detection of ammonia was measurable by the UV-vis absorbance spectra associated with the plasmonic properties of silver nanoparticles

and trancparency of bacterial cellulose. Consequently, it revealed a reduction in the intensity of a plasmonic peak by increasing the concentration of ammonia and time of exposure. As ammonia is one of the primary compounds of bacterial spoilage in meat and fish, the proposed platform was assessed against the produced gases during spoilage. We also discovered that the size of silver nanoparticles embedded in the bacterial cellulose endured a reduction due to the etching by exposure to the ammonia. As observed, because of this phenomenon, the nanopaper exhibited a color change from amber to a light amber by interacting with ammonia vapor and, to a gray or taupe upon the presence of ammonia in fish spoilage or for meat, respectively. Thus, these results opened the window to an innovative technique for examining the spoilage in meat and fish by smart packaging.

In the second part of this research, we studied the development of a biosensor for detection of bacteria relying on the fluorescent based-method. This biosensor was developed by using Förster (fluorescence) resonance energy transfer (FRET) approach that is a non-radiative energy transfer from a photoexcited fluorophore to an acceptor molecule with strong dependency on the distance between these molecules. Among various donor-acceptor pairs, nano-crystal quantum dot and gold nanoparticles are known as the high efficient ones in FRET technique. In order to design a promising biosensor, a solid surface platform was considered with the appropriate features to support the biorecognition and transducer elements. Interestingly, we found that bacterial cellulose impregnated with gold nanoparticles addressed the demands for such a system, owing to the plasmonic properties of gold nanoparticles (served as the acceptor) and abundant functional groups available in the bacterial cellulose. Our result showed that it functioned to absorb the energy transfer from photoexcited fluorescent materials, caused a reduction their photoluminescence. Accordingly, the high population density of gold nanoparticle-bacterial cellulose was intended as a strong quencher while this ability reduced by the reduction of the nanoparticle population density. Successfully, the synthesized nano paper presented a novel solid surface with quenching ability that can be utilized in fluorescence detection approaches such as FRET.

In the last step, a biosensor for bacterial detection was assembled based on the obtained results from the pervious step of this research and by applying FRET approach. The carboxylated bacterial cellulose embedded with gold nanoparticles served as the acceptor and simultaneously cross-linked to the biorecognition element as the solid platform. Quantum dot (QD) conjugated to anti-*E. coli*

played as the donor which bonded to the protein A/G immobilized on the surface of carboxylated bacterial cellulose. The photoluminescence of the QD endured a reduction once the anti-*E. coli* conjugated QD interacted with the respective bacteria. So, the distance between the QD and the surface of the acceptor was reduced, as the consequence of the inherent conformational change in the antibody structure after interacting. Through this strategy, *E. coli* was recognized with a LOD (limit of detection) about 10 CFM.mL^{-1}. Thus, this immunosensor identified the bacteria directly without employing extra treatments. Given the simplicity and selectivity, the proposed biosensor has the potential to be implemented as a portable device in food packaging.

Finally, the results of this research involve multidisciplinary and novel outcomes that can influence several fields of science. 1) the environmental sector, by introducing a new generation of smart packaging that allows early recognition of foodborne pathogens and spoilage bacteria to prevent infections outbreak, 2) biosensing technology, by introducing plasmonic nanopaper as a versatile and sensitive platform for the detection of vapor; and suggesting the intrinsic properties of an antibody for straightforward detection of antigens.

TABLE OF CONTENTS

DEDICATION III

ACKNOWLEDGEMENTS IV

RÉSUMÉ VI

ABSTRACT IX

TABLE OF CONTENTS XII

LIST OF TABLES XVII

LIST OF FIGURES XVIII

LIST OF ABBREVIATIONS XXIII

CHAPTER 1 INTRODUCTION 1

CHAPTER 2 LITERATURE REVIEW 4

2.1 Sensor 4

2.1.1 Receptor 5

2.1.1.1 Antibody 5

2.2 Transducer 10

2.2.1 Electrochemical sensor 10

2.2.2 Optical sensor 10

2.2.2.1 Fluorescent-based detection 11

2.3 Quantum Dots 16

2.3.1 Quantum dots properties 16

2.3.2 Quantum dot applications in bioassay 17

2.4 Noble metal nanoparticles in bioassay 18

2.4.1 Gold nanoparticles as quencher 20

2.4.2 Gold nanoparticle in optical density 21

2.5 Solid-based FRET assay 22
2.5.1 Cellulosic-based substrate 23
2.6 Volatile organic compounds and detection of fish and meat spoilage 28
2.7 Problem identification 30
CHAPTER 3 OBJECTIVES AND ORGANIZATION OF THE ARTICLES 32
3.1 Objectives 32
3.1.1 General objective 32
3.1.2 Specific objectives 32
3.2 Organization of Articles 33
CHAPTER 4 ARTICLE 1: MODULATION OF POPULATION DENSITY AND SIZE OF SILVER NANOPARTICLES EMBEDDED IN BACTERIAL CELLULOSE VIA AMMONIA EXPOSURE: VISUAL DETECTION OF VOLATILE COMPOUNDS IN A PIECE OF PLASMONIC NANOPAPER 35
4.1 Abstract 36
4.2 Introduction 36
4.3 Experimental 38
4.3.1 Reagents and equipments 38
4.3.2 Synthesis of plasmonic nanopaper 41
4.3.3 Preparation of the gas sensing set-up 41
4.3.4 Sample preparation for TEM analysis 42
4.3.5 Raman analysis 42
4.4 Results and discussion 42
4.4.1 The effect of ammonia vapor on AgNPs embedded in bacterial cellulose nanopaper 42
4.4.2 Specificity upon ammonia exposure 43

4.4.3 Sensing performance 45
4.4.4 Raman analysis 49
4.5 Conclusions 50
4.6 Acknowledgements 51
4.7 References 51
4.8 Supporting Information 55
4.8.1 Supporting information content 55
4.8.1.1 Figures 56
4.8.1.2 Estimation of Evaporation rates and Limits of Detection 58
4.8.2 Supplementary References 59
CHAPTER 5 ARTICLE 2: NANOPAPER-BASED PLATFORM APPLICABLE IN SOLID-BASED FRET TECHNIQUE 60
5.1 Abstract 61
5.2 Introduction 61
5.3 Materials and methods 63
5.3.1 In-situ synthesis of AuNP within BC 63
5.3.2 Sample preparation for TEM 64
5.3.3 Estimation of quenching efficiency 64
5.4 Results and discussion 65
5.4.1 Characterizing the in-situ synthesized AuNP-BC 65
5.4.2 Estimating the fluorescence quenching efficiency 68
5.5 Conclusion 71
5.6 Acknowledgments 72
5.7 References 72

CHAPTER 6 ARTICLE 3: TOWARD A NANOPAPER-BASED AND SOLID PHASE IMMUNOASSAY USING FRET FOR RAPID DETECTION OF BACTERIA 76

6.1 Abstract 77

6.2 Introduction 77

6.3 Experimental methods 79

6.3.1 Reagents and instruments 79

6.3.2 Carboxylation of bacterial cellulose (CBC) 80

6.3.3 In-situ synthesis of AuNP within CBC (AuNP-CBC) 81

6.3.4 Protein A/G immobilization on the CBC and the AuNP-CBC 81

6.3.5 Conjugation of antibody to quantum dot 82

6.3.6 Characterization of the immobilized protein A/G on nanopaper-based platform 83

6.3.7 Pathogen recognition platform 83

6.4 Results and discussion 84

6.4.1 Carboxylation of bacterial cellulose (CBC) 84

6.4.2 In-situ synthesis of AuNP within CBC 85

6.4.3 Protein A/G immobilization on the nanopaper platform and its characterization 86

6.4.4 Bacteria recognition 89

6.5 Conclusions 90

6.6 Acknowledgments 91

6.7 References 91

6.8 Supporting information 95

6.8.1 Bacteria growth and preparation 96

CHAPTER 7 GENERAL DISCUSSION 99

CHAPTER 8 CONCLUSIONS AND RECOMMENDATIONS 106

8.1 Summary and Conclusions 106

8.2 Original contribution and novelty 108

8.3 Recommendations 109

LIST OF REFERENCES 110

LIST OF TABLES

Table 2-1. Identified compounds from P. aeruginosa, S. aureus, E. coli, and S. Typhimurium through SEMSI-MS [115] 28

Table 2-2. Strains of bacteria are commonly found in the raw meat stored in different conditions, vacuum packaging (VP) and modified atmosphere packaging (MAP) [126]. 29

Table 4-1. Limits of detection of the explored system [a] 47

Table 4-2. Modulation of population density (PD) and average size (AS) of the AgNPs embedded in the nanopaper via volatile compound exposure. 49

Table S 4-1. Estimation of initial evaporation rate of NH_3. 58

Table S6-1. A comparison between the amount of immobilized protein A/G in different condition and various platforms. These amounts are estimated through the Bradford assay analysis. .97

LIST OF FIGURES

Figure 2-1. (A) a schematic of the integration of a biosensor [7], (B) a popularity of the applied transducers for the pathogen detection [13]. 5

Figure 2-2. The schematic of the IgG structure and its differentiation to the various blocks of amino acids. The dark and light blue chains represent the heavy (H) and light (L) chains of an antibody, respectively. Each one is composed of the variable (V) and constant (C) region [17]. 6

Figure 2-3. The probabilities of an antibody positions after immobilization on the surface of a substrate [18] 7

Figure 2-4. The illustration of EDC/S-NHS chemistry [25]. 8

Figure 2-5. A schematic of optical sensing along with the representative components and techniques applied to a biosensor for the detection of pathogen: (A) various types of receptors, (B) the established substrates and (D) the sensing approaches [38]. 11

Figure 2-6. An illustration of Jablonski diagram which shows the fluorescent mechanism [39]. .12

Figure 2-7. A schematic of FRET process and the overlap between the absorbance spectra of acceptor and emission spectra of donor [47]. 14

Figure 2-8. Demonstrating the dependence of FRET efficiency on the distance between donor and acceptor [48]. 15

Figure 2-9. (A) a schematic and TEM image of a quantum dot composed of CdSe/ZnS core/shell, (B) the change in the emission spectra and color of CdSe/ZnS with increasing the nanocrystal size [57]. 16

Figure 2-10. An illustration of the detection of bacteria through establishing a sandwich model. [62]. 17

Figure 2-11. Colors change of various sized monodispersed (A) silver nanoparticles and (C) gold nanoparticles. (B) and (D) graphs show the respective UV-Vis spectra of dispersed silver and gold nanoparticles, respectively [72]. 19

Figure 2-12. (A) a schematic of colorimetric detection of E. coli through anti- E. coli conjugated nanorods. (B) TEM image of anti- E. coli conjugated nanorods, (C) the color change of anti-

E. coli conjugated nanorods upon addition of E. coli (10^4 CFU.mL^{-1}) and (D) TEM image showing the aggregation of gold nanorods on the surface bacteria [86].....22

Figure 2-13. A schematic of the chemical structure of cellulose and effect of hydrogen bonds on its formation [98].....24

Figure 2-14. The presented figures show the differences in the structure of various nanocelluloses [101]. 25

Figure 2-15. SEM of the composit nanopapers (A) bare bacterial cellulose nanopaper. (B) AgNP-BC: (B-a) AgNPs synthesized in-situ BC (B-b,c) AgNP-BC in the presence of 10 μg mL^{-1} of methimazole and 4 μg mL^{-1} of iodide, respectively (C) SEM of AuNP-BC: (C-a) AuNP-BC; (C-b, c) AuNP-BC in the presence of 8 μg mL^{-1} of thiourea and 4 μgmL^{-1} of cyanide, respectively. (D) SEM of QDs embedded within bacterial cellulose nanopaper. (E) SEM of UCNP-BC. (F) Graphene oxide-coated QD-BC. (G) Graphene oxide-coated UCNP-BC [112]. 27

Figure 4-1. Modulation of the population density of AgNPs embedded in bacterial cellulose via corrosive vapor (ammonia) exposure. Appearance of AgNP-BC without ammonia vapor exposure (A) and after ammonia vapour exposure (C). TEM micrographs of AgNP-BC without ammonia vapour exposure (B and B′) and after ammonia vapour exposure (D and D′). Estimation of the size distribution of the studied AgNPs (E) without ammonia vapour exposure (control) and after ammonia vapour exposure. The box plots show the median, 25th and 75th percentiles and the extreme values of the respective size distributions (5–95 percentile). 40

Figure 4-2. Specificity of the nanoplasmonic membrane as a corrosive vapor (ammonia) sensing platform. A. UV-Vis spectra of plasmonic nanopaper upon vapor exposure using an initial volume of 1000 μL of different volatile compounds spontaneously volatilized for 18 hours. B. Blue shift observed in the UV-Vis spectra depending on the volatile compound exposed. C. Changes in optical density according to the volatile compound exposed. The error bars represent the standard deviation of three parallel experiments. a. Methanol. b. Ethanol c. Propanol. d. Acetic acid. e. Ethyl acetate. f. Acetonitrile. g. Ammonia. h. Acetone. i. Toluene. j. Indole. k. Water. l. Triethylamine. 44

Figure 4-3. Behavior of the nanoplasmonic membrane as a corrosive vapor sensing platform. A. UV-Vis spectra of the plasmonic nanopaper upon corrosive vapour (ammonia) exposure using 10 and 1000 µL of 30% ammonia solution spontaneously volatilized for between 2 and 12 hours. B. Calibration curves displaying changes in optical density depending on the initial volume to be volatilized (from 10 to 1000 µL) and the exposure time (2–12 hours). The error bars represent the standard deviation of three parallel experiments. 46

Figure 4-4. Food spoilage monitoring via plasmonic nanopaper. A. UV-Vis spectra of the nanoplasmonic membranes before food spoilage exposure (Ctrl) and after food spoilage exposure (ammonia and several volatile organic compounds are released during fish and meat spoilage). B. Appearance of the nanoplasmonic membranes before/after food spoilage monitoring. C. TEM micrographs, from left to right: control, fish spoilage and meat spoilage. D. Size distribution of the AgNPs embedded in the nanopaper before/after food spoilage monitoring, the box plots show the median, 25th and 75th percentiles and the extreme values of the respective size distributions (5–95 percentile).....48

Figure 4-5. Raman signature of the explored materials: bare bacterial cellulose (BC), bacterial cellulose decorated with silver nanoparticles (AgNP-BC) and AgNP-BC exposed to ammonia and fish/meat spoilage.....50

Figure 5-1. AuNP-BCs characterization by (A) their color appearance (from right to left, high, medium and low-density AuNP-BC and bare BC) and, (B) UV-Vis absorbance spectra of AuNP-BC synthesized with different densities of AuNPs. Also, the emission spectra of FSS (exited at 460 nm) and QD (exited at 350 nm) are illustrated for more comparison. 66

Figure 5-2. Scanning electron microscopy of AuNP-BC with high density (A and A'), medium density (B and B'), low density (C and C'), and bare BC (D). 67

Figure 5-3. Transmission electron microscopy (TEM) of AuNPs dissociated from the high density (A) and medium density (B) of AuNP-BC platforms and their respective size distribution histograms (A' and B').....68

Figure 5-4. Evaluation of FSS quenching efficiency cast on nanopaper-based platform of AuNPs with different density. 69

Figure 5-5. Distribution of the evaluated FSS quenching efficiency regarding to AuNP-BCs densities over different concentrations of FSS. 70

Figure 5-6. A comparison between FSS fluorescent intensity cast on the surface of nitrocellulose and BC. The graph insight is just a magnification of the last two concentrations. The measured fluorescent intensities were the result of applying 5 µl of FSS with different concentration on the surface of BC or nitrocellulose. 70

Figure 6-1. Characterization of the obtained AuNP-CBC, (A) scanning electron microscope (SEM) imaging from AuNP-CBC, (B) UV-Vis absorbance spectra of as-synthesized AuNP-CBC along with its overlap with emission spectra of QD (excited at 350 nm). 85

Figure 6-2. The optical density recorded at 460 nm as a result of the enzymatic reaction of HRP and TMB. It presents the situation of the protein A/G immobilized on the surface of CBC by the interaction between the amounts of HAb linked to protein A/G as well as captured HRP. (A) the effect of pH on the immobilization of protein A/G and, (B) the effect of the initial amount of protein A/G on its immobilization. 87

Figure 6-3. (A) Estimated optical density of HRP response attached to HAb and HAb-QD which are linked to protein A/G in two different platforms, AuNP-CBC and bare CBC. (B) Quenching efficiency evaluated by the capture of HRP to HAb-QD which is linked to protein A/G on the surface of AuNP-CBC. 88

Figure 6-4. Performance of proposed immunosensor presented by (A) the quenching efficiency of QD corresponding to the concertation of E. coli (orange bars) and control bacteria S. aureus (blue bars) and (B) the change in fluorescent intensity QD after its response to E. coli detection. 90

Figure S4-1. TEM micrographs showing the population density of AgNPs embedded in BC without NH3 vapor exposure (A-C) and after NH3 vapor exposure (D-F). The population density of AgNPs at the foreground in images A-C has been estimated to be 1473 ± 227 AgNP μm^{-2}, whereas the population density of AgNPs at the foreground in images D-F is around 302 ± 38 AgNP μm^{-2}. AgNP-BC in images D-F was exposed at an initial vapor rate of around ~1.2 µg $s^{-}1$ for 12 hours. TEM micrographs were analyzed via image processing through ImageJ 1.48v

(Wayne Rasband, National Institutes of Health, Bethesda, MD) in order to estimate the population density of nanoparticles embedded in the BC-based composite. 56

Figure S4-2. SEM micrographs of AgNP-BC without NH3 vapor exposure (A) and after NH3 vapor exposure (B). No damage or structural changes were observed in the nanofibers. 57

Figure S4-3. Calibration curves displaying changes in optical density depending on the initial evaporation rate and the exposure time. The error bars represent the standard deviation of three parallel experiments. 57

Figure S6-1. (A) TEM image of QD which was conjugated to antibody and (B) The size distribution of QD obtained by analyzing the diameter of 200 individual QD particles. 98

LIST OF ABBREVIATIONS

2D	Two-dimensional
3D	Three-dimensional
Ab	Antibody
AgNP	Silver nanoparticle
AuNP	Gold nanoparticle
BC	Bacterial Cellulose
BNC	Bacterial Nanocellulose
CBZ	Carbamazepine
CBC	Carboxylated Bacterial Cellulose
BSA	Bovine Serum Albumin
CNC	Cellulose Nanocrystal
CNF	Cellulose Nanofibers
CNP	Carbon Nanoparticle
E. coli	*Escherichia coli*
EDC	1-Ethyl-3-(3-dimethylaminopropyl)carbodiimide
FE-SEM	Field Emission Scanning Electron Microscopy
FITC	Fluorescein-5-Isothiocyanate
FSS	Fluorescein Salin Salt
FRET	Fluorescence Resonance Energy Transfer
GO	Graphene Oxide
HRP	Horseradish Peroxidase
LOD	Limit of Detection
LSPR	Localized Surface Plasmon Resonance
MES	2-(N-Morpholino) ethanesulfonic acid

NC	Nanocellulose
NCC	Nanocrystalline Cellulose
NF	Nanofibers
NFC	Nanofibrillated Cellulose
NP	Nanoparticle
NHS	N-hydroxysuccinimide
PAGE-gel	Polyacrylamide gel electrophoresis
PBS	Phosphate-Buffered Saline
PET	Polyethyleneterephthalate
PEI	Poly(ethylenimine)
Phe	Phenylalanine
P. aeruginosa	Pseudomonas aeruginosa
QD	Quantum Dot
SDS	Sodium Dodecyl Sulfate
SERS	Surface Enhanced Raman Scattering
S-NHS	N-hydroxysulfosuccinimide
S. aureus	*Staphylococcus aureus*
T-paper	Transparent nanopaper
Trp	Tryptophan
Tyr	Tyrosine
TEMPO	2,2,6,6-tetramethylpiperidine-1-oxyl
UCNP	Up-Conversion Nanoparticle
VOC	Volatile Organic Compounds

CHAPTER 1 INTRODUCTION

Food has always been regarded as the primary source of energy for mankind that may be served in a variety of recipes either raw or cooked. Although our ancestors were used to provide their needs locally, developments and enhancements of transport systems, as well as improvements in food packaging, has made it much easier to conserve food varieties from all over the world.

However, storage and shelf conditions serve as effective parameters for controlling the freshness and safety of foods, but it cannot be guaranteed that food is free of contaminations such as foodborne pathogens or spoilage microorganism. As such, food quality control is necessary not only to protect customers against foodborne illness but also to minimize wasting food resulting from microbial spoilage [1, 2].

Despite all precautions and preservations used, the outbreak of foodborne diseases has remained a remarkable threat to public health and safety which has significantly increased over the last two decades [3]. For instance, the Centers for Disease Control and Prevention (CDC) has estimated that every year 48 million people in the United States alone are infected by foodborne pathogens, leading to approximately 128,000 hospitalizations and 3000 deaths [3, 4].

Generally, an outbreak of foodborne diseases results from the consumption of food contaminated with pathogens. Among the different types of foodborne pathogens, bacteria such as *Listeria monocytogenes*, *Escherichia coli* O157:H7, *Staphylococcus aureus*, *Salmonella enterica* and *Bacillus cereus* remain the most common [5, 6].

Due to very low infection dose of pathogenic bacteria (10-1000 bacterial cells), their ability to multiply rapidly and their high resistance to antibiotics, recall and disposal of contaminated food products are considered as an essential step in keeping consumers safe. Therefore, rapid, precise and early recognition of contaminated food has been argued as the most important priority in the public health domain [7].

Conventional methods for foodborne pathogens detection are practically carried out by culturing microorganisms in agar plates followed by a chemical-biochemical analysis. Despite their high accuracy and reliability, their application has been limited because they are time-consuming, dependent on technician and equipment and are not flexible for on-site diagnosis [7].

Recent development in material science and nanotechnology has successfully promoted the recognition tools and bioassays. Nanomaterials with a diameter of 1-100 nm, owing to phenomenal physical and chemical properties such as high surface area, capacity to carry functional groups, and flexibility to conjugate to biomolecules, are currently of great interest to researchers [8-11]. For example, integration of biomolecules (such as antibodies, aptamers, enzymes, etc.) with nanoparticles (such as quantum dots, gold nanoparticles and, graphene, etc.) has facilitated the improvement of analytical devices called sensors or biosensors. These sensors offer several advantages such as sensitivity, selectivity, rapid detection, and accuracy as well as in-situ and real-time detection. Besides, their cost-efficiency, miniaturized design, and unnecessary sample preparation have made them an attractive alternative to incorporate into food packaging [7, 12].

Thus, the main objective of this research is to develop and fabricate a biosensor to detect bacteria, directly through the whole cell or indirectly through its by-products, which is portable, easy-to-use, and can be easily integrated into food packaging materials.

The first part of the work is a proof-of-concept investigation, proving the potential of bacterial cellulose with nanofibrils structure impregnated with plasmonic nanoparticles to detect volatile organic compounds. The second part of this work investigates the improvement of a solid-based platform to address the demands for the design of biosensors for fluorescent-based methods. Therefore, we explored the properties of bacterial cellulose embedded with gold nanoparticles as a plasmonic nanopaper which has the ability to absorb the energy transfer from photoexcited fluorescent material. The obtained results lead to a new assembly of biomolecules relying on the fluorescent-based technique for direct detection of bacteria, which was the subject of the third part of this research. It consists in the proof-of-concept of a novel biosensor which was developed on solid-surface using FRET method.

This dissertation involves eight chapters and is arranged according to the main objective and three scientific articles, one published and two submitted.

- Chapter 1: Introduction
- Chapter 2: Literature review
- Chapter 3: Explanation of the main objective as well as specific objectives of this research, and arrangement of the articles
- Chapter 4, 5 and 6: Report of three articles as well as their main outcomes

- Chapter 7: Presentation of general discussion with respect to the reported articles
- Chapter 8: Conclusion of this work along with the summary, the originality, and suggested recommendations for future works.

CHAPTER 2 LITERATURE REVIEW

What are biosensors and their properties? Why are they needed? What are the strategies in fabricating biosensors? What are the roles of nanoparticles and biomolecules in developing a high efficient biosensor? How will it be possible to improve biosensor for smart packaging? This chapter seeks evidence and information from the published scientific reports to answer these questions along with others.

2.1 Sensor

The biosensor is a novel technology widely utilized in the fields such as food safety, medical, process control and biosecurity. Typically, the biosensor evolves two main parts: a receptor and a transducer. The receptor (biorecognition element), known as the heart of any biosensor, is a functionalized platform can specifically capture and recognize the analyte of interest. Due to the interaction between the analyte and biorecognition element, a physical or chemical change is produced which is translated to a measurable signal by the transducer [13]. Regarding the applied approach as a transducer, sometimes an additional device is necessary to modify or amplify the generated signal to a detectable one. Therefore, the measured signal is directly corresponded to the concentration of an analyte, allowing the real-time quantitative and qualitative measurement. Figure 2-1A represents the two main parts of a biosensor and their integration.

Usually, biosensors are classified with respect to the transducer approaches such as optical, electrochemical and mass sensitive. The Figure 2-1B shows the most popular reported biosensor in the field of pathogen detection.

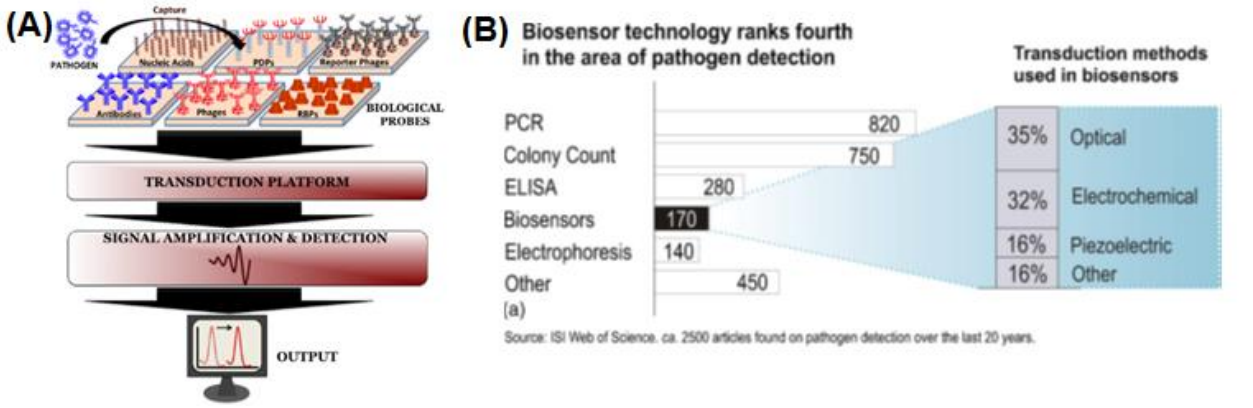

Figure 2-1. (A) a schematic of the integration of a biosensor [7], (B) a popularity of the applied transducers for the pathogen detection [13].

The biosensor will be ideal when it exhibits high selectivity and sensitivity to the specific target analyte. Selectivity is the ability of biosensor to distinguish different substances and not be affected by the presence of other interfering substances. While sensitivity refers to the sensing ability in the range of sub-milligram and lower. The efficiency of these parameters will be defined by the type of receptor, applied transducer and the design integrity.

2.1.1 Receptor

The main receptors which have been exploited for the fabrication of biosensors are antibodies, aptamers, nucleic acids, and bacteriophages [14]. Besides the biomolecule, the use of a specific carbohydrate has been reported for detection of pathogens such as *E. coli* [15]. The parameters such as stability, ease of immobilization and conjugation to biosensor platform, high affinity in interacting with the specific analyte and low reactivity with interfering contamination are taken into account for the selection of an appropriate bioreceptor that can significantly influence the efficiency and quality of the biosensor. Among them, antibodies are of great interest to researchers as a biorecognition element, explored in the configuration of the various biosensors, especially those used for pathogen detection. The section below clarifies antibodies and their importance in the biosensor fabrication.

2.1.1.1 Antibody

Antibodies (immunoglobulin) have been widely investigated in the development of biosensors as promising receptors for detection of an analyte. The biosensors integrated to antibodies are usually

called as immunosensors [16]. Antibodies, found as monoclonal, polyclonal or recombinant, are discriminated by their affinity of attachment to the analyte. Antibodies are known as a biopolymer composed of different blocks of amino acids that their sequence and composition have shaped a three-dimensional structure. Depending on the type of the antibody, it may possess a different molecular weight, for instance, the abundant type of antibody (immunoglobulin G, IgG) has a molecular weight around 150 kD and approximated dimensions of 14×10×5 nm [16]. Figure 2-2 exhibits a classical schematic of IgG with the different blocks of amino acids chains.

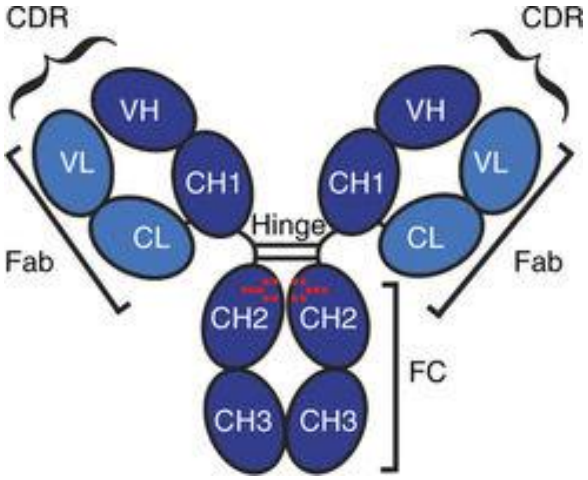

Figure 2-2. The schematic of the IgG structure and its differentiation to the various blocks of amino acids. The dark and light blue chains represent the heavy (H) and light (L) chains of an antibody, respectively. Each one is composed of the variable (V) and constant (C) region [17].

This Y-shape structure of the antibody is due to two parts: 1) two variable fragments, F(ab), contains the binding region to the antigen and 2) the constant region, Fc, is the tail which determines the orientation of the antibody. According to this specific structure, the immobilized antibody will be desirable when it is located on the surface of the substrate through its Fc in an oriented-shape and, as a result, the specific binding regions are free for attachments [17]. So, this “end-on” configuration has a maximum affinity to bind with antigen. While its efficiency can be remarkably reduced by random immobilization referred as “head-on”, “side-on” and “lying-on” [18]. As illustrated in Figure 2-3, in the random immobilization one or both active regions may link to the substrate which would cause their blockage and preventing the interaction with the antigen.

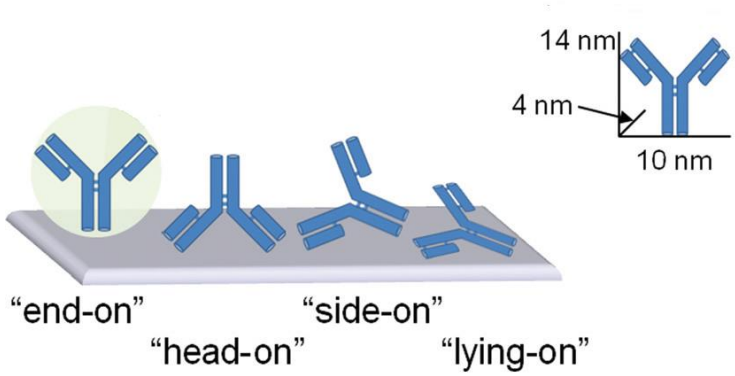

Figure 2-3. The probabilities of an antibody positions after immobilization on the surface of a substrate [18]

The exploited immobilization strategies would thoroughly justify the position of antibodies on the surface of the respective solid substrate [19, 20]. Various functional groups on the surface of antibody derived from amino acids blocks may be targeted for the crosslinking and immobilization strategies [21]. The most applied strategies are covalent binding and affinity immobilization techniques, subjected in detail in the next session.

To develop an immunosensor, antibodies are immobilized on the surface of a transducer which can specify the antibody-antigen binding. Consequently, the binding event is measured and revealed by either the changes in electron charge via impedance measurement or a change in the optical properties of the substrate. The bioassays using the antibody as biorecognition element are very selective, sensitive and robust enough to detect the antigen.

2.1.1.1.1 Antibody immobilization

Functional groups of the antibody are the main targets of its attachment to the chemically engineered surface. Covalent binding can significantly improve the density and reliability of attached antibody and provide a more robust immunosensor. On the other hand, the covalent bond provides a strong immobilization of antibody to the functionalized surface, highly efficient. Various chemistries have been applied for achieving a high-throughout attachment which totally corresponds to the functionality of the surface and the target group on the antibody. Commonly employed groups of the antibody are amine, carboxyl, thiol and carbohydrate moieties [19, 21].

Amine and carboxyl groups are abundantly available on the surface of the antibody. Reactive amino groups are a primary amine side chain, generally derived from amino acid like lysine while

carboxyl groups are mostly derived from amino acids such as glutamate and aspartate [22]. Owing to the widespread presence of these groups especially lysine all over the structure of an antibody, it is difficult to define and justify the immobilization; nevertheless, it remains as the favorite functional group. The common chemistry for amine and carboxyl coupling (between a substrate and protein) is carbodiimide reaction that uses EDC associated with succinimidyl esters, e.g., NHS or S-NHS, as shown in Figure 2-4. This chemistry known as EDC/NHS binding causes the formation of a robust amide bond [20]. This covalent attachment method has been widely applied for immobilization of protein as well as preparation and activation of a surface. By adjusting the conditions of the experiment, researchers have improved the efficiency of attachments through this method. For example, Parolo and coworkers could improve the immobilization of the antibody to the surface of carboxylated gold nanoparticles by simply adjusting the pH of reaction [23]. The activated carboxyl groups of gold nanoparticles by EDC/NHS chemistry were conjugated to antibodies in pH 5 that resulted in a greater contribution of the Lys groups. This strategy prevented the amine groups at the active sites of antibody to be conjugated to AuNP. Therefore, the final platforms demonstrated more sensitivity for capturing the antigen. Likewise, Sun and co-workers have employed a novel approach for oriented immobilization of an antibody through carbodiimide chemistry by controlling the electric field. In their work, the Fc region of the antibody was activated through EDC/NHS, coupled to the self-assembled monolayer of cysteine with amino groups. By inducing an appropriate electric field and adjusting pH, antibodies were immobilized orientally through their native charge [24].

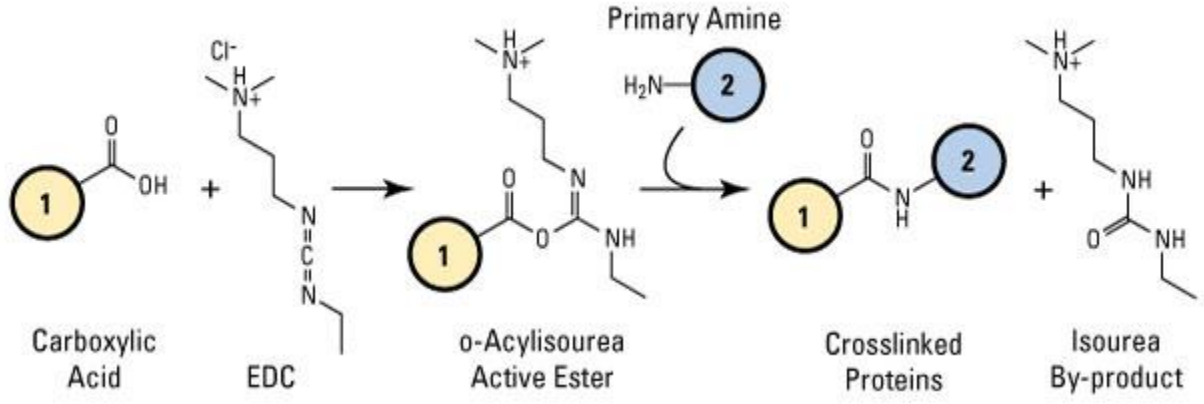

Figure 2-4. The illustration of EDC/S-NHS chemistry [25].

Other active groups in the antibody are disulfide bonds derived from cysteine that are responsible for the 3D structure of an antibody, such as disulfide bonds in the Hinge-region. By reducing this bond with chemical agents such as dithiothreitol (DTT) and 2-mercaptoethylamine (2-MEA), a free thiol bond can be created on the antibodies [26, 27]. Crosslinkers that involve maleimide or iodoacetyl groups are the most efficient for sulfhydryl-directed conjugation. As an example, the thiol groups on the antibody were conjugated to the amine group of a solid surface with Succinimidyl-4-(N-maleimidomethyl) cyclohexane-1-carboxylate (SMCC) containing NHS-ester and maleimide reactive groups [26]. Although the thiol groups (sulfhydryl groups) can directly immobilize on the surface of gold [27], their creation is followed by the pretreatments of antibody. Thus, it causes the fragmentation of the antibody that may influence their active sites [27].

Besides, carbohydrates located in the Fc region of antibodies is another reactive group which can contribute to immobilization. However, these groups are not reactive in their native state, and oxidization treatment is necessary for converting into active aldehydes (–CHO) for coupling [26]. Although this group allows a desired immobilization of antibodies in an oriented shape, the harsh oxidation may affect the other available amino acids in the antibody [28].

Although covalent immobilization can provide a highly stable conjugation, it may lead to randomly oriented placements of an antibody blocking its active sites, necessary for capturing bacteria. It is reported that this approach decreased the capacity of capturing 2-3 fold in compared with the well-oriented antibodies [29].

Another alternative that provides an oriented immobilization of antibodies, free from any chemical reaction, is affinity binding. Remarkably, this method has promoted the immobilization strategies and been widely employed in the biosensor development. The most commonly applied method is to use Protein A, Protein G or recombinant Protein A/G that can bind particularly with the Fc region of the antibody. It allows immobilizing an antibody through a tail-on position that keeps the two active sites free for capturing the antigen. The Protein A and G have two and five binding domains respectively while the protein A/G has the ability of both [18, 28, 30-34]. Extensive studies have investigated the immobilization of these Proteins on various functionalized surfaces by using different experimental conditions. Several researchers had proved the improvement in biosensor performance when it was compared with randomly immobilized antibodies [35-37].

2.2 Transducer

Several types of transducers have been studied for a high-throughout design of biosensors, such as electrochemical, optical and piezoelectric. As illustrated in Figure 2-1Bs, optical and electrochemical biosensors are the most popular approaches for developing of a promising biosensor due to ease of use, rapid, low-cost and portable detection.

2.2.1 Electrochemical sensor

Electrochemical biosensors are also classified as the most widespread recognition tools because of their low-cost, simple operation and multiplex sensing in a chip-like device [8]. This bioassay mainly relies on the measurement of changes in current or potential once the interaction between analyte and sensor occurs. In respect to the measured parameter, the technique of sensing can be identified differently such as current (amperometric), the potential (potentiometric) or impedance (impedimetric) [13].

2.2.2 Optical sensor

The optical biosensors referring to those use the light (electromagnetic radiation) for the detection technique. Surface plasmon resonance (SPR), surface-enhanced Raman scattering (SERS), fluorescent and colorimetric methods are among the most popular optical sensing technologies [38]. The optical sensing allows a direct visual detection of the analyte whose advantage can surpass other methods [38]. Although for quantitative and precise recognition, the optical signal measurement provides more information, the visual detection would be possible through this approach. Figure 2-5 represents an overview of optical sensors integrated with different parts. Despite the electrochemical sensors, the optical sensors don’t need a conductive substrate, so it makes them an attractive and simple method for detection of vapor or gases in the headspace of food packages. The focus of this dissertation is mainly dedicated to fluorescent-based technique and colorimetric detection as will be explained in the next sessions.

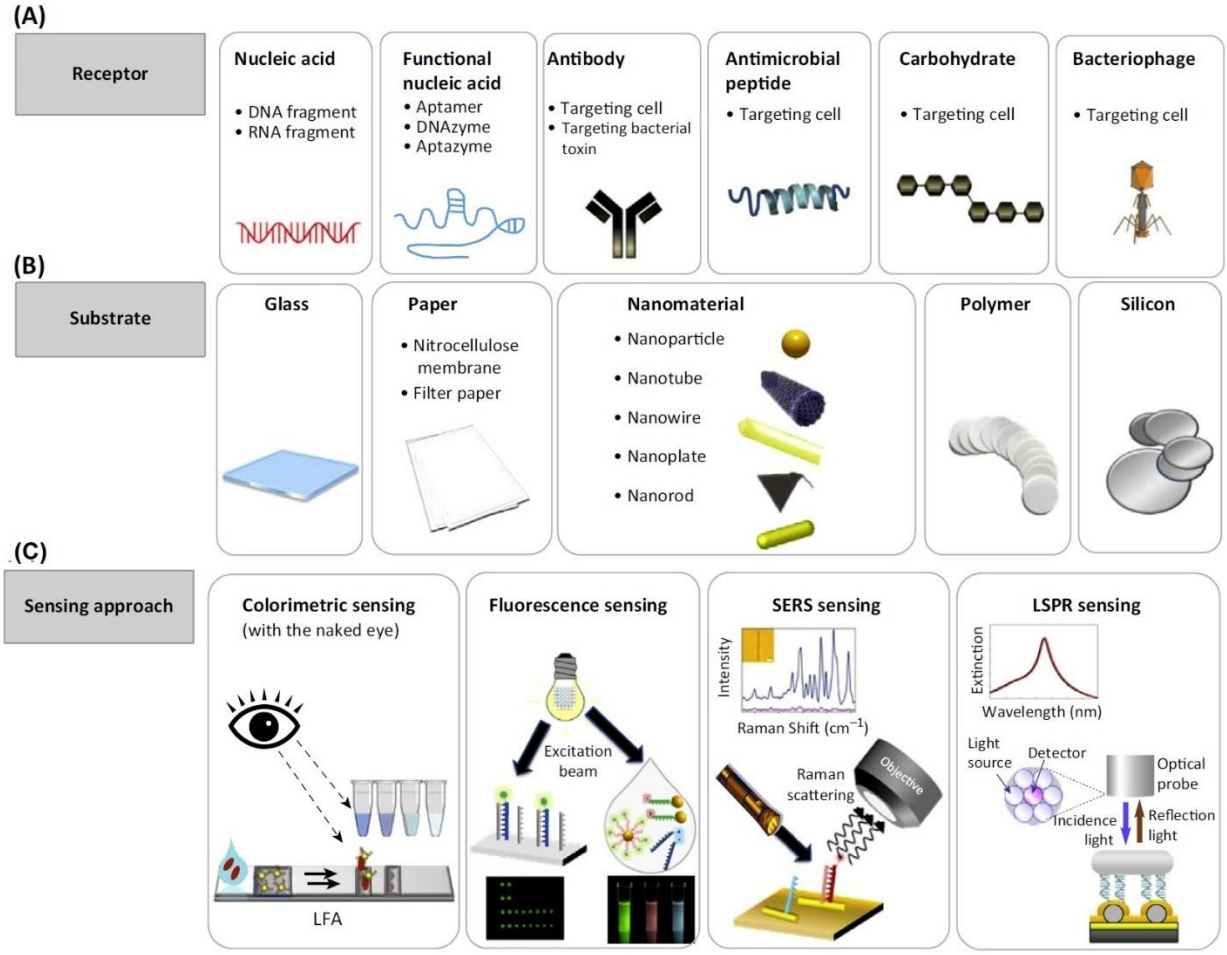

Figure 2-5. A schematic of optical sensing along with the representative components and techniques applied to a biosensor for the detection of pathogen: (A) various types of receptors, (B) the established substrates and (D) the sensing approaches [38].

2.2.2.1 Fluorescent-based detection

There has been a remarkable involvement of fluorescent materials in the design of biosensors as it has proven to be a versatile tool for a myriad of applications. Since the fluorescence technique is a non-invasive sensing technology, the biomolecules are not influenced or damaged during measurements or toxified by hazardous by-products. The fluorescent-based approaches can be measured by either the alteration in their fluorescent intensity or decay time while the last one is mostly used for in-vivo investigations [39, 40].

Fluorescent emission is followed by the absorption of light with enough energy. As a result, the fluorophore can be excited and proceeded with several phenomena. As illustrated in the Jablonski

diagram in Figure 2-6, the electronic states of fluorophore molecules can be divided into the singlet states and triplet states. In excited singlet states, all the electrons in the molecule orbits are spin paired. The electronic state of singlet ground, first, second is indicated by S0, S1, and S2, respectively. The transition between states is drawn as vertical lines to illustrate the instantaneous nature of light absorption. During the first absorption step, the molecule is excited from the ground to some higher vibrational level of either S1 or S2 (singlet). It then tends to release the excess of energy by fast relaxation to lower electronic states. This may be done through two possible ways, 1) a non-radiative method called the internal conversion (IC) process, which occurs within 10^{-12} s that generally completes prior to emission, 2) a radiative way by emitting light, i.e., a fluorescence process with lifetime about 10^{-8} s [39, 40]. When a molecule possesses a heavy atom, the emission of light from triplet excited states results in Phosphorescence in which the electron in the excited orbital has the same spin orientation as the ground-state electron [39, 40].

By returning the electron to the original ground state, a photon with lower energy will emit. On the other hand, the observed emission wavelength is usually longer than the absorbed light wavelength due to an energy cap, known as Stoke's shift. This energy cap should be large enough to prevent the interference of emission and absorbance spectra of fluorescent substances [39]

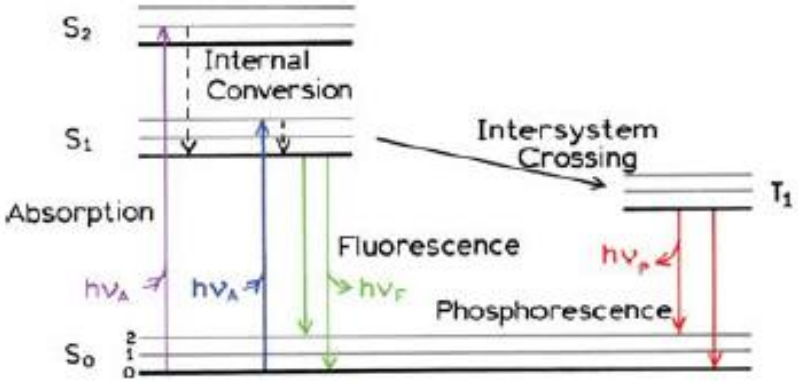

Figure 2-6. An illustration of Jablonski diagram which shows the fluorescent mechanism [39].

Various fluorophores with distinctive structures and features have been used in bioassay tools. They are mainly categorized as intrinsic or natural fluorophores and extrinsic fluorophores. Intrinsic fluorophores show natural fluorescent properties. The most dominant types are the proteins composed of aromatic amino acids groups such as tryptophan (Trp), tyrosine (Tyr) and phenylalanine (Phe). They absorb light near 280 nm with and emit spectra around 350 nm. Thus,

the presence of protein with these amino acids residues in the bacteria causes autofluorescence of bacteria [41]. Consequently, this phenomenon has been considered as a suitable method for rapid detection, identification, and differentiation of the various bacteria, including foodborne pathogenic bacteria [42, 43]. Through fluorescent spectroscopy the limit of detection for *E. coli*, *Salmonella* and *Campylobacter* were estimated 10^3 cells/mL [42]. Given the advantages, such as direct detection, low cost, sensitivity and time-saving, this method shows a high potential for rapid bacteria detection.

Extrinsic fluorophores are those linked to the other molecule (with or without spectral properties) to provide fluorescence. The extrinsic fluorophores can conjugate to sample via covalent or non-covalent bonding and are available in the various types of dyes, crystal quantum dots (made from heavy metal or carbon) and green fluorescent proteins [44].

The quantum yield (Q) and the lifetime of fluorescence are the most important features of fluorophores. The quantum yield is defined by the ratio of emitted photons from fluorescence to the absorbed photons. When the fluorophore has the larger quantum yields, it shows brighter photoluminescence. The lifetime is the average time that the fluorophore stays in the excited state before relaxing and returning to ground state. It determines the time that is available for the fluorophore to interact with its environment. Also, fluorescence lifetime indicates the time it takes for 69% of the population to emit. Typical fluorescence lifetime is around 10 ns [39].

The fluorescent intensity of a fluorophore can be reduced through various mechanisms which are known as quenching. One possible way is the deactivated of the excited state fluorophore by a contact with another molecule especially in solution, that is called collisional quenching. Also, quenching can occur at the ground state due to the formation of nonfluorescent complexes composed of a quencher and fluorophores [39].

2.2.2.1.1 Fluorescent resonance energy transfer

Besides, the autofluorescent molecules and direct detection of the molecule by fluorophores, some fluorescence-based bioassays employ Förster (fluorescence) resonance energy transfer (FRET). This mechanism is a non-radiative energy transfer from the initially photoexcited fluorophores (donors) to an acceptor molecule which can absorb the energy transfer. This phenomenon causes a reduction in the fluorescent intensity of the donor or even its quenching while the fluorescent intensity of acceptor increases if it is another fluorophore. The energy transfer would effectively

occur when the emission spectrum of a donor has maximum overlap with the absorbance spectra of the acceptor molecule. Moreover, the donor and acceptor molecules should be located close enough together, approximately between 10–100Å [45, 46].

Figure 2-7 shows a schematic of FRET phenomena and interaction between a donor and acceptor.

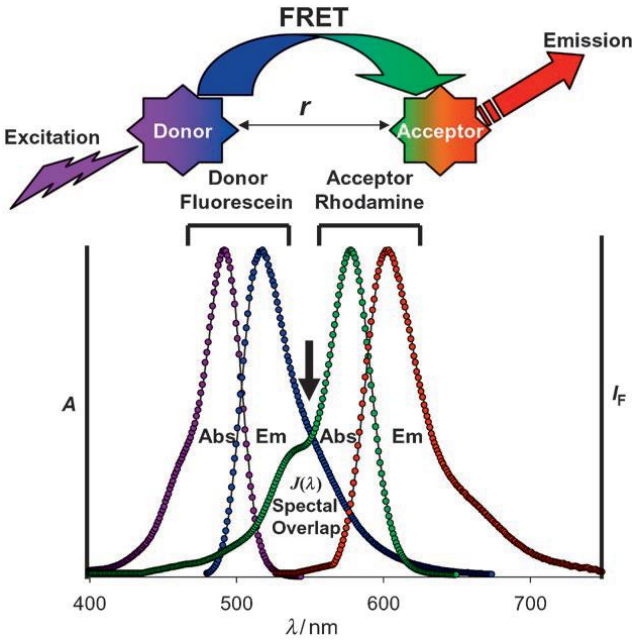

Figure 2-7. A schematic of FRET process and the overlap between the absorbance spectra of acceptor and emission spectra of donor [47].

The efficiency of the energy transfer is defined as the ratio of the photons absorbed by the donor to the parts that are transferred to the acceptor [48]. FRET efficiency for a single donor and acceptor pair in the defined distance is estimated by the following equation

$$E = \frac{R_0^6}{R_0^6 + r^6}$$

Whereas r is the distance between the donor and acceptor. R_0 is Förster distance where the FRET efficiency is 50% and it depends on donor-acceptor characteristics as illustrated in Figure 2-8.

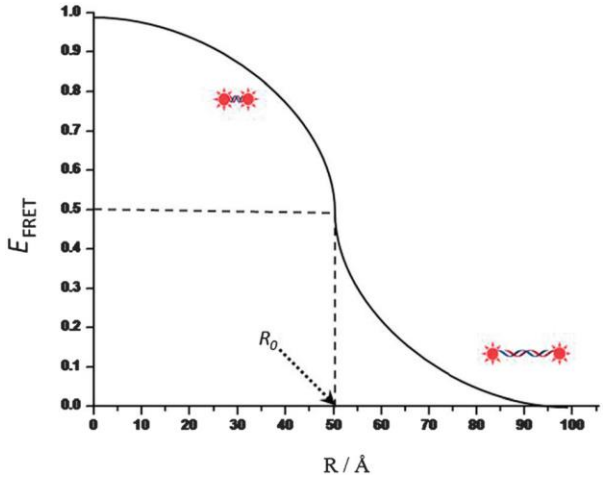

Figure 2-8. Demonstrating the dependence of FRET efficiency on the distance between donor and acceptor [48].

As the size of biomolecules is comparable with the Förster distance, FRET has widely used to measure the nanometer scale changes in the biomolecules either in-vitro or in-vivo. On the other hand, it has been introduced as a powerful technique to measure the distance changes between specific sites on macromolecules upon their conformational changes or moving domains in the proteins [39, 49].

Varieties of materials have been explored to develop high-efficient FRET structures. Generally, they can be classified into different categories: organic materials such as traditional dye fluorophores, dark quencher, and polymers; inorganic materials such as metal or semiconductor nanoparticles and fluorophores originated from biological components such as fluorescent proteins or amino acids [47]. According to the experimental design, these materials may serve as an acceptor or a donor or even both since a selected pair is compatible with FRET criteria.

Owing to the unique optical properties of semiconductor QDs and gold nanoparticles, these are a promising FRET pair according to their interaction [23, 50-56]. As such, their application in FRET-based bioassays has been extensively studied and are still the main focus of many researchers. The following parts will explain their properties and the proposed applications in bioassay systems.

2.3 Quantum Dots

2.3.1 Quantum dots properties

Quantum dots (QDs) are semiconductor nanocrystals composed of elements of groups II-VI, III-V and IV-VI of the periodic table. Typically, they have spherical or approximately ellipsoidal shape with a range size of 1-10 nm. Their optical and electronics features have made them distinctive over the usual fluorescent dyes. Those remarkable characters are: size-tuned and narrow emission spectra, broad absorbance spectrum, photostability, high resistance to photobleaching and chemical degradation as well as their high quantum yield in comparison with fluorescent dyes [44, 57, 58]. Figure 2-9 exhibits a schematic of core/shell quantum dot and the dependency of color and emission spectra of QD on the size of the nanocrystal.

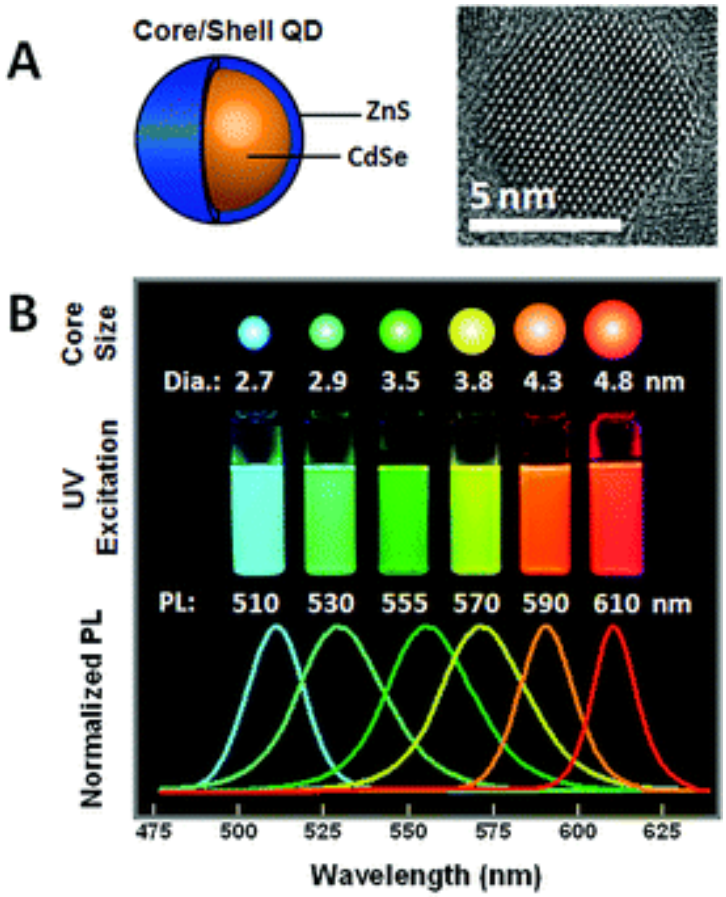

Figure 2-9. (A) a schematic and TEM image of a quantum dot composed of CdSe/ZnS core/shell, (B) the change in the emission spectra and color of CdSe/ZnS with increasing the nanocrystal size [57].

The most popular ones have the core of CdSe and CdTe which may cover with an inorganic shell layer such as ZnS to improve not only their luminescence properties but also protect them from oxidation. Due to the use of insoluble salts in the synthesis of QDs, they are usually insoluble in water. So, the decorated QDs with various types of biofunctional groups have improved their solubility and facilitated their conjugation to the desired biomolecules [58, 59]. Given these properties, QDs remain favorite candidate applied as biomarkers and the development of FRET-based bioassays.

2.3.2 Quantum dot applications in bioassay

The application of a quantum dot as the biomarker for monitoring foodborne pathogens such as *Salmonella Typhimurium* [60], *E. coli* [61, 62] and *Listeria monocytogenes* [63] or their toxin [64] has been widely investigated. Mainly, the pathogen is detected through forming a sandwich model which is established between the QD conjugated antibody/ pathogen/ and a secondary antibody conjugated to magnetic nanoparticles or immobilized on the surface of a membrane, as illustrated in Figure 2-10. The obtained fluorescent intensity of the separated and collected sandwich model corresponds linearly to the concentration of pathogen.

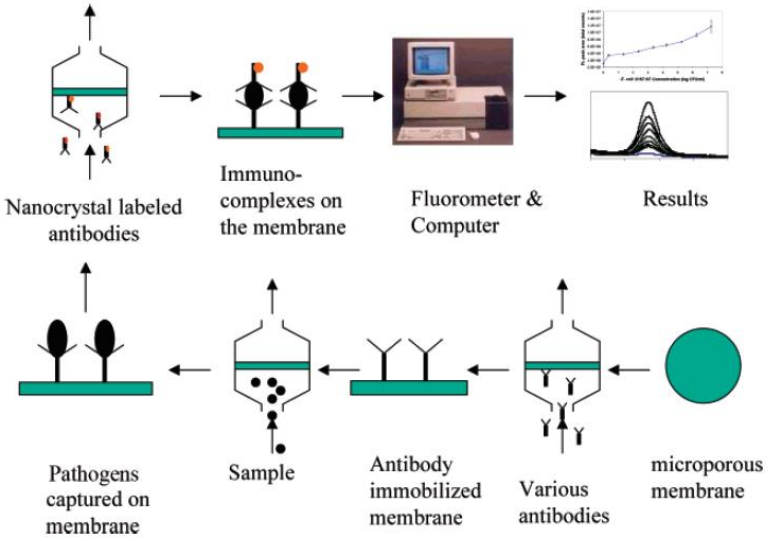

Figure 2-10. An illustration of the detection of bacteria through establishing a sandwich model. [62].

Aside from that, QDs have been assessed as a donor in various configurations for the development of FRET-based bioassays for the recognition of bacteria. For instance, in the proposed design by

Morales et al., the whole cell of *E. coli* was detected by energy transfer from the QD to graphene oxide (GO) acting as the acceptor [65]. This approach was introduced as "on and off state" method. In this case, the GO was added to the platform after capturing the bacteria using QD conjugated antibodies. In the presence of bacteria, the system was "on-state" because the distance between GO and QD was large enough to prevent the energy transfer. While in the absence of bacteria the system was "off-state" resulted from the interaction of GO through π-π stacking with the antibody, followed by the FRET occurrence and quenching of QD. Moreover, Duan and coworkers developed a simultaneous detection of two pathogenic bacteria, *Vibrio parahaemolyticus* and *Salmonella typhimurium*, by using green and red emitting QDs conjugated to their respective aptamers [66]. Their developed method relied on the competitive affinity binding between aptamer-carbon nanoparticles and aptamer-analyte. While the QDs didn't fluoresce in the presence of carbon nanoparticles as the result of affinity binding, their fluorescent light detected upon the addition of the target analyte. It was due to the attachment of QDs-aptamer to the target followed by dissociating from the carbon nanoparticles.

Moreover, QD acting as a donor may quench another QD of different size. Wang and coworkers have developed a FRET-based immunosensor for the detection of *Salmonella Enteritidis* on an eggshell by a pair of QDs with two different emitting photoluminescence [67]. The green and orange emitting QD were conjugated to anti-*S. Enteritidis* produced in rabbit and anti-rabbit antibody produced in goat. Similar to the previously described FRET, in the absence of bacteria, the antibodies were linked together through their affinity binding which allowed an efficient energy transfer from the green emitting QD (donor) to the orange one (acceptor). In the presence of bacteria (*S. Enteritidis)*, the green QD conjugated anti-*S. Enteritidis* was attached to bacteria due to its higher affinity and the increase in the photoluminescence of the green QD which successfully revealed the pathogen. FRET-based immunosensor have shown a high sensitivity to detect the analyte of interest.

2.4 Noble metal nanoparticles in bioassay

Noble metal nanoparticles especially gold and silver nanoparticles have been widely explored in the development of optical bioassay owing to the unique optical properties, biocompatibility, ease of modification and conjugation to a biomolecule, size-tunable synthesis and high surface ratio [56]. The optical properties of these nanoparticles strongly rely on the localized surface plasmon

resonance (LSPR), which is resulted by the collective oscillation of their conductive electrons when they are excited by electromagnetic wavelength larger than the metal nanostructure [68, 69]. The LSPR spectral position is extremely dependent on the particles size, the distance between the particles, dimension and also the reflective index of surrounding the environment [70]. As the primary consequence of LSPR feature, the nanoparticles have the potential to scatter and absorb light at a specific wavelength [71], which is the main reason of their use as the plasmonic nanoparticles for sensitive transducers. When nanoparticles undergo an alteration as the result of a change in one of the mentioned parameters, it would be revealed in their absorption band and plasmonic peak. Consequently, the accurate measurement of these changes would be directly recorded by UV-Vis spectroscopy. Figure 2-11 exhibits the dependency of absorbance spectrum and color of monodispersed silver and gold nanoparticles on the change of their size.

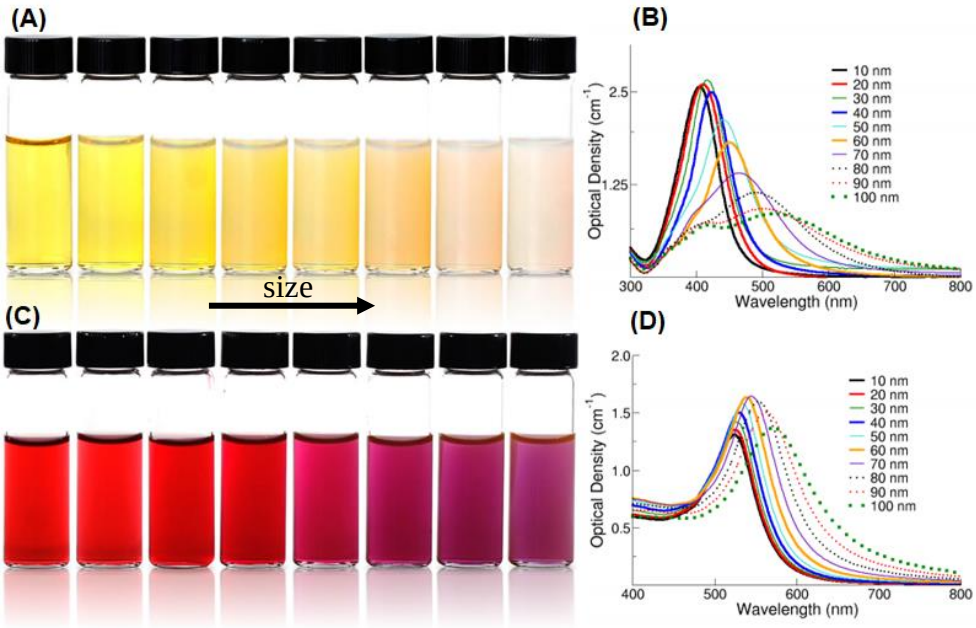

Figure 2-11. Colors change of various sized monodispersed (A) silver nanoparticles and (C) gold nanoparticles. (B) and (D) graphs show the respective UV-Vis spectra of dispersed silver and gold nanoparticles, respectively [72].

Additionally, LSPR enables metal nanoparticles to quench the photoexcited fluorophores which have a spectral overlap with them. Given to this feature, they are known as strong quenchers used in the FRET technique. Among the noble metal nanoparticles, gold nanostructures have drawn more attention due to the chemical stability and no-toxicity. Although silver nanoparticles show a

more intense plasmonic peak, its application is restricted in the bioassay because of its toxicity toward bacteria and fast oxidation in solution phase [73].

2.4.1 Gold nanoparticles as quencher

It is likely gold nanoparticle (AuNP) the most remarkable plasmonic nanoparticle which has been extensively used in FRET system as a quencher. There are some reasons attributed to its excellent quenching behavior. Firstly, gold nanoparticles generally adopt a spherical shape which causes no defined dipole moment in comparison with dye molecules. As a result, the energy transfer occurs in any direction for the donor molecule which is relative to the surface of gold nanoparticle [52]. Secondly, a broad absorbance spectra with a high cross-section near its plasmon resonance encourages an enhancement of energy transfer [49]. Finally, due to resonant oscillation of gold nanoparticles, the energy transfer efficiency is dependent on the (R^{-4}) in comparison with that of (R^{-6}) for the energy transfer to other types of acceptors [49].

Detailed studies have investigated the effect of size and shape of gold nanoparticles on the energy transfer. Accordingly, the dye molecule, Cy3 or Cy5 were attached to the surface of gold nanoparticles (with diameter from 1 to 30 nm) in the fixed distance (adjusted by the length of DNA or RNA) from 1 nm up to 100 nm [51, 74, 75]. It was shown that the gold nanoparticle was able to quench the excited donor located at the distance of around 40 nm which was quite longer than the FRET distance. Moreover, the size of AuNP affected the FRET efficiency where the increase in the size of gold nanoparticle caused the enhancement of the energy transfer.

The use of AuNP and QD as a pair of acceptor-donor in FRET configuration suggests tremendous advantages, such as the lower background signal, robust sensitivity, and ability of both to link with various biological groups [47]. Moreover, the broad absorbance spectra of AuNP has a large overlap with emission spectra of size-tunable QDs. Fundamental studies have also investigated the energy transfer of QDs to AuNP in a FRET system. As the results, the experimental observations have proved the increase of distance in energy transfer for QD-AuNP that was beyond the traditionally allowed distance in FRET [54]. Also, the energy transfer directly corresponded to the size of AuNP whereas the larger AuNPs absorbed a higher rate of energy transfer in comparison with smaller nanoparticles [76].

Aside from the fundamental studies, the pair of AuNP- QD has been widely explored in nanoscale biosensor technology using FRET. Although plenty of bioassays have been applied by this pair such as DNA hybridization [77, 78], protein detection [50, 79] and chemical targets [80-82], it has rarely been reported for bacteria and pathogen detection. This may attribute to the lack of understanding of the mechanism of energy transfer from QD to AuNP. In addition, their size compatibility with the size of a biomolecule such as antibodies may remain another issue, restricted their applications in this specific area of detection [83].

2.4.2 Gold nanoparticle in optical density

The following section reviews some optical bioassays which have exploited the metal nanoparticles as transducers, especially for pathogenic bacteria. In this case, various nanoscale structures of gold have been fabricated in different sizes and shapes such as gold nanoparticles, gold nanorods and gold nanowire. The varying morphologies and structures cause a tunable plasmonic and optical properties which are visible in the near-infrared region. Given these unique properties, the nanostructures of gold antibodies have been used to detect bacteria. For example, Wang and coworkers have developed multiplex pathogen detection method for *E. coli* O157: H7 and *S. Typhimurium*, by using gold nanorods with different aspect ratios [84]. The modified gold nanorods with amino groups were conjugated to the antibodies. Thus, the recognition of bacteria was monitored by the change in the plasmonic peak of the nanorods due to the aggregation of gold nanorods on the surface of pathogens. Through this approach, the limit of detection was estimated less than 10^2 CFU.mL^{-1} for each type of bacteria. According to this fact, the oval-shaped gold nanoparticles linked to antibodies has also been applied for the detection of *S. Typhimurium* [85]. By adding bacteria to the solution of nanoparticles-antibodies and the attachment of gold nanoparticles to the surface of bacteria, the color of solution for detection changed from pink to blue. In fact, the LSPR technique is provided a simple way of visual detection. So, taking advantage of aggregation and dissociation of metal nanoparticles due to its impact on the interparticle distance, it led to the development of a colorimetric assay. Figure 2-12 represents an example of the color change of anti-*E. coli* conjugated gold nanorods solution upon addition of *E. coli* bacteria which tuned from light to dark blue [86]. Owing to its simplicity, sensitivity and, low cost of synthesis this method has been improved for paper based-detection by lateral flow immunoassay [87] allowed to be used for in-situ analysis.

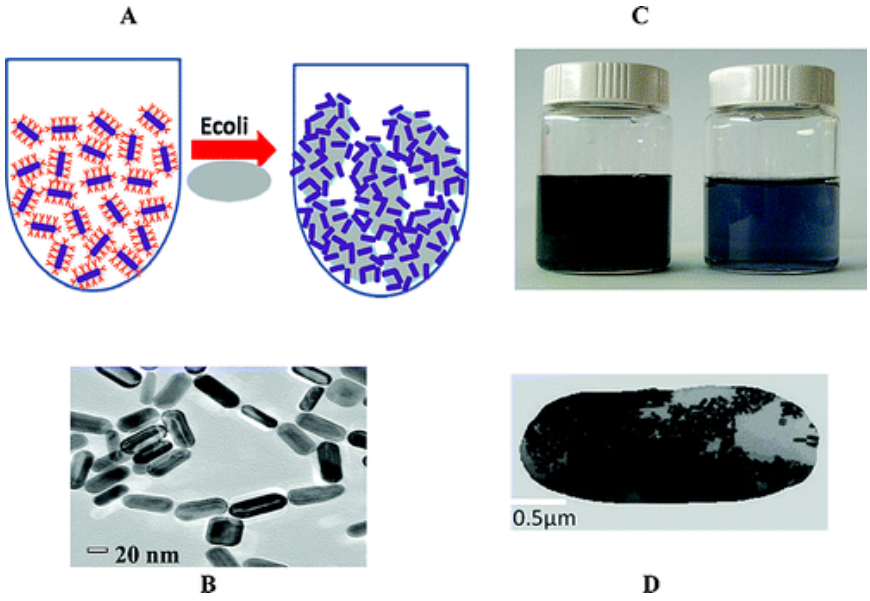

Figure 2-12. (A) a schematic of colorimetric detection of *E. coli* through anti- *E. coli* conjugated nanorods. (B) TEM image of anti- *E. coli* conjugated nanorods, (C) the color change of anti- *E. coli* conjugated nanorods upon addition of *E. coli* (10^4 CFU.mL^{-1}) and (D) TEM image showing the aggregation of gold nanorods on the surface bacteria [86].

Despite their extensive application in solution based-detection, there is a lack of appropriate building blocks to improve the plasmonic devices in a solid state [88]. To address this challenge, recently developed plasmonic nanopaper provided a novel optical sensing platform which will be discussed in details as below.

2.5 Solid-based FRET assay

Mostly, the developed FRET-based bioassays are a solution-based technique which are not generally applicable for food packaging. Besides, aggregation of nanoparticles and alteration of their photoluminescence remain another major challenge for the solution-phase bioassays. Recent efforts have investigated the design of a solid-phase bioassay to overcome the drawback of the traditional solution-phase FRET which allows for simple, fast and portable sensing tools. Generally, in the fabricated model, the fluorophore molecules as donors are immobilized on the surface of the solid substrate, and then the energy transfer is triggered by the interaction of the acceptor conjugated to a biomolecule [53, 89-91].

The functionalized glass is an attractive surface which has been investigated for the assembly of FRET bioassay. For example, Kim et al. investigated the multiplexed assay for proteases activity by AuNP and QD conjugated on a glass slide as nanoprobes. By employing this strategy, they could reduce background noise and photobleaching [53]. Moreover, a positively charged glass side was modified to carry graphene oxide (GO) sheets to be able to conjugate to antibodies. The fluorescent intensity of GO was reduced by the energy transfer mechanism when the analyte (microcystin) conjugated to AuNP was absorbed to the GO sheet [92]. Furthermore, a similar sandwich structure of GO and AuNP was arrayed on the surface of amino-functionalized glass for rotavirus detection [93].

Although the glass is an attractive surface in diagnostic devices, the strong groups of SiO_2 make it very stable against functionalization. In this case, some harsh chemical modifications are essential to achieve a proper immobilization of the biomolecule [94]. Also, lack of flexibility is another drawback of the glass substrate that makes it an undesired substrate for developing the novel bioassays.

2.5.1 Cellulosic-based substrate

There is an increasing interest in fabricating sensing platforms using cellulose-based substrates [95]. Among the renewable polymers, cellulose is known as the most abundant natural polymer which is the main component of plants structure. The molecular structure of cellulose is derived from a long chain of carbohydrate generated by repeating blocks of β-D-glucopyranose molecules that are covalently bound together by β(1→4)-glycosidic bonds [96] (see Figure 2-13). As such, obtaining wood pulp is one of the first and probably the most popular method used for the extraction of cellulose from plants prior to its transformation to cellulosic products such as paper. Although the paper has been used for over centuries for many purposes, its marvelous advantages (such as flexibility, compatibility, biodegradability, capillary action, and porous structure) have made it an attractive substrate for the development of advanced diagnostic devices. A well-reviewed article by Nery et al. has discussed the usage of the paper platform for the fabrication of various sensing approaches [97]. Interestingly, the developed sensitive and selective optical (colorimetric and fluorescent-based methods) and electrochemical (voltage, potential and conductivity-based methods) of different types of paper prove its revolutionary role as a substrate for the fabrication of solid-based diagnostic tools.

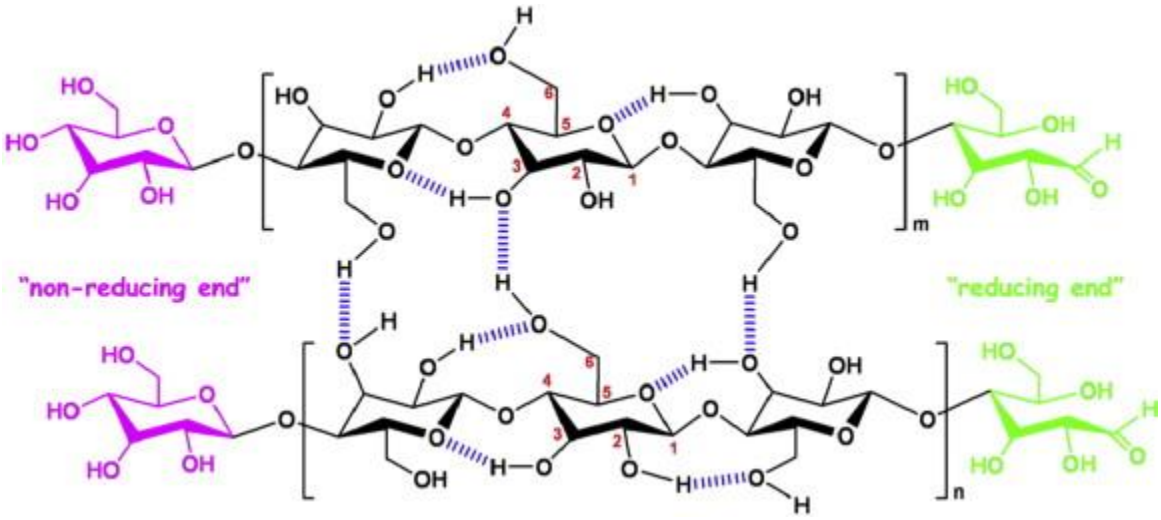

Figure 2-13. A schematic of the chemical structure of cellulose and effect of hydrogen bonds on its formation [98].

Given these reasons, few studies have explored the assembly of the FRET technique on the surface of the paper, mostly dedicated to nucleic acid hybridization [90, 91, 99]. Practically, the QDs and upconversion nanoparticles immobilized on the surface of the functionalized paper have served as a donor. Upon adding the targeted oligonucleotide labeled with the acceptor, the hybridization caused the occurrence of FRET. The researchers have claimed a rapid, sensitive and specify detection through the developed bioassays on the surface of the paper.

Although the traditional derivation of cellulosic material such as paper has its place in this field of science, it cannot meet all the demands of modern technology especially in the fabrication of a new generation of cellulosic nanocomposites. Ongoing investigations for extraction of cellulose in the form of a nanoscale structure have led to improve the deficiency of the traditional one [100]. As regarding the preparation and extraction methods, various forms of nanocellulose (NC) are induced such as cellulose nanocrystals (CNCs), nanofibrillated cellulose (NFCs) and bacterial cellulose (BCs) [101]. While CNCs and NFCs result from plants (e.g., wood pulp), BC is produced during the growth of particular bacteria (known as *Acetobacter xylinum*) under controlled culture conditions [101]. The resulted physical shape and size of nanocellulose are defined according to the source and isolation process, as observed in Figure 2-14. For example, while the lengths of NFC and CNC are less than 50 nm, the ones of BC are around micrometer [101]. Besides, the degree of cellulose purity in the presented forms have been directly affected by the way it is

produced. Thus, it has been shown that BC owns a higher degree of cellulose purity due to direct synthesis in the lignin free medium.

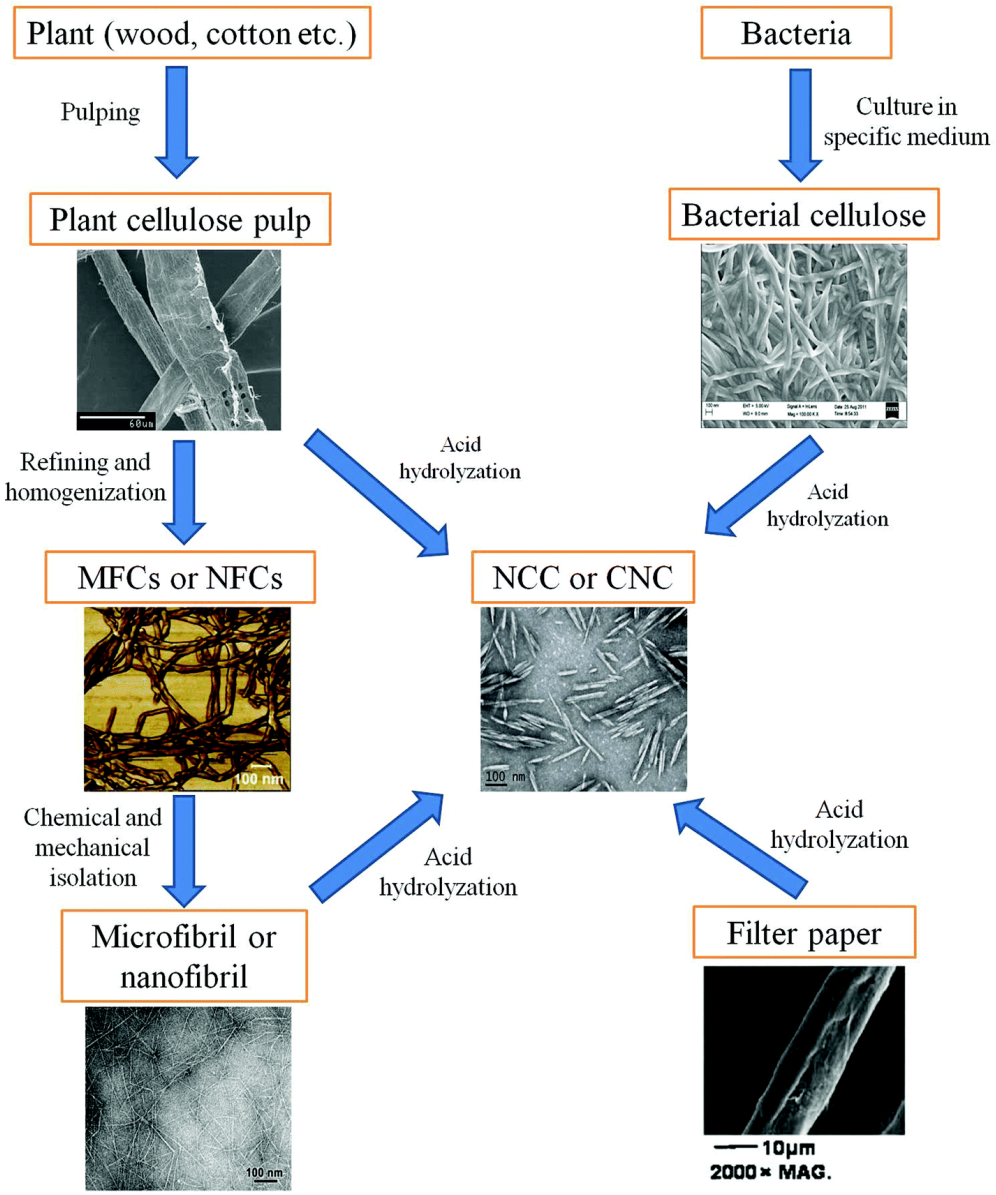

Figure 2-14. The presented figures show the differences in the structure of various nanocelluloses [101].

Recently, modified nanocellulose in various forms such as paper, hydrogel, or nanoparticles has been widely considered in the field of bioengineering, medicine, electronic devices application, etc. [98, 102, 103]. The paper obtained from NC especially BC, called nanopaper or cellulose nanopaper, displays high optical transparency due to the nanosized diameter of its fibrils and the

nano-space between the fibrils network which is less than the visible light wavelength [104]. Additionally, owing to its nano-shaped structure, renewability, sustainability, high surface area, high porosity, ease of chemical modification, incredible mechanical strength (high tensile strength and stiffness, high Young's modulus) [105], it has acquired plenty of attention for developing sensing and diagnostic tools [95].

Interestingly, however, different forms of NC don't inherently possess conductive properties, it has been implemented in the fabrication of electrical sensing techniques. As such, its modification through various types of conductive agents such as carbon-based materials (e.g., carbon nanotubes and graphene) [106], gold and silver nanoparticles [107] and conductive polymers [108] has led to advance the hybrid nanopaper with electrical properties. Therefore, these multifunctional features of nanopaper caused its employment to produce new composites with the characteristics dislike the native one.

Additionally, the optical transparency of nanopaper is considered to be another notable feature, resulting in the development of innovative optical nanocellulosic transducers. Successfully, this was advanced by inducing noble metal nanoparticles, organic/inorganic dye, and fluorescent materials within nanopaper through in-situ synthesis or covalent crosslinking [109-113]. For example, the in-situ synthesized Au, and Ag nanoparticles within NC was investigated in SERS method (Surface-Enhanced Raman scattering) which is a sensitive and selective tool for biochemical detections [109-111]. In this method, the molecules are absorbed to the interstice between the adjacent metal nanoparticles (known as the hot-spot), it leads to the enhancement of Raman spectra due to the electromagnetic field resulting from the SPR of metal nanoparticles. As explained before, SPR is dependent on size, shape and interparticle distances; therefore, they can affect the enhancement of Raman spectra. On the other hand, their fixation or immobilization on the porous and flexible substrate can increase the number of hot spots [114]. Consequently, the use of NCs as a nano-based platform with such unique features have improved the SERS as a detection tool.

Recently, researchers have explored the BCs integration to noble metal and photoluminescent nanoparticles as highly sensitive composite nanopapers for colorimetric detection [112, 113]. Interestingly, the AgNPs were embedded within BC through a green synthesis mechanism in which

the abundant hydroxyl groups of BC served as a reducing and stabilizing agent. Besides, the nanostructural network of BC was exploited for the synthesis of AuNP, reduced and stabilized by

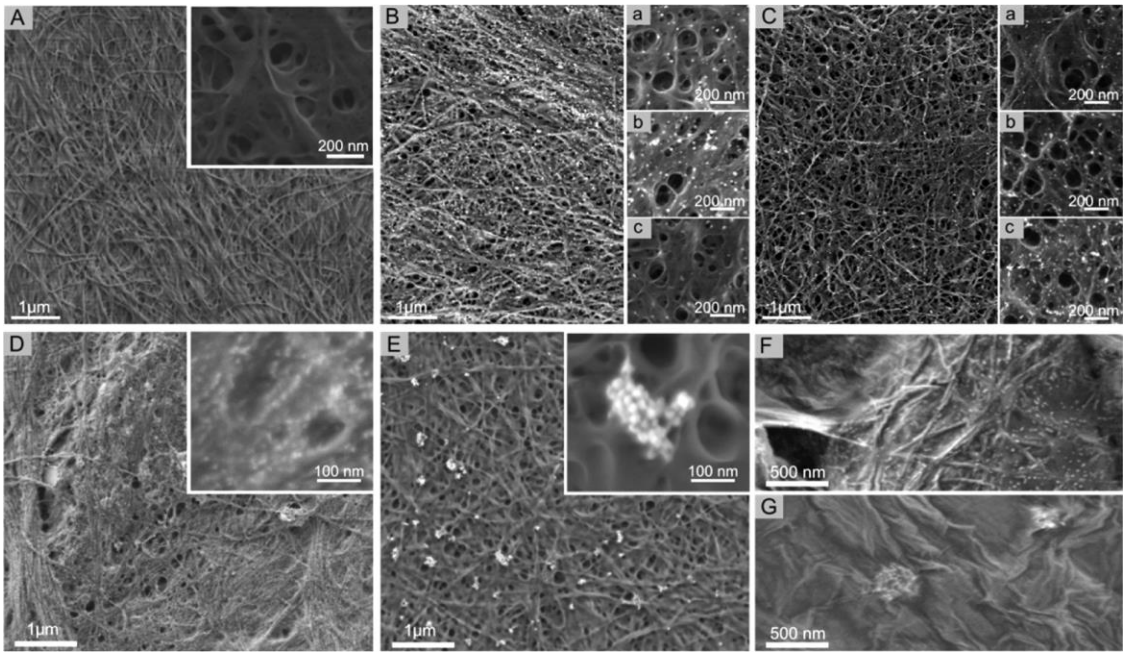

Figure 2-15. SEM of the composit nanopapers (A) bare bacterial cellulose nanopaper. (B) AgNP-BC: (B-a) AgNPs synthesized in-situ BC (B-b,c) AgNP-BC in the presence of 10 µg mL^{-1} of methimazole and 4 µg mL^{-1} of iodide, respectively (C) SEM of AuNP-BC: (C-a) AuNP-BC; (C-b, c) AuNP-BC in the presence of 8 µg mL^{-1} of thiourea and 4 µgmL^{-1} of cyanide, respectively. (D) SEM of QDs embedded within bacterial cellulose nanopaper. (E) SEM of UCNP-BC. (F) Graphene oxide-coated QD-BC. (G) Graphene oxide-coated UCNP-BC [112].

chemical agents like PEI. QDs and upconversion nanoparticles were also immobilized through amine-carboxyl groups reaction. Prior to crosslinking, the carboxyl groups were created on the surface of BC nanofibrils by TEMPO oxidation (see Figure 2-15). Besides, the researchers have noticed that the plasmonic or fluorescent properties of embedded nanoparticles could modulate upon the addition of some analytes. Accounting to this fact, they could detect the chemicals such as 2-mercaptobenzothiazole (MBT), cyanide, iodide, thiourea, methimazole in solution by using the developed composite nanopaper (see Figure 2-15B and C). For instance, they have observed the change in the color of AgNP-BC platform from dark amber to a light amber upon the addition of cyanide due to the etching of silver nanoparticles. Also, the aggregation of AgNP caused the increase in the intensity of AgNP-BC color since it interacted with MBT solution. Although the

change in the color intensity of AgNP-BC was visually detectable, the small changes were also revealed through the slight change in the plasmonic peak in UV-vis absorbance spectra of the nanoplasmonic platform [113].

2.6 Volatile organic compounds and detection of fish and meat spoilage

The focus of the pervious sections was mainly dedicated to the detection of bacteria through its whole cell. Recently, the waste products of bacteria such as volatile organic compounds (VOCs), the reason of characteristic odors, have been considered to recognize specific species of microorganism and bacteria [115-117]. For example, 2-aminoacetophenone, a grape like odor, synthesized by *P. aeruginosa* in the culture medium can be used for detection of this bacteria [118]. Likewise, *E. coli* is recognizable by its odor due to the presence of indole known as a marker VOC for identification of this type of bacteria [119]. Generated profile from the combination of VOCs can provide a fingerprint, specified for each type of bacterium. Table 2-1 presents the various VOCs produced by different bacteria. Approaches such as secondary electrospray ionization mass spectrometry (SESI-MS) and gas chromatography coupled with mass spectrometry (GC-MS) have been applied for fast and selective analysis of VOCs in the headspace of cultured bacteria [115, 120].

Table 2-1. Identified compounds from *P. aeruginosa*, *S. aureus*, *E. coli*, and *S. Typhimurium* through SEMSI-MS [115]

	Relative signal intensity [b]			
	P. aeruginosa	*S. aureus*	*E. coli*	*S.* Typhimurium
Acetonitrile	+	+	+	++
Ethanol	+++	++	++	+
Butanol	-	+++	-	++
Acetone	++	+++	-	++
Acetic acid	++	+++	-	+++
Ethylene glycol	++	+	-	++
Isopentanol	-	++	-	++
Pyrimidine	-	+	-	++
2-Pentanone	+	++	-	++
4-Methylphenol	+++	+	-	+++
Indole	++	-	+++	++

2-Aminoacetophenone	+	-	-	-
2-Nonanone	-	+	-	++

[b] +++, 25% to 100%; ++, 5% to 25%; +, 1% to 5%; -, below the 1% threshold.

Given the complexity of detection through these methods, sensors such as colorimetric sensor array have been developed for detection and identification of VOCs [121, 122]. The array was composed of chemo-responsive dyes, leads to create a distinctive color pattern by exposing to VOC. Considering this fact, Janzen et al. have reported a discrimination of 100 VOCs [121]. Similarly, Carey and coworkers have implemented the colorimetric sensor array for rapid identification of 10 strains of bacteria. As the consequent, they have found 10 distinct colorimetric patterns assigned to each strain of bacteria with 98% accuracy within 10 h [122].

Furthermore, monitoring of changes in the quality of meat and fish is facilitated by recording the alteration in the produced VOCs. Microbial spoilage of meat and fish is a complex event which is recognizable by the change in the odor and physical appearance of the food product. In particular, the spoilage process derived from the microbial growth and consumption of proteinic substrate by bacteria generates the characteristic profile of VOCs. For instance, amine-based components such as trimethylamine (TMA), dimethylamine (DMA), ammonia, histamine, putrescine (Put), cadaverine (Cad), short-chain carbonyls, acids, sulfur compounds, N-cyclic compounds and unsaturated aldehydes have been considered for monitoring the spoilage of fish and meat [123-125]. However, the produced VOCs may be varied in the different environments and storage conditions due to its dependency on the growth of bacteria [126]. Table 2-2 compares the type of bacteria that may grow in raw meat stored in the various conditions.

Table 2-2. Strains of bacteria are commonly found in the raw meat stored in different conditions, vacuum packaging (VP) and modified atmosphere packaging (MAP) [126].

Gram-positive	Storage conditions			Gram-negative	Storage conditions		
	Air	MAP	VP		Air	MAP	VP
Bacillus	+		+	*Achromobacter*	+		
Brochothrix	+	+	+	*Acinetobacter*	+	+	+
Carnobacterium	+	+	+	*Aeromonas*	+		+
Corynebactenum	+			*Alcaligenes*	+	+	+
Clostridium			+	*Alteromonas*	+	+	+
Enterococcus	+	+		*Campylobacter*	+		

Kocuria	+			*Chromobacterium*	+			
Kurthia	+			*Citrobacter*	+	+		
Lactobacillus	+	+	+	*Enterobacter*	+	+		
Lactococcus	+			*Escherichia*	+			
Leuconostoc	+	+	+	*Flavobacterium*	+			
Listeria	+	+		*Hafnia*	+	+	+	
Microbacterium	+	+	+	*Klebsiella*	+			
Micrococcus	+	+		*Kluyvera*	+			
Paenibacillus	+			*Moraxella*	+			
Staphylococcus	+	+	+	*Pantoea*	+		+	
Streptococcus	+	+		*Proteus*	+	+		
Weissella	+	+	+	*Providencia*	+	+	+	
				Pseudomonas	+	+	+	
				Serratia	+	+	+	
				Shewanella	+			
				Vibrio	+			
				Yersinia	+		+	
				Moraxella	+			

Given the sensitivity of colorimetric sensor array, it has also been reported for the detection of fish spoilage by Morsy and coworkers [127]. This array has successfully revealed a distinctive color pattern due to the spoilage of fish in various stored conditions (24 h at room temperature and 9 days at 4°C). Similarly, the freshness of fish has been monitored through the colorimetric sensor array [128]. Therefore, such colorimetric methods are attracted plenty of researchers' attention due to the ease of use, its integration into the food packaging and sensitivity.

2.7 Problem identification

This review has focused on illustrating the most convenient type of biosensors which are user-friendly, sensitive and selective for detecting microorganisms, either their whole cell or their by-products. Nevertheless, most of them don't meet the necessary demands to be applicable in the food packaging industry because of their solution-based functionality, needing a secondary biomarker to accomplish the recognition procedures and complexity in detecting devices to read the signal. Besides, the aggregation of nanoparticles including their stability and propensity to nonspecific binding may remain as other challenges that should be comprehensively addressed.

In order to develop an approach for the fabrication of biosensors applicable in the food packaging, we have to consider some criteria. Firstly, it should be user-friendly for consumers. As such, optical-based biosensors, especially those that are fluorescent and colorimetric, can be introduce as a favorite candidate that is visually detectable in most of the cases. Also, thanks to the advancement in smartphone technology to provide the optical detection system by supporting the appropriate apps. Secondly, the detection system should proceed directly after the capture of the analyte that makes a biosensor suitable for smart packaging. Taking into account the shapes and structure of the nanoparticles as well as a conformational change of the biomolecule upon interacting with the analyte, their forthcoming integration by appropriate design can allow straightforward solutions. Thirdly, solid-based detection transpires the need not only for the applicability in the food packaging but also overcoming the aggregation of nanoparticles. However, paper-based biosensors have offered myriad properties but the recently developed nanopapers, composed of nanocellulose, have surpassed and excelled the structure and optical properties of traditional paper. The nanopaper-based biosensor is the latest technology which has not yet been fully studied. It is envisaged that such a biosensor would open windows for excellent and efficient opportunities in smart packaging.

CHAPTER 3 OBJECTIVES AND ORGANIZATION OF THE ARTICLES

The biosensor is a promising tool to overcome the environmental and economical problems resulted from outbreak of the foodborne infection. According to the literature review presented in Chapter 2, various biosensors have been developed for the bacteria detection and food spoilage. Nevertheless, there is a large gap between the advanced ones and those of one are practical in the food packaging. On the other hand, in-situ and user-friendly detection are among those limitations for biosensors that should be taken into attention to achieve a straightforward approach in the field of packaging. Thus, it is needed to design a proper structure with considering all effective parameters.

3.1 Objectives

3.1.1 General objective

The main objective of this research is:

To Develop a Sustainable Solid-Based Sensor for Bacteria and Gas Detection applicable in food packaging

3.1.2 Specific objectives

To conduct the main objective, the specific objectives were defined as follow:

1. To design a solid-based substrate which supports the receptor and transducer,
2. To fabricate an optical-based platform to detect some degradation by-products such as ammonia,
3. To develop the solid-based biosensor for direct detection of bacteria through fluorescent-based approach.

3.2 Organization of Articles

This section is dedicated to the scientific contribution of this thesis in the form of three original articles.

The first part of the study presented in chapter 4 involves the synthesis of plasmonic nanopaper and its implementation for ammonia vapor detection. The article is entitled “Modulation of population density and size of silver nanoparticles embedded in bacterial cellulose via ammonia exposure: visual detection of volatile compounds in a piece of plasmonic nanopaper.” In this paper, we investigated a colorimetric detection of ammonia vapor by relying on plasmonic properties of silver nanoparticles. To take advantages of plasmonic properties of silver nanoparticles in the solid state, it was successfully synthesized in-situ of bacterial cellulose. The bacterial cellulose due to its transparency with nanofibrous structure was served as the promising platform. The sensitivity of as-synthesized plasmonic nanopaper was examined in the exposure of various concentrations of ammonia vapor. Considering this fact that ammonia is one of the major components of meat and fish spoilage due to the bacterial growth, this novel assay was explored for the detection of spoilage. To the best of our knowledge, no report has studied such a technique for vapor detection. This paper has been published in “Nanoscale, 2016, Vol. 8”.

The second article in chapter 5 entitled “Nanopaper-based platform applicable in solid-state based FRET technique” studied another aspect of the plasmonic nanopaper for optical biosensing technology, specifically fluorescent based-technique. Here, gold nanoparticles were integrated into the bacterial cellulose by in-situ synthesis. By comparing the bacterial celluloses decorated with various population density of gold nanoparticles, we illustrated the potential of these platform in quenching photoexcited fluorophores. This work established the foundation for our third and last paper which is the application of such a hybrid plasmonic platform in the development of the FERT-based technique for pathogen detection. This article has been submitted to the journal of “Biochimica et Biophysica Acta (BBA) - General Subjects.”

Having generated the solid platform with appropriate characteristics for assembly of biomolecules as well as AuNP for FRET technique, we can finally test our hypothesis that the whole cell of bacteria can be detected directly through FRET technique. This work is a proof-of-concept of straightforward detection of bacteria by considering the conformational change of antibody structure after the interaction. In order to obtain a high-throughout immunosensor, some important

parameters were explored that might have an impact on its functionality. The original paper entitled "Toward a nanopaper-based and solid phase immunoassay using FRET for rapid detection of bacteria" has been submitted to the journal of "Biosensors & Bioelectronics."

CHAPTER 4 ARTICLE 1: MODULATION OF POPULATION DENSITY AND SIZE OF SILVER NANOPARTICLES EMBEDDED IN BACTERIAL CELLULOSE VIA AMMONIA EXPOSURE: VISUAL DETECTION OF VOLATILE COMPOUNDS IN A PIECE OF PLASMONIC NANOPAPER

B. Heli [ab], **E. Morales-Narváez** [a], **H. Golmohammadi** [c], **A. Ajji** *[b] **and A. Merkoçi** *[d]

[a]*Catalan Institute of Nanoscience and Nanotechnology (ICN2), CSIC and The Barcelona Institute of Science and Technology, Campus UAB, Bellaterra, Barcelona 08193, Spain*

[b]*3SPack, CREPEC, Département de génie chimique, Polytechnique Montréal, Montréal, Québec, Canada*

[c]*ACECR-Production Technology Research Institute, Ahvaz, 6139684689, Iran*

[d]*ICREA – Catalan Institution for Research and Advanced Studies, Barcelona, 08010, Spain.*

***Published in: NANOSCALE,* 2016, Vol. 8, Page 7984–7991**

DOI: 10.1039/c6nr00537c

4.1 Abstract

The localized surface plasmon resonance exhibited by noble metal nanoparticles can be sensitively tuned by varying their size and interparticle distances. We report that corrosive vapor (ammonia) exposure dramatically reduces the population density of silver nanoparticles (AgNPs) embedded within bacterial cellulose, leading to a larger distance between the remaining nanoparticles and a decrease in the UV-Vis absorbance associated with the AgNP plasmonic properties. We also found that the size distribution of AgNPs embedded in bacterial cellulose undergoes a reduction in the presence of volatile compounds released during food spoilage, modulating the studied nanoplasmonic properties. In fact, such a plasmonic nanopaper exhibits a change in color from amber to light amber upon the explored corrosive vapor exposure and from amber to a grey or taupe color upon fish or meat spoilage exposure. These phenomena are proposed as a simple visual detection of volatile compounds in a flexible, transparent, permeable and stable single-use nanoplasmonic membrane, which opens the way to innovative approaches and capabilities in gas sensing and smart packaging.

4.2 Introduction

Nanomaterials display outstanding and high-powered phenomena that are not present in bulk materials [1], such as localized surface plasmon resonance in noble metal nanoparticles (NPs) [2], where incident light triggers collective motion of their electrons, amplifying the local electromagnetic field. Noble metal NPs are stable, easy to synthesize and, unlike photoluminescent NPs, endowed with a relatively endless amount of photons for sensing applications over long time periods, which can even be visually detected [3-6]. Given these extraordinary behaviors, nanosensing technology is capitalizing on analyte-nanoparticle interactions that modulate the size, shape, composition, and interparticle distance of the NPs, the dielectric properties or the refractive index of the surrounding medium to engineer advantageous nanoplasmonic sensing systems [3,7-10].

Recently, we have proposed bacterial cellulose nanopaper decorated with optically active nanoparticles, including plasmonic NPs and photoluminescent NPs, as a novel sensing platform targeting analytes in the liquid phase [11]. On the other hand, plasmonic NPs have generally been exploited to detect analytes in the liquid phase [3]. However, the detection of biologically relevant analytes in the gas phase using simple platforms based on plasmonic NPs is scarcely explored. For

example, in early 2016, a search on Web of Science using the formula topic: ((localized surface plasmon resonance) and (gas detection)), produces results pointing to less than 50 articles, none of which are related to visual detection.

Some gaseous analytes, particularly volatile compounds are often associated with environmental pollution, hazardous chemicals and potential biomarkers [12-15]. Furthermore, these agents can also be found as a by-product of bacteria and food spoilage or even in the headspace of cancer cells and blood samples [16-18]. Therefore, the detection of volatile compounds is a paramount research field and related technologies remain under development. On the one hand, emerging approaches intended for volatile compound sensing are expected to be simple, safe, low-power, stable, inexpensive and easy-to-use. On the other hand, commercially available paper tests offer fast and sensitive detection strips to measure dangerous gases in the air. However, they are often hazardous items themselves and/or require a moistening step or external reagents [19,20]. Here, we demonstrate a simple-to-use plasmonic nanopaper designed as a hybrid material based on silver nanoparticles embedded in bacterial cellulose that is amenable to the detection of analytes in the gas phase with no extra reagents. In particular, we discovered that corrosive vapor (ammonia) exposure dramatically reduces the population density or size distribution of silver nanoparticles (AgNPs) embedded within the studied nanoplasmonic membrane, leading to a modulation of the UV-Vis absorbance corresponding to the explored nanoplasmonic properties, which can even be determined visually. Scheme 6-1 conveys the proposed sensing principle and depicts the overall set-up utilized throughout this research, which represents a straightforward way to follow plasmonic nanopaper interaction with gases.

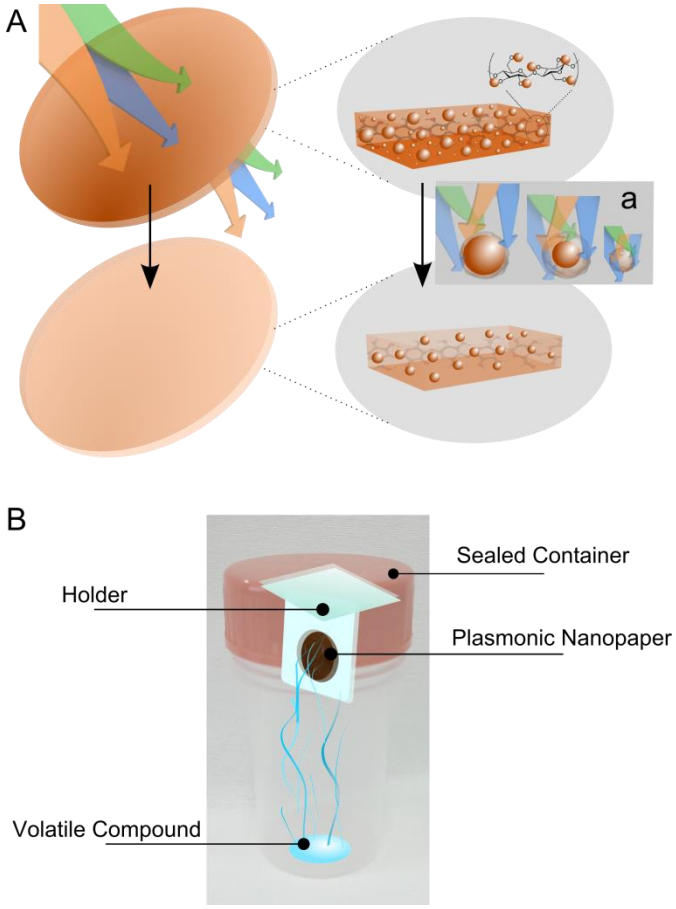

Scheme 1. A. Schematic representation of the nanoplasmonic membrane upon volatile compound exposure. Corrosive vapor (ammonia) triggers etching of the nanoparticles embedded within the studied nanoplasmonic membrane (a). Therefore, the population density of the AgNPs falls and the interparticle distance increases, and/or the size distribution undergoes a dramatic change, changing the color of the plasmonic nanopaper. B. Schematic representation of the set-up utilized throughout this research. A sealed container with a capacity of 50 mL is used. A piece of plasmonic nanopaper is attached underneath the container lid and vertically aligned through a holder being exposed to a volatile compound, which was previously introduced.

4.3 Experimental

4.3.1 Reagents and equipments

The commercial reagents were handled according to the material safety data sheets suggested by the suppliers. Bacterial cellulose nanopaper was kindly provided free of charge by Nanonovin Polymer Co. (Mazandaran, Iran). Ammonia (30%), methanol (99.9%), ethanol (99.8%), propanol (99.8%), acetic

acid (100%), ethyl acetate (99%), acetonitrile (99.8%), acetone (99.5%), and toluene (99.8%) were purchased from Panreac AppliChem (Castellar del Vallès, Barcelona, Spain). NaOH, $AgNO_3$, indole (99%), trimethylamine (99.5%) and microwell plates were acquired from Sigma-Aldrich (Taufkirchen, Germany). The thickness of bare bacterial cellulose (BC) and the nanoplasmonic membrane was respectively measured using a digital calliper (Alfa Mirage Co. Ltd, Osaka, Japan) and reported as an average of 10 different points in various pieces of paper. Particle size distributions and population density were estimated using ImageJ 1.48v (Wayne Rasband, National Institutes of Health, USA). UV-Vis absorbance spectra were recorded using a SpectraMax M2e spectrophotometer (Molecular Devices, California, USA). SEM imaging was performed using a Magellan 400L SEM High-Resolution SEM (FEI, Oregon, USA). TEM imaging was carried out using a FEI Tecnai F20 S/TEM (Oregon, USA). Nanopaper samples were prepared using a Precision Ion Polishing System, Model 691 with camera, (GATAN, California, USA) before the TEM analysis. Raman spectroscopy was performed using a Renishaw Invia Raman Microscope System (Gloucestershire, UK). The error bars in the figures represent the standard deviation of three parallel experiments. The box plots in Figure 4-1 and Figure 4-4 show the median, 25th and 75th percentiles and the extreme values of the respective size distributions (5–95 percentile). All of the experiments were carried out using the experimental set-up described in eme 1B.

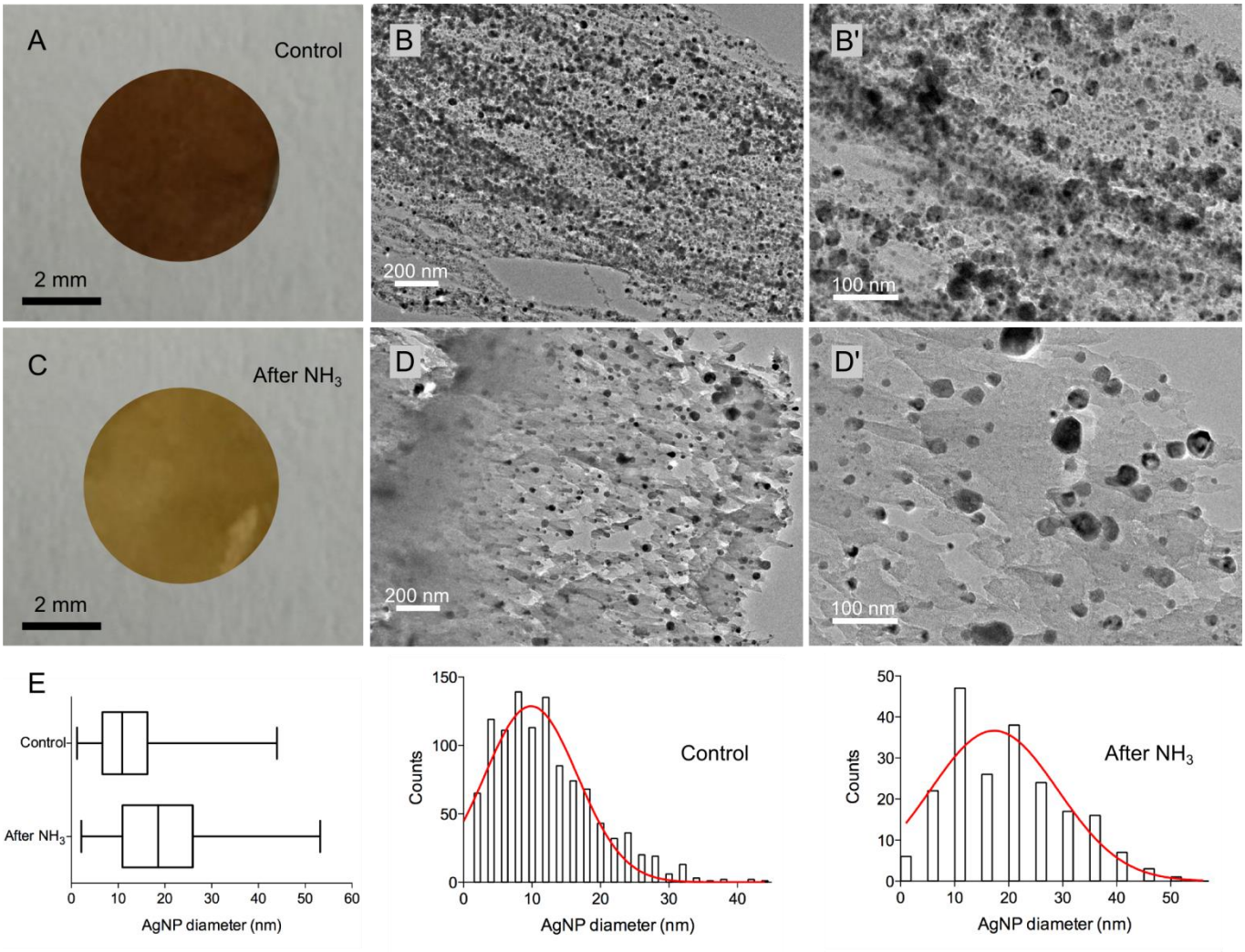

Figure 4-1. Modulation of the population density of AgNPs embedded in bacterial cellulose *via* corrosive vapor (ammonia) exposure. Appearance of AgNP-BC without ammonia vapor exposure (A) and after ammonia vapour exposure (C). TEM micrographs of AgNP-BC without ammonia vapour exposure (B and B′) and after ammonia vapour exposure (D and D′). Estimation of the size distribution of the studied AgNPs (E) without ammonia vapour exposure (control) and after ammonia vapour exposure. The box plots show the median, 25th and 75th percentiles and the extreme values of the respective size distributions (5–95 percentile).

4.3.2 Synthesis of plasmonic nanopaper

Silver nanoparticles were synthesized *in situ* within bacterial cellulose following previous procedures [11,21]. Particularly, 15 pieces of wet bacterial cellulose (2 × 2.5 × 0.3 cm) were soaked in 50 ml of milli-Q water at pH 12 adjusted using 2 M NaOH. Then, the mixture was kept under heating and stirring to reach 65 °C. At this time, 5 ml of a fresh solution of 0.1% $AgNO_3$(v/w) was added to the mixture dropwise. During vigorous stirring at 65 °C, silver ions diffused into the fibril network of the cellulose and gradually converted to silver nanoparticles. After 2 h, silver nanoparticle formation was confirmed by the color change of the colorless bacterial cellulose to amber. Then the heating process was stopped and the mixture was cooled down to room temperature. Bacterial cellulose pieces containing *in situ* synthesized AgNPs (plasmonic nanopaper pieces) were separated from the mixture and completely washed through the squeezing of BC and redispersing in milli-Q water. This step was repeated 3 times to remove all of the unreacted silver ions and free silver nanoparticles from the cellulose fibrils. The nanoplasmonic membranes were dried at room temperature while they were kept between filter paper and glass slides to prevent any twisting and tearing. The original thickness of bare BC was not dramatically affected after the synthesis of AgNPs embedded within the BC as the thickness of the dried nanoplasmonic and BC membranes were estimated to be 16 ± 1.7 and 16 ± 2.5 μm, respectively. Once it is dried, the composite can be stored in the dark at room temperature for more than 6 months. Following the described procedure systematically, we observed that the synthesis of the nanoplasmonic membrane can be reproduced with a similar absorbance spectrum and nanoparticle population.

4.3.3 Preparation of the gas sensing set-up

Volatile compound sensing experiments were carried out in sealable containers with a total volume of 50 mL. To explore the gas effect on the nanoplasmonic membrane, tiny amounts of volatile compounds (from 5 to 1000 μL) were drop-casted onto the bottom of the container aiming to spontaneously volatilize the studied compound and expose it to the nanoplasmonic membrane which was at the top of the sealed container (as described in Scheme 6-1B). The plasmonic nanopaper pieces were assembled inside a holder made of PDMS films, which was attached underneath the container lid but vertically aligned. Previously, original UV-Vis absorbance spectra of completely dried AgNP-BC pieces (5 × 5 mm) were recorded. All of the experiments were carried out in triplicate.

4.3.4 Sample preparation for TEM analysis

The samples made of BC and nanopaper embedding AgNPs were prepared *via* three different steps using a Precision Ion Polishing System. (i) The samples were treated with an energy of 4 keV for 30 minutes (angle from the plane of the sample to the incident ion beam 1 of +7 units, and to the incident beam 2 of +7 units). (ii) The samples were treated with an energy of 3 keV for 10 minutes (angle from the plane of the sample to the incident ion beam 1 of +7 units, and to the incident beam 2 of +7 units). (iii) The samples were treated with an energy of 0.5 keV for 5 minutes (angle from the plane of the sample to the incident ion beam 1 of +7 units, and to the incident beam 2 of +7 units).

4.3.5 Raman analysis

Raman spectroscopy was carried out using an argon laser of 514 nm (25 mW), an objective lens of 50× and a CCD exposure time of 30 seconds.

4.4 Results and discussion

Nanopaper exhibits a myriad of functional properties which are advantageous in optical sensing, including optical transparency [22], sustainability, flexibility [23], high mechanical strength, hydrophilicity, high porosity, broad chemical-modification capabilities and high surface area [24-26]. The nanopaper utilized in this research was synthesized *via Acetobacter xylinum*, as previously described and characterized [11]. Among other features, this cellulose exhibits a crystallinity around 82%, an approximate Young's modulus of 17 GPa, an average fiber diameter of *ca.* 45 ± 10 nm and a length that is approximately greater than 10 μm. The plasmonic nanopaper exploited throughout this research was synthesized following recently reported methods, where AgNPs are synthesized *in situ* using nanopaper as the reducing agent of a salt-containing Ag precursor such as $AgNO_3$ [11.21].

4.4.1 The effect of ammonia vapor on AgNPs embedded in bacterial cellulose nanopaper

For the present study, we employed ammonia as a model corrosive agent, which is known as an environmental and clinically relevant analyte [14, 15, 27]. In order to explore the effect of corrosive vapor exposure on the nanoplasmonic membrane, 1 mL of 30% ammonia solution was introduced and spontaneously volatilized at room temperature for 12 hours using the set-up described in Scheme 6-1B. Remarkably, the plasmonic nanopaper displayed a change in color from amber to light amber, which

can be readily observed by the naked eye when compared with a control piece of plasmonic nanopaper (without ammonia vapor exposure, see Figure 4-1A and C). Once the explored nanopaper samples were analyzed *via* transmission electron microscopy (TEM), we discovered that the population density of the AgNPs embedded in the nanopaper was dramatically decreased. In fact, the population density of the AgNPs in the images of the control plasmonic nanopaper has been estimated to be 1473 ± 227 AgNP μm^{-2}, whereas the population density of the AgNPs in the images of the plasmonic nanopaper exposed to ammonia in the aforementioned conditions is estimated to be 302 ± 38 AgNP μm^{-2} (see Figure S4-1). Moreover, the control nanoplasmonic membrane (without ammonia exposure) displays a broad size distribution of AgNPs with an average particle diameter of around 10 ± 7 nm, whereas the nanoplasmonic membrane exposed to ammonia showed an average particle diameter of around 17 ± 12 nm (see Figure 4-1). These results suggest that the AgNPs embedded in the nanopaper are prone to be partially or completely etched by corrosive vapor exposure, leading to a larger distance between the remaining nanoparticles, whereas the average particle size increases, modulating the plasmonic properties of the explored nanoplasmonic membrane. Interestingly, we observed through scanning electron microscopy (SEM) imaging that this phenomenon occurs with virtually no damage to the structure of the nanocellulose (see Figure S4-2).

4.4.2 Specificity upon ammonia exposure

We expected that the modulation of the population density of the AgNPs embedded in bacterial cellulose *via* ammonia exposure would lead to a sensing platform. Aiming at exploring whether the modulation of plasmonic properties discussed above is specific to corrosive vapour (ammonia) exposure, the nanoplasmonic membrane was exposed to other volatile compounds under harsh conditions, including methanol (99.9%), ethanol (99.8%), propanol (99.8%), acetic acid (100%), ethyl acetate (99%), acetonitrile (99.8%), acetone (99.5%), toluene (99.8%), indole (99%) and trimethylamine (99.5%). Using the set-up described in Scheme 6-1B, 1 mL of each of these volatile compounds was spontaneously volatilized at room temperature for 16 hours, respectively. Likewise, 1 mL of water was also included in these experiments to evaluate the moisture effect on the plasmonic nanopaper. Afterwards, the UV-Vis absorbance of each piece of plasmonic nanopaper was analyzed. We ascertained that the moisture gave rise to a blue shift of approximately 10 nm in the UV-Vis spectra of the nanoplasmonic membrane, whereas the intensity of the absorbance peak was negligibly affected (see Figure 4-2A). These spectral changes may be due to a possible motion of the AgNPs and/or a change

in the refractive index of the nanoplasmonic membrane facilitated by humidity across the experiment. We also spotted a blue shift of up to 20 nm in the experiments carried out with the other 10 volatile compounds and the absorbance peak was slightly increased or decreased (see Figure 4-2A). The origin of these spectral changes might be attributed to a reorganization of the AgNPs embedded in the nanocellulose triggered by humidity and the effect of the volatile compound on the nanopaper.

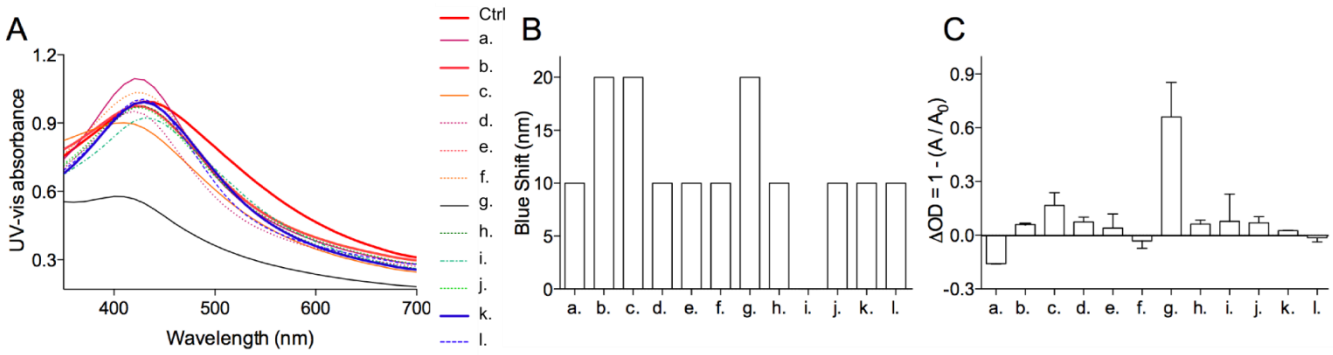

Figure 4-2. Specificity of the nanoplasmonic membrane as a corrosive vapor (ammonia) sensing platform. A. UV-Vis spectra of plasmonic nanopaper upon vapor exposure using an initial volume of 1000 µL of different volatile compounds spontaneously volatilized for 18 hours. B. Blue shift observed in the UV-Vis spectra depending on the volatile compound exposed. C. Changes in optical density according to the volatile compound exposed. The error bars represent the standard deviation of three parallel experiments. a. Methanol. b. Ethanol c. Propanol. d. Acetic acid. e. Ethyl acetate. f. Acetonitrile. g. Ammonia. h. Acetone. i. Toluene. j. Indole. k. Water. l. Triethylamine.

On the other hand, the color of the nanoplasmonic membranes exposed to the other volatile compounds has not been observed to change by the naked eye. As a consequence, we exploited the formula $\Delta OD = 1 - (A/A_0)$ to analyze the absorbance peak modulation, where ΔOD represents the changes in optical density; A_0 is the original intensity of the absorbance peak of the nanoplasmonic membrane; and A is the final intensity of the absorbance peak of the studied nanoplasmonic membrane. The plasmonic nanopaper exposed to ammonia changed in color, which can be detected smoothly by the naked eye as described above. It also exhibited a blue shift of around 20 nm and, most importantly, its ΔOD values were dramatically different, as can be noticed in Figure 4-2B and C. These results prove that the explored phenomenon is specific to ammonia exposure. Moreover, AgNPs have been reported to undergo a continuous release of silver ions from their surface [28], which are known to react with

ammonia forming the complex $[Ag(NH_3)_2]^+$. This complex can occur simultaneously with hydrogen bonding between the hydroxyl groups of nanocellulose and ammonia, which may boost the dissociation of the silver atoms and modulate the AgNP size. This mechanism is likely to contribute to the specificity of the explored sensing system.

4.4.3 Sensing performance

We explored several ammonia dose exposures for different times in order to determine the overall performance of the sensing principle using the experimental set-up described in Scheme 6-1B. Particularly, ammonia volumes from 10 μL to 1000 μL, were spontaneously volatilized at room temperature for 2, 4, 8 and 12 hours. The corresponding initial evaporation rates were estimated as described in the ESI, and range from *ca.* 15.7 ng s^{-1} to *ca.* 1200 ng s^{-1}.

Figure 4-3A shows the UV-Vis spectra of the plasmonic nanopaper exposed to an initial ammonia volume of 10 μL and 1000 μL between 2 and 12 hours. The intensity of the UV-Vis absorbance was observed to be modulated as a function of ammonia dose and exposure time. The general behavior of this modulation was represented in terms of the ΔOD values (obtained as discussed above); see Figure 4-3B, which displays a two-phase response with a sharp transition for the ammonia doses below an initial evaporation rate of 121 ng s^{-1} (corresponding to 50 μL) and a steady response for the ammonia doses with an initial evaporation rate between 176 and 1200 ng s^{-1} (100 and 1000 μL, respectively). ΔOD values corresponding to the exposure to water were considered as blank values. Different limits of detection were estimated by interpolating the ΔOD blank value plus eight times its standard deviation into the respective calibration curve, that is, according to the exposure time of the explored corrosive vapor (ammonia).

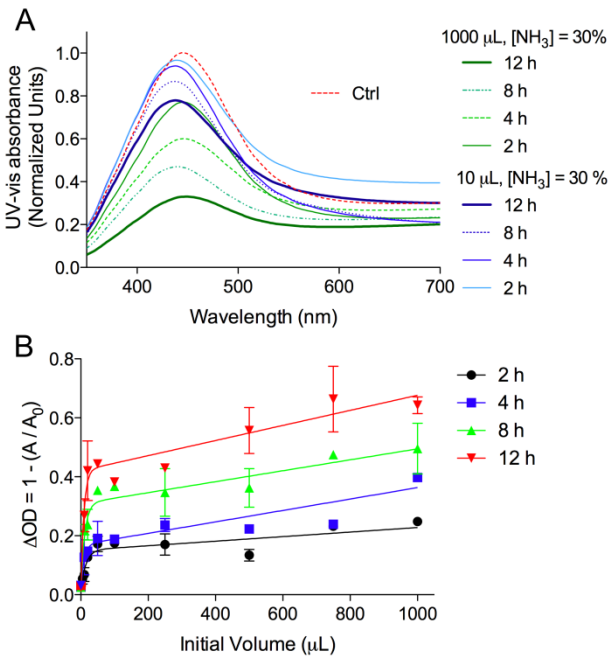

Figure 4-3. Behavior of the nanoplasmonic membrane as a corrosive vapor sensing platform. A. UV-Vis spectra of the plasmonic nanopaper upon corrosive vapour (ammonia) exposure using 10 and 1000 µL of 30% ammonia solution spontaneously volatilized for between 2 and 12 hours. B. Calibration curves displaying changes in optical density depending on the initial volume to be volatilized (from 10 to 1000 µL) and the exposure time (2–12 hours). The error bars represent the standard deviation of three parallel experiments.

Among the explored exposure times, the proposed sensing platform exhibited a limit of detection of 1515 µg of ammonia spontaneously volatilized at room temperature during 2 h in a sealed 50 mL container (*i.e.*, 30.3 ppmv). On the other hand, the explored sensing system displayed a limit of detection of 28.7 µg of ammonia spontaneously volatilized at room temperature in a sealed 50 mL container for 8 hours (*i.e.*, 0.574 ppmv), which was the lowest limit of detection observed. Table 4-1 summarizes the estimated limits of detection and their related initial evaporation rates (details on these estimations are discussed in the ESI).

Table 4-1. Limits of detection of the explored system [a]

Exposure time (h)	LOD[b]	RIER[c](ng s^{-1})
2	~30.3	~2.48
4	~6.42	~0.51
8	~0.574	~0.09
12	~4.18	~0.32

[a] Details on these estimations are discussed in the ESI. [b] Limit of detection. [c] Related initial evaporation ratio. Food spoilage monitoring: a proof-of-concept

Aiming at demonstrating a practical application for this approach, as a proof-of-concept, we reasoned that the studied phenomenon could be useful for food spoilage monitoring given that ammonia is released as a major agent along with other volatile compounds during the degradation process, in particular trimethylamine, dimethylamine, histamine, putrescine, cadaverine, short-chain carbonyls, acids, sulfur compounds, and *N*-cyclic compounds as well as unsaturated aldehydes in fish spoilage [29], and alcohols, aldehydes, esters, ketones, and carbon dioxide in meat spoilage [30].

We again used the experimental set-up illustrated in Scheme 6-1B. 5 g of fish or meat was placed inside the sealed container, and was left at room temperature for 60 hours. Unexpectedly, the original amber color of the nanoplasmonic membranes became grey for the fish spoilage monitoring and a taupe colour for the meat spoilage monitoring. Furthermore, the UV-Vis spectrum was dramatically modulated and the original peak absorbance disappeared (see Figure 4-4A and B). Interestingly, the size distribution of the AgNPs embedded in the nanocellulose was also dramatically modulated upon food spoilage exposure. As discussed above, the original size distribution bears an average particle diameter of around 10 ± 7 nm, whereas we ascertained that the average particle diameter upon food spoilage exposure was approximately 6 ± 3 nm for fish spoilage monitoring, and *ca.* 6 ± 5 nm for meat spoilage monitoring.

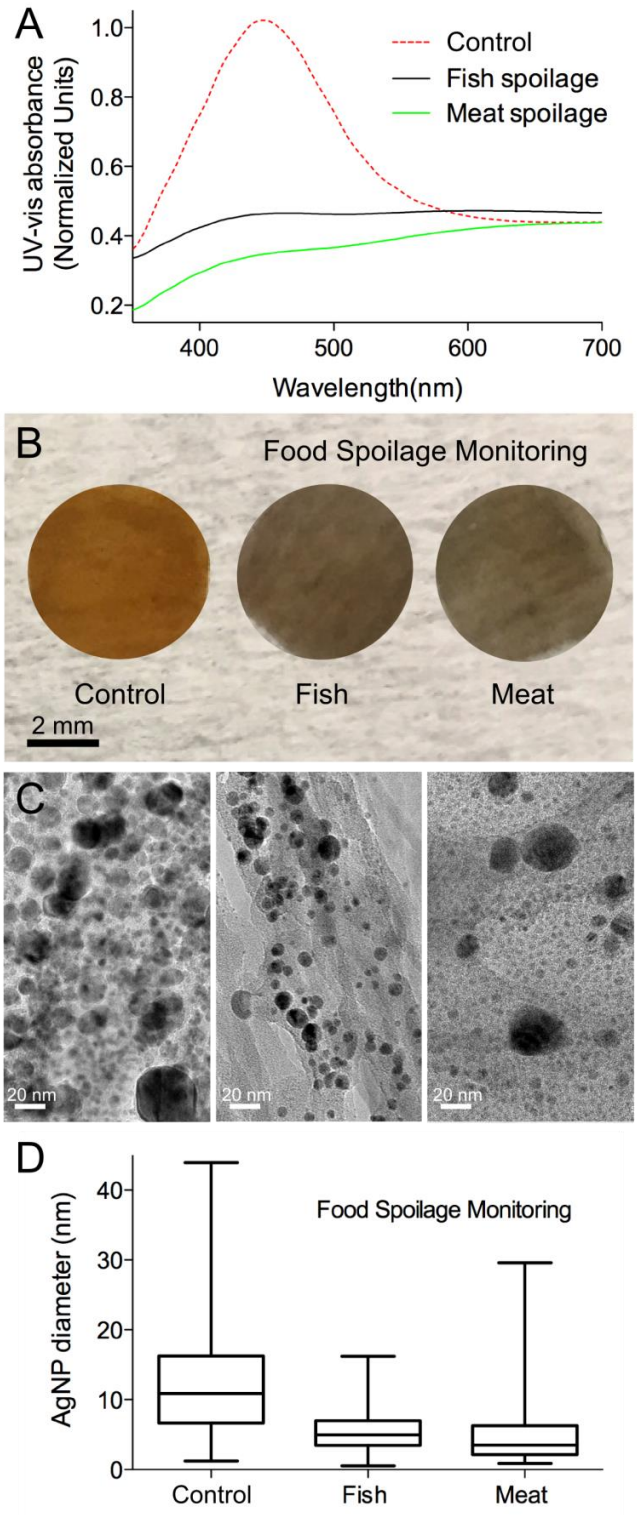

Figure 4-4. Food spoilage monitoring *via* plasmonic nanopaper. A. UV-Vis spectra of the nanoplasmonic membranes before food spoilage exposure (Ctrl) and after food spoilage exposure (ammonia and several volatile organic compounds are released during fish and meat spoilage). B.

Appearance of the nanoplasmonic membranes before/after food spoilage monitoring. C. TEM micrographs, from left to right: control, fish spoilage and meat spoilage. D. Size distribution of the AgNPs embedded in the nanopaper before/after food spoilage monitoring, the box plots show the median, 25th and 75th percentiles and the extreme values of the respective size distributions (5–95 percentile).

On the other hand, we found that the distribution size of the embedded AgNPs ranged from 1 to 16 nm upon fish spoilage exposure, and from 1 to 30 nm upon meat spoilage exposure. However, the population density of the embedded AgNPs was not dramatically affected during food spoilage monitoring. Thus, we concluded that the volatile compounds released during food spoilage effectively modulated the size of the embedded AgNPs and consequently the plasmonic properties of the sensing platform. Figure 4-4C displays the corresponding TEM micrographs and Figure 4-4D plots the estimated size distributions. Table 4-2 summarizes our study on the modulation of the population density and size distribution of the AgNPs embedded in the nanopaper *via* volatile compound exposure.

Table 4-2. Modulation of population density (PD) and average size (AS) of the AgNPs embedded in the nanopaper *via* volatile compound exposure.

Exposure	**PD[a](AgNP per µm^2)**	**AgNP-AS[a] (nm)**	**Resulting colour**
Control	~1473 ± 227	~10 ± 7	Amber
Ammonia	~302 ± 38	~17 ± 12	Light amber
Fish spoilage	~1213 ± 251	~6 ± 3	Grey
Meat spoilage	~1376 ± 244	~6 ± 5	Taupe

[a] Three TEM micrographs corresponding to each type of exposure were analyzed to estimate these values.

4.4.4 Raman analysis

Additionally, we performed a Raman analysis of the explored materials. In particular, we observed that the employed bare bacterial cellulose displays its main Raman signature from 900 to 1500 cm^{-1} and

from 2700 to 3500 cm^{-1}, with the most prominent peaks being those centred at ~2900 and ~3375 cm^{-1}. Moreover, the peak centred at ~3375 cm^{-1} disappears after synthesizing the AgNPs using the nanocellulose as a reducing agent, and a new set of peaks rise from 1500 to 1700 cm^{-1} due to the presence of the AgNPs. Interestingly, the Raman signature of the nanoplasmonic membrane around 1350 ± 450 cm^{-1} was modulated upon ammonia exposure, whereas the peaks centred at 2900 and 3375 cm^{-1} were similar to those of bare nanocellulose. Likewise, the Raman fingerprint of the nanoplasmonic membrane was modulated upon fish/meat spoilage, with those prominent peaks centred at ~2900 cm^{-1} and ~3375 cm^{-1} being renewed, which can be ascribed to the partial or complete etching of the embedded AgNPs and can be considered further evidence of the studied phenomena (see Figure 4-5).

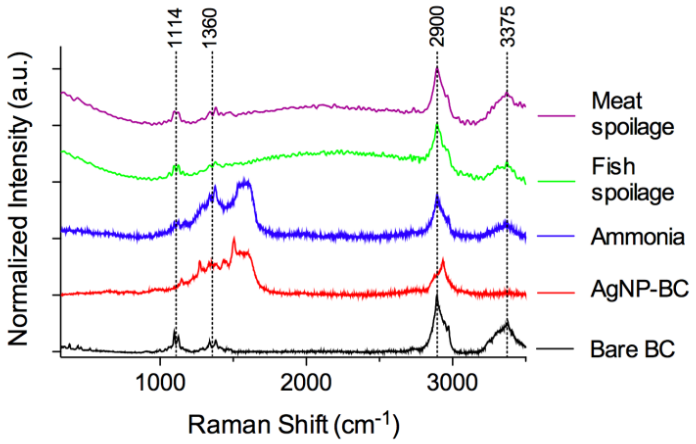

Figure 4-5. Raman signature of the explored materials: bare bacterial cellulose (BC), bacterial cellulose decorated with silver nanoparticles (AgNP-BC) and AgNP-BC exposed to ammonia and fish/meat spoilage.

4.5 Conclusions

We discovered that the population density and size of silver nanoparticles embedded within bacterial cellulose nanopaper can be easily modulated *via* corrosive vapor (ammonia) exposure even in a mixture of volatile compounds released during food spoilage. In fact, AgNPs embedded in nanopaper were partially or completely etched by the explored corrosive vapor exposure, modulating the plasmonic properties of the studied plasmonic nanopaper. As a consequence, the nanoplasmonic membrane changed in color from amber to light amber upon ammonia exposure and from amber to grey or taupe in colour upon fish or meat spoilage exposure, respectively. These phenomena are proposed for a

straightforward volatile compound sensing platform principle that can be applied for visual detection using a flexible, transparent, permeable and stable single-use nanoplasmonic membrane. This approach opens the way to new possibilities and capabilities for smart packaging and gas sensing-related applications.

4.6 Acknowledgements

This work was supported by MINECO (Spain, MAT2014-52485-P). ICN2 acknowledges support from the Severo Ochoa Program (MINECO, Grant SEV-2013-0295). Nanobiosensors and Bioelectronics Group acknowledges the support from Secretaria d'Universitats i Recerca del Departament d'Economia i Coneixement de la Generalitat de Catalunya (2014 SGR 260). B. H. thanks the FRQNT (Quebec, Canada), NSERC (Canada) and the industrial partners of 3SPack Chair Saputo and Prolamina for funding her research stay in Spain. The authors are grateful to Dr. Hossein Yousefi for providing the bacterial cellulose utilized in this research.

4.7 References

[1] H. Goesmann and C. Feldmann, "Nanoparticulate functional materials," *Angewandte Chemie International Edition,* vol. 49, pp. 1362-1395, 2010.

[2] X. Chen, S. G. Parker, G. Zou, W. Su, and Q. Zhang, "β-Cyclodextrin-functionalized silver nanoparticles for the naked eye detection of aromatic isomers," *ACS nano,* vol. 4, pp. 6387-6394, 2010.

[3] P. D. Howes, R. Chandrawati, and M. M. Stevens, "Colloidal nanoparticles as advanced biological sensors," *Science,* vol. 346, p. 1247390, 2014.

[4] J. N. Anker, W. P. Hall, O. Lyandres, N. C. Shah, J. Zhao, and R. P. Van Duyne, "Biosensing with plasmonic nanosensors," *Nature materials,* vol. 7, pp. 442-453, 2008.

[5] M.-P. N. Bui, S. Ahmed, and A. Abbas, "Single-Digit Pathogen and Attomolar Detection with the Naked Eye Using Liposome-Amplified Plasmonic Immunoassay," *Nano Letters,* vol. 15, pp. 6239-6246, 2015/09/09 2015.

[6] T. Xu, H. Shi, Y.-K. Wu, A. F. Kaplan, J. G. Ok, and L. J. Guo, "Structural Colors: From Plasmonic to Carbon Nanostructures," *Small,* vol. 7, pp. 3128-3136, 2011.

[7] M. I. Stockman, "Nanoplasmonic sensing and detection," *Science,* vol. 348, pp. 287-288, 2015.

[8] E. Busseron, Y. Ruff, E. Moulin, and N. Giuseppone, "Supramolecular self-assemblies as functional nanomaterials," *Nanoscale,* vol. 5, pp. 7098-7140, 2013.

[9] S. Szunerits and R. Boukherroub, "Sensing using localised surface plasmon resonance sensors," *Chemical Communications,* vol. 48, pp. 8999-9010, 2012.

[10] S. Su, X. Zuo, D. Pan, H. Pei, L. Wang, C. Fan, *et al.*, "Design and applications of gold nanoparticle conjugates by exploiting biomolecule-gold nanoparticle interactions," *Nanoscale,* vol. 5, pp. 2589-2599, 2013.

[11] E. Morales-Narváez, H. Golmohammadi, T. Naghdi, H. Yousefi, U. Kostiv, D. Horák, *et al.*, "Nanopaper as an Optical Sensing Platform," *ACS nano,* vol. 9, pp. 7296-7305, 2015.

[12] D. Fine, F. Rufeh, and D. Lieb, "Group analysis of volatile and non-volatile N-nitroso compounds," *Nature,* vol. 247, pp. 309-310, 1974.

[13] K. D. van de Kant, L. J. van der Sande, Q. Jöbsis, O. C. van Schayck, and E. Dompeling, "Clinical use of exhaled volatile organic compounds in pulmonary diseases: a systematic review," *Respiratory Research,* vol. 13, p. 117, December 21 2012.

[14] B. H. King, A. Gramada, J. R. Link, and M. J. Sailor, "Internally Referenced Ammonia Sensor Based on an Electrochemically Prepared Porous SiO2 Photonic Crystal," *Advanced Materials,* vol. 19, pp. 4044-4048, 2007.

[15] T. A. Kumar, E. Capua, M. Tkachev, S. N. Adler, and R. Naaman, "Hybrid Organic-Inorganic Biosensor for Ammonia Operating under Harsh Physiological Conditions," *Advanced Functional Materials,* vol. 24, pp. 5833-5840, 2014.

[16] E. Tait, J. D. Perry, S. P. Stanforth, and J. R. Dean, "Identification of Volatile Organic Compounds Produced by Bacteria Using HS-SPME-GC–MS," *Journal of Chromatographic Science,* vol. 52, pp. 363-373, 2014.

[17] Y. Xu, W. Cheung, C. L. Winder, and R. Goodacre, "VOC-based metabolic profiling for food spoilage detection with the application to detecting Salmonella typhimurium-

contaminated pork," *Analytical and Bioanalytical Chemistry,* vol. 397, pp. 2439-2449, July 01 2010.

[18] M. Hakim, Y. Y. Broza, O. Barash, N. Peled, M. Phillips, A. Amann, *et al.*, "Volatile organic compounds of lung cancer and possible biochemical pathways," *Chemical reviews,* vol. 112, pp. 5949-5966, 2012.

[19] "http://www.environmental-expert.com/products/ammonia-test-paper-301704, 2015."

[20] http://www.ctlscientific.com/cgi/display.cgi?item_num=90722.

[21] N. Pourreza, H. Golmohammadi, T. Naghdi, and H. Yousefi, "Green in-situ synthesized silver nanoparticles embedded in bacterial cellulose nanopaper as a bionanocomposite plasmonic sensor," *Biosensors and Bioelectronics,* vol. 74, pp. 353-359, 2015.

[22] H. Zhu, S. Parvinian, C. Preston, O. Vaaland, Z. Ruan, and L. Hu, "Transparent nanopaper with tailored optical properties," *Nanoscale,* vol. 5, pp. 3787-3792, 2013.

[23] M.-C. Hsieh, C. Kim, M. Nogi, and K. Suganuma, "Electrically conductive lines on cellulose nanopaper for flexible electrical devices," *Nanoscale,* vol. 5, pp. 9289-9295, 2013.

[24] D. Klemm, F. Kramer, S. Moritz, T. Lindström, M. Ankerfors, D. Gray, *et al.*, "Nanocelluloses: A New Family of Nature-Based Materials," *Angewandte Chemie International Edition,* vol. 50, pp. 5438-5466, 2011.

[25] D. Klemm, B. Heublein, H.-P. Fink, and A. Bohn, "Cellulose: Fascinating Biopolymer and Sustainable Raw Material," *Angewandte Chemie International Edition,* vol. 44, pp. 3358-3393, 2005.

[26] W. Kang, C. Yan, C. Y. Foo, and P. S. Lee, "Foldable Electrochromics Enabled by Nanopaper Transfer Method," *Advanced Functional Materials,* vol. 25, pp. 4203-4210, 2015.

[27] L. R. Narasimhan, W. Goodman, and C. K. N. Patel, "Correlation of breath ammonia with blood urea nitrogen and creatinine during hemodialysis," *Proceedings of the National Academy of Sciences,* vol. 98, pp. 4617-4621, April 10, 2001 2001.

[28] J. Liu, D. A. Sonshine, S. Shervani, and R. H. Hurt, "Controlled Release of Biologically Active Silver from Nanosilver Surfaces," *ACS Nano,* vol. 4, pp. 6903-6913, 2010/11/23 2010.

[29] M. K. Morsy, K. Zór, N. Kostesha, T. S. Alstrøm, A. Heiskanen, H. El-Tanahi*, et al.*, "Development and validation of a colorimetric sensor array for fish spoilage monitoring," *Food Control,* vol. 60, pp. 346-352, 2016/02/01/ 2016.

[30] B. Zhang, S. Ye, G. Xiao, and D. Dong, "Identification of beef spoilage via the analysis of volatiles using long optical-path Fourier transform infrared spectroscopy," *Analytical Methods,* vol. 7, pp. 5891-5897, 2015.

4.8 Supporting Information

Modulation of population density and size of silver nanoparticles embedded in bacterial cellulose via ammonia exposure: Visual detection of volatile compounds in a piece of plasmonic nanopaper

B. Heli [ab], **E. Morales-Narváez** [a], **H. Golmohammadi** [c], **A. Ajji** *[b] **and A. Merkoçi** *[d]

[a]*Catalan Institute of Nanoscience and Nanotechnology (ICN2), CSIC and The Barcelona Institute of Science and Technology, Campus UAB, Bellaterra, Barcelona 08193, Spain*

[b]*3SPack, CREPEC, Département de génie chimique, Polytechnique Montréal, Montréal, Québec, Canada*

[c]*ACECR-Production Technology Research Institute, Ahvaz, 6139684689, Iran*

[d]*ICREA – Catalan Institution for Research and Advanced Studies, Barcelona, 08010, Spain.*

4.8.1 Supporting information content

1. Supporting Figures

2. Estimation of Evaporation Rates and Limits of Detection

4. Supplementary References

4.8.1.1 Figures

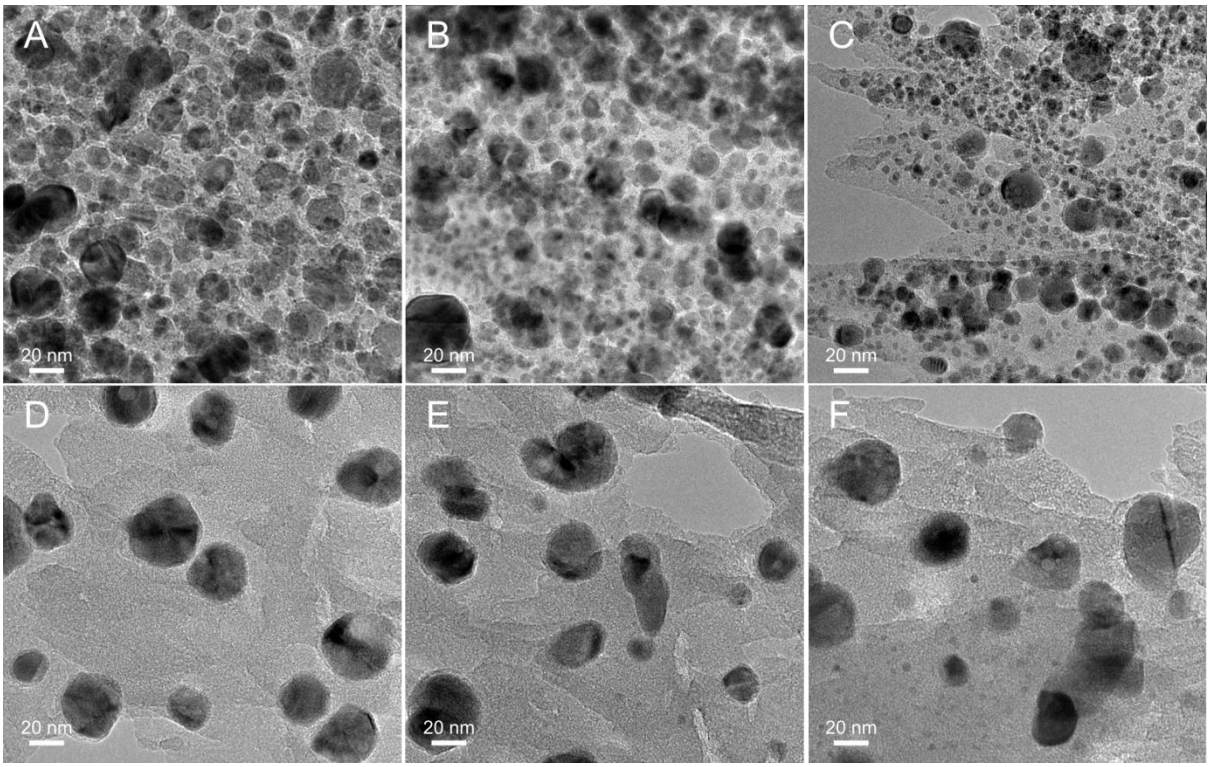

Figure S4-1. TEM micrographs showing the population density of AgNPs embedded in BC without NH3 vapor exposure (A-C) and after NH3 vapor exposure (D-F). The population density of AgNPs at the foreground in images A-C has been estimated to be 1473 ± 227 AgNP μm^{-2}, whereas the population density of AgNPs at the foreground in images D-F is around 302 ± 38 AgNP μm^{-2}. AgNP-BC in images D-F was exposed at an initial vapor rate of around ~1.2 µg $s^{-}1$ for 12 hours. TEM micrographs were analyzed via image processing through ImageJ 1.48v (Wayne Rasband, National Institutes of Health, Bethesda, MD) in order to estimate the population density of nanoparticles embedded in the BC-based composite.

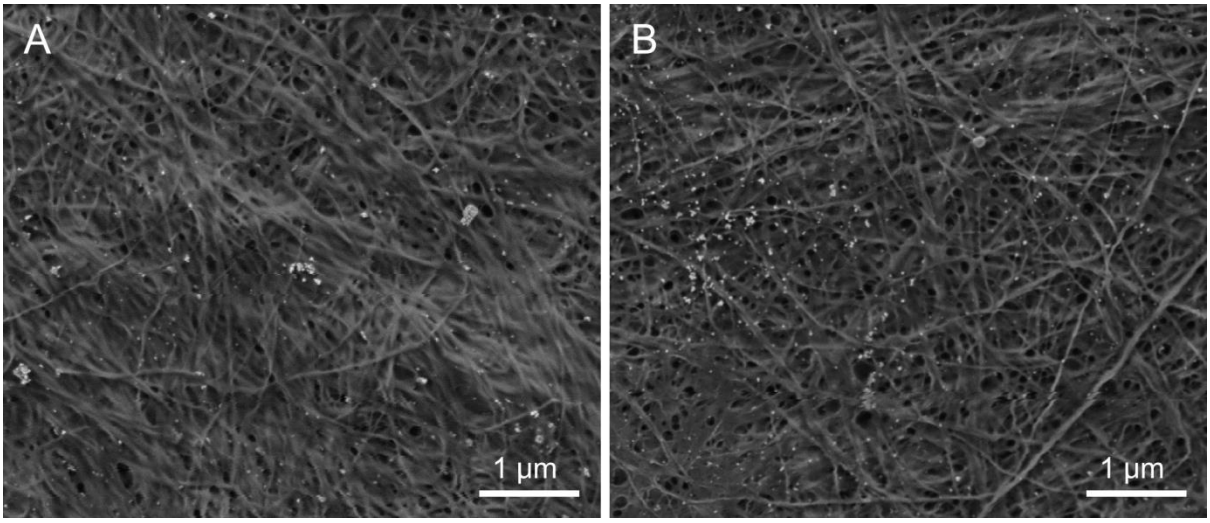

Figure S4-2. SEM micrographs of AgNP-BC without NH3 vapor exposure (A) and after NH3 vapor exposure (B). No damage or structural changes were observed in the nanofibers.

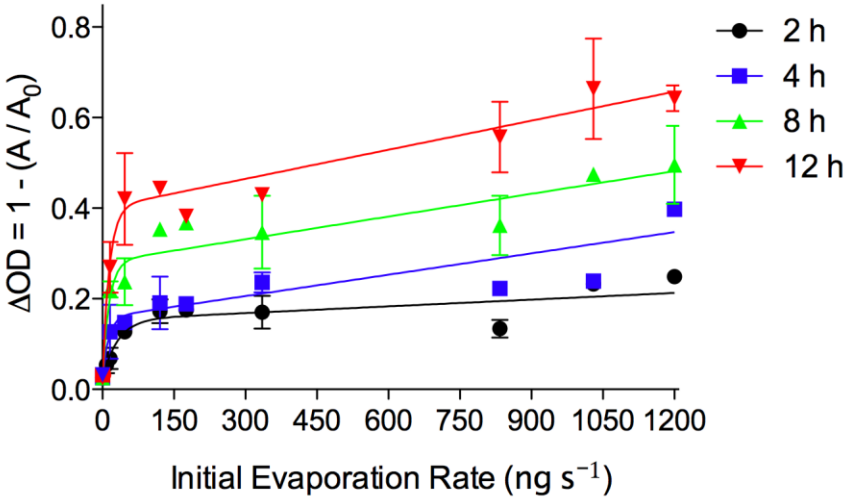

Figure S4-3. Calibration curves displaying changes in optical density depending on the initial evaporation rate and the exposure time. The error bars represent the standard deviation of three parallel experiments.

4.8.1.2 Estimation of Evaporation rates and Limits of Detection

Estimation of Evaporation rates and Limits of Detection The evaporation rate was estimated via the computations suggested by the National Ocean Service, (2013, National Oceanic and Atmospheric Administration, http://goo.gl/ebOf2T), which are based on the model proposed by Kawamura and Mackay [1]. This estimation was carried out considering a negligible wind speed of 1 μm s^{-1}, an ammonia concentration of 30%, an ambient temperature of 25 ºC and measuring the dimensions of the drops belonging to the respective studied volumes after being deposited onto the bottom of the kind of container employed throughout this research, see details in Table S1 below.

Table S 4-1. Estimation of initial evaporation rate of NH_3.

Volume (μL)	Dimensions of the drop		Evaporation rate	
	Length (cm)	Width (cm)	(ng s^{-1})	(μg h^{-1})
5	0.21 ± 0.11	0.21 ± 0.01	8.51	30.6
10	0.29 ± 0.01	0.29 ± 0.01	15.7	56.5
20	0.54 ± 0.05	0.5 ± 0.05	46.9	168.8
50	0.88 ± 0.10	0.83 ± 0.07	121.0	435.6
100	1.15 ± 0.05	0.96 ± 0.02	176.0	633.6
250	1.61 ± 0.05	1.35 ± 0.05	335.0	1206.0
500	2.96 ± 0.15	1.96 ± 0.05	834.0	3002.4
750	3.03 ± 0.05	2.36 ± 0.11	1030.0	3708.0
1000	3.1 ± 0.00	2.71 ± 0.10	1200.0	4320.0

We utilized the formula $\Delta OD = 1 - (A/A_0)$ to analyze the absorbance peak modulation, where ΔOD represents the changes in optical density; A_0, the original intensity of the absorbance peak of the

nanoplasmonic membrane; and A the final intensity of the absorbance peak of the nanoplasmonic membrane. ΔOD values corresponding to the exposure to water were considered as blank values. Different limits of detection were estimated by interpolating the ΔOD blank value plus eight times its standard deviation into the respective calibration curve, that is, according to the exposure time of the explored corrosive vapor.

These resulting interpolations are expressed in terms of µL. As the analyzed ammonia (30%) has a density of 897 µg μL^{-1}, the mass corresponding to these calculated values was estimated using this density value as a conversion factor. The limits of detection in terms of initial evaporation rate (ng s^{-1}) were obtained by interpolating the respective ΔOD values using the curves plotted in Figure S4-3.

Author Contributions A. M. and E. M-N. conceived the overall concept. E. M-N., B. H. and H. G. designed the experiments. E. M-N., B. H., H. G. and A. M. analyzed the data. B. H. performed the experiments. E. M-N., wrote the manuscript with input of B.H., A. A. and A. M. E. M-N. performed the figures with input of B.H. A. M. and E. M-N. supervised the overall project.

4.8.2 Supplementary References

[1] P. I. Kawamura and D. Mackay, "The evaporation of volatile liquids," *Journal of hazardous Materials,* vol. 15, pp. 343-364, 1987.

CHAPTER 5 ARTICLE 2: NANOPAPER-BASED PLATFORM APPLICABLE IN SOLID-BASED FRET TECHNIQUE

Bentolhoda Heli[1], Abdellah Ajji[1*]

[1] *3SPack, CREPEC, Département de Génie Chimique École Polytechnique de Montréal, Montréal, Québec, Canada.*

Corresponding Author

***** Email: abdellah.ajji@polymtl.ca

Submitted to: Biochimica et Biophysica Acta (BBA)

5.1 Abstract

The fluorescence (Föster) resonance energy transfer (FRET) functionality has been widely investigated in solution-based bioassays by varying the donor-acceptor pairs and their designed arrangement. Recently, FRET has been integrated into solid-based substrates to overcome the drawbacks of nanoparticle aggregation. This paper explores the performance of a nanopaper based configuration as a solid-based quencher applicable in FRET assay. To design a solid-based FRET platform, bacterial cellulose (BC) nanofibers were employed as robust nano-based template due to its nanofiber structure. Beside its plasmonic properties, AuNP is one of the main candidates as a strong quencher in FRET based bioassay. So, AuNP was synthesized within BC (AuNP-BC) by reducing and stabilizing the gold ions through the PEI agent. The integrated AuNP-BC showed high functionality to accept the transfer energy from the photoexcited donor whereas its performance was adjusted by controlling the AuNP densities embedded in BC. The quenching efficiency was assessed as 94±4%, 82±6%, and 56±11% through drop casting of fluorescein sodium salt (FSS) on the surface of the platform of AuNP embedded in BC, for high, medium and low densities, respectively.

5.2 Introduction

For over the past few decades, fluorescence (Föster) resonance energy transfer (FRET) has been investigated as a powerful spectroscopic technique in biosensing and bioanalysis applications [1]. FRET is a nonradiative phenomenon in which the excited energy from a donor fluorophore is transferred, and then, absorbed by an acceptor molecule [2,3]. The performance and design of FRET are strongly dependent on the type of donor and acceptor, which are generally conjugated to a biomolecule located at a desired distance between 10 to 200 Å [4]. The most popular molecular pairs are fluorescent organic dyes, quantum dots (QDs), upconversion nanoparticles (UPCNPs), noble metallic nanoparticles like gold (AuNP), silver (AgNP), and carbon-based materials, such as graphene (G), carbon nanotubes (CNT), and graphene oxide (GO) [3, 5].

Due to the unique plasmonic characteristics of the gold nanoparticle, it shows high potential to accept the energy transfer from the photoexcited donor in comparison with the other types of acceptors. Dubertret and co-workers have studied that the effective distance of donor and a single gold nanoparticle was enhanced up to 100-fold compared with a traditional quencher [6]. Moreover, it has been indicated that the dependency of quenching efficiency is directly

correspondent to the size of gold nanoparticles, whereas larger gold nanoparticles caused a stronger quenching [7]. Besides, owing to their wide absorbance spectra, ease of surface modification, size-controlled synthesis and biocompatibility, AuNPs have been extensively exploited as acceptors in FRET-based bioassays [8, 10].

Currently, the most developed FRET configurations have been designed for a solution-based assay with single nanoparticles, while the aggregation of nanoparticles, especially gold nanoparticles, remains a challenge. To overcome this drawback and to provide a user-friendly and more sensitive bioassay, some attempts have explored the solid-based FRET confirmations. Functionalized glass [11, 12] and paper [13-16] are of great interest to the researchers as substrates to assemble solid-based bioassays.

Although paper is a very attractive candidate for designing biosensors due to its low cost, flexibility, ease of use, and varieties [17, 18], a recently developed nanopaper (e.g. bacterial cellulose) offered more opportunities over traditional paper [19]. Owing to the nanofibrous structure, a high degree of cellulose purity, abundant natural functional groups, and its ease of modification [20, 21], bacterial cellulose has been exploited as a marvellous nanoscale support for nanoparticle synthesis and immobilization. Successfully integrated nanoparticles (such as gold, silver, quantum dot and upconversion NP) with bacterial cellulose has led to the development of the promising optical-based platform [22]. Specifically, plasmonic nanopapers composed of bacterial cellulose with noble metal nanoparticles (gold and silver) are applied as a highly sensitive optical and colorimetric detection approach to recognize chemicals which are either dissolved in water [23] or presented in the headspace of food packaging [24].

Up to now, neither the bacterial cellulose nor its composites is described as a substrate for FRET-based bioassays. Herein, we study the efficiency of gold nanoparticles embedded in bacterial cellulose (AuNP-BC) in the quenching of a fluorophore, such as a fluorescent dye. The dependency of fluorescein quenching efficiency on the density of AuNP-BC is examined for the various fluorescein concentrations. The characteristics of BC and AuNP have a huge potential to carry biomolecules either through covalent bonding or electrostatic interaction. As such, it can serve as an excellent solid-based substrate for FRET technique to improve in-situ bioanalytical devices applicable in food and environment industries.

5.3 Materials and methods

The following chemicals: polyethylenimine (PEI) with a molecular weight of 25,000, tetrachloroauric (III) acid ($HAuCl_4.3H_2O$) and fluorescein sodium salt ($C_{20}H_{10}Na_2O_5$) (FSS) were purchased from Sigma-Aldrich Co. LLC (Okaville, Ontario, Canada). The bacterial cellulose was provided by Nanonovin Polymer Co. (Mazandaran, Iran). The carboxyl quantum dot (Qdot 525 ITK) was acquired from Invitrogen Co. (Carlsbad, CA). Costar 96 micro plates (black and transparent, flat bottom) were provided by Corning Inc. (Kennebunk, Me) as samples holders. All the materials were stored and handled with respect to the conditions specified in the safety datasheet. Milli-Q water was used for all aqueous solutions in our experiments.

UV-Vis absorbance spectra and fluorophores emission spectra were recorded by Infinite 200 PRO (Tecan, Switzerland) microplate reader. Scanning electron microscopy (SEM) was performed by Hitachi's ultra-high resolution SU8200 FE-SEM operated at 1 kV (Hitachi High-Technology Cor., Japan). Transmission electron microscopy (TEM) was carried out by JEM 2100F (JEOL USA Inc., CA).

5.3.1 In-situ synthesis of AuNP within BC

In-situ synthesizing of AuNPs was performed through the method as described [22]. So, the synthesis was proceeded by soaking 15 pieces of cut, wet BCs (1×1 in) in 100 ml of $HAuCl_4$ solution under heating and stirring. Once the temperature reached the boiling point, PEI solution was added to the precursor mixture. The synthesis of AuNPs within BCs was completed after 1 h under the same conditions of heating and stirring. The color of the BC pieces changed from colorless BCs to red-violet and pink, indicative of AuNP formation. Here, to modulate the density of the AuNPs embedded in BCs, the concentration of $HAuCl_4$ was adjusted to 0.34, 0.17 and 0.02 mM which was reduced to AuNPs by adding 400, 200 and 30 µl of 15% (V/V) PEI solution.

After cooling the mixture to room temperature, AuNP-BCs were separated from the rest of the solution in the container. Then, the free and unattached nanoparticles were removed from AuNP-BCs by washing with an adequate amount of Milli-Q water. Afterwards, the AuNP-BCs were properly dried at room temperature by putting them between a filter paper under mild pressure.

The samples were prepared from the dried AuNP-BCs by punching them in a circle shape (d=5 mm). To measure the absorbance and emission spectra, they were placed in transparent and black

microplates, respectively. The absorbance band of dried BC, without any treatment, was considered as the blank sample.

5.3.2 Sample preparation for TEM

In order to define accurately the size and shape of AuNP, a piece of the synthesized of AuNP-BC was soaked in 3 ml of Mili-Q water. It was then treated under sonication in an ultrasonic bath (Thermo Fischer, 40 KHz) for 1 h, which resulted in the dissociation of AuNPs from the platform. Next, the obtained mixture was filtered by syringeless filtering device (WhatmanTM, 0.45 µm PEFE membrane) to remove impurities. The filtered mixture containing AuNP was dropped on the surface of a copper grid with supporting carbon film (CF400-Cu, Electron Microscopy Sciences) prior to TEM observation. This procedure was repeated separately for the different AuNP-BC platforms.

5.3.3 Estimation of quenching efficiency

The ability of AuNP-BC to absorb the energy transfer was assessed by examining the quenching efficiency of FSS (excited and emitted at wavelengths of 460 and 520 nm, respectively). In order to measure the samples' background, the emission intensities of AuNP-BCs and BCs were also recorded by the microplate reader at the same excitation wavelength before adding FSS. Next, 5 µl of different FSS concentration dissolved in Milli-Q water was drop-casted to each piece of AuNP-BCs and BCs located in the black microplate. After drying it at room temperature for 20 min, the fluorescent emission intensity was scanned again at the same excitation wavelength. The quenching efficiency (φ_q) of FSS was evaluated through the following equation:

$$\varphi_q = \frac{I_0 - I_i}{I_0}$$

Where, I_0 and I_i are the emission intensities of the dispersed FSS on the BC and AuNP-BC, respectively. These values are applied in the equation after subtraction from their respective background.

To confirm repeatability of experiments, all the represented graphs were evaluated from those obtained through three parallel experiments with mean and standard deviation.

5.4 Results and discussion

5.4.1 Characterizing the in-situ synthesized AuNP-BC

The employed bacterial cellulose (BC) in this study was produced by *Acetobacter xylinum* under a controlled culture conditions [25]. The synthesized BC sheet through this approach is a gel-like with a nanofibrils network whose nanofibers have the average diameter of 45±10 nm and the estimated length more than 10 micrometers [22]. As such, the native form of BC was implemented as the bio-based platform in our investigation.

Through the Au precursor adjustment (by 0.34, 0.17, and 0.02 mM), the population density of the synthesized AuNPs embedded in a BC network can be controlled. Here, Poly(ethyleneimine) (PEI) serves as a reducing agent that also stabilizes and protects the formed AuNPs in the BC network [26]. Due to the cationic structure of PEI, composed of primary, secondary, and tertiary amino groups, the ionic $AuCl_4^-$ is absorbed by PEI, which is then followed by its transformation into metallic Au atoms [27]. Once AuNPs are formed, the color of BCs tent from colorless to red-violet and pink, with their color intensity being highly dependent on the concentration and the density of AuNPs, as shown in Figure 5-1A. The UV-Vis absorbance spectra, as illustrated in Figure 5-1B, proves also the impregnated BCs with the different densities of AuNPs. While there isn't any absorbance peak for BC between 400 to 650 nm, the absorbance spectrum of AuNP-BCs reveals a peak at 530 nm, as the result of the plasmon resonance absorption of AuNPs. Upon decreasing the AuNP density within the BC, the intensity of this plasmonic peak declined and became broader, as studied before [26]. Thus, the absorbance spectra demonstrated that the plasmonic properties of AuNPs can be preserved while they are embedded in the BC network.

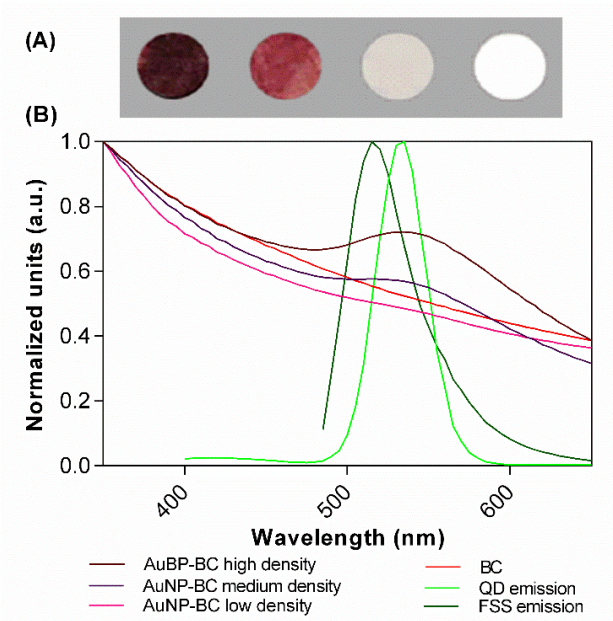

Figure 5-1. AuNP-BCs characterization by (A) their color appearance (from right to left, high, medium and low-density AuNP-BC and bare BC) and, (B) UV-Vis absorbance spectra of AuNP-BC synthesized with different densities of AuNPs. Also, the emission spectra of FSS (exited at 460 nm) and QD (exited at 350 nm) are illustrated for more comparison.

Moreover, the SEM pictures (Figure 5-2) clearly illustrate a uniform distribution of AuNPs on the BC surface, which is also significantly affected by AuNP density. As it can be observed, for the high AuNPs density, clusters of AuNPs are more dominant in comparison with a single distributed AuNP. This effect was less prominent when AuNPs density was reduced to the lowest amount, where single nanoparticles can be distinctly recognized.

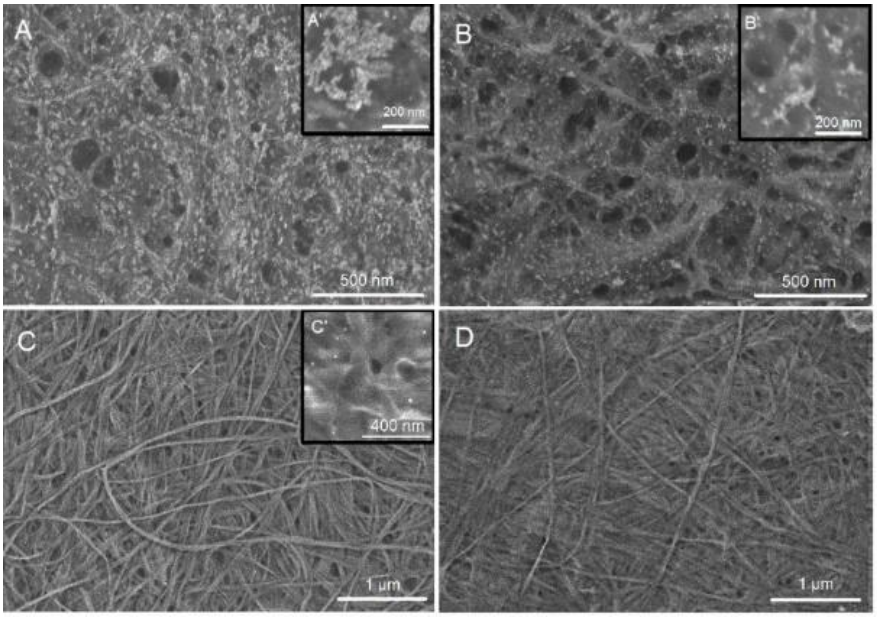

Figure 5-2. Scanning electron microscopy of AuNP-BC with high density (A and A'), medium density (B and B'), low density (C and C'), and bare BC (D).

Furthermore, the structure and size of AuNPs were investigated using TEM imaging as shown in Figure 5-3. Interestingly, we observed the spherical AuNPs dissociated from the high and medium density AuNP-BCs platform with the average diameter of about 5.5±1.2 and 5.1±1.2 nm, respectively. As such, the increase of the Au precursor concentration affected directly the density of embedded AuNP, with a negligible effect on the size of AuNP. However, the suggested methodology of sample preparation didn't provide enough cluster of AuNP for the exploration of AuNP embedded in the low density platform.

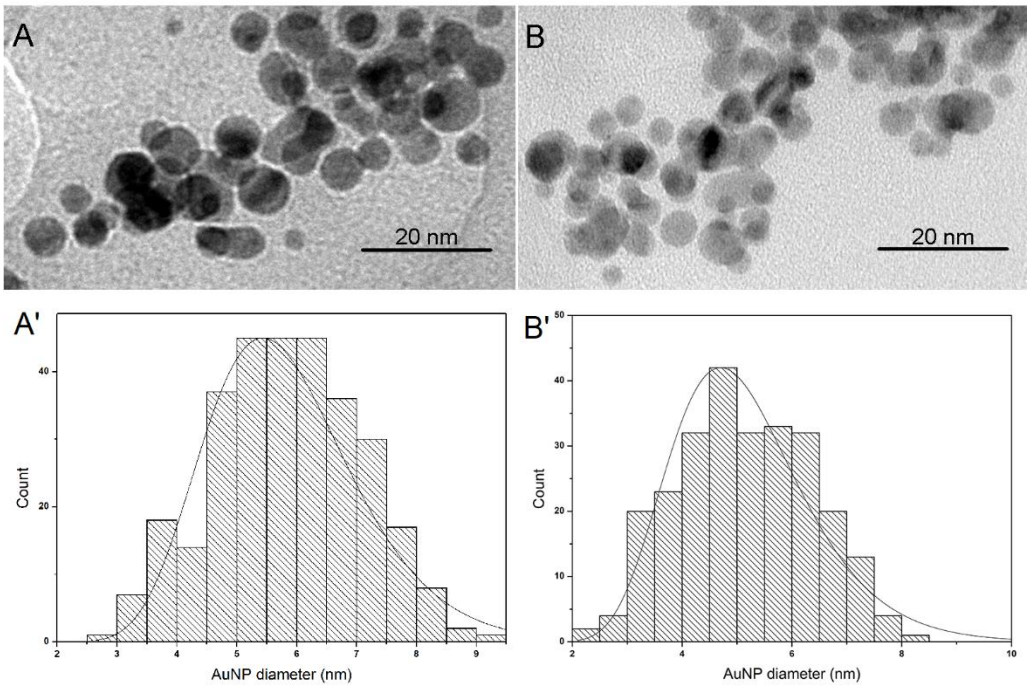

Figure 5-3. Transmission electron microscopy (TEM) of AuNPs dissociated from the high density (A) and medium density (B) of AuNP-BC platforms and their respective size distribution histograms (A' and B').

5.4.2 Estimating the fluorescence quenching efficiency

The energy transfer from donor to acceptor in FRET can be significantly enhanced by maximizing the spectral overlap of acceptor absorption and donor emission [2]. Interestingly, as seen in Figure 5-1B, the board absorbance spectra of AuNP-BCs provided an incredible overlap with FSS emission spectra whereas it became larger by the increase in the density of AuNP-BC. To examine the effect of AuNP-BCs density on FSS quenching, the fluorescent intensity of 5 µl FSS with concentrations of (5, 2, 1, 0.5 and 0.25 µg/ml) were spotted on AuNP-BCs and measured through microplate reader. Its comparison with the similar amount of FSS spotted on the surface of the bare BC revealed the quenching efficiency of FSS as shown in Figure 5-4. As observed, high-density AuNP-BC behave as a strong acceptor and it could even quench a high concentration of FSS (5 µg/ml), up to 95%. The decrease in the density of AuNP-BCs caused a reduction in the quenching efficacy – less than 70% for the same FSS concentration. Interestingly, a similar quenching efficiency was estimated by the change of the concentration of FSS, whereas the quenching behavior wasn't affected notably by lowering the concentration of FSS. On the other hand, FSS

quenching efficiency was strongly dependent on the AuNP density, as a reduction in the density of the AuNPs, caused less acceptance of the transferred photons from the excited FSS. This reduction is a result of the decrease in the number of AuNPs located in the BC and therefore, an increase in the distance of the interparticles (see SEM imaging). Although AuNPs are completely dispersed within the BC network, it is expected that the particles located on the surface of the BC can, more effectively, absorb the photons from the excited FSS compared to the AuNPs located underneath the nanofibrils layers.

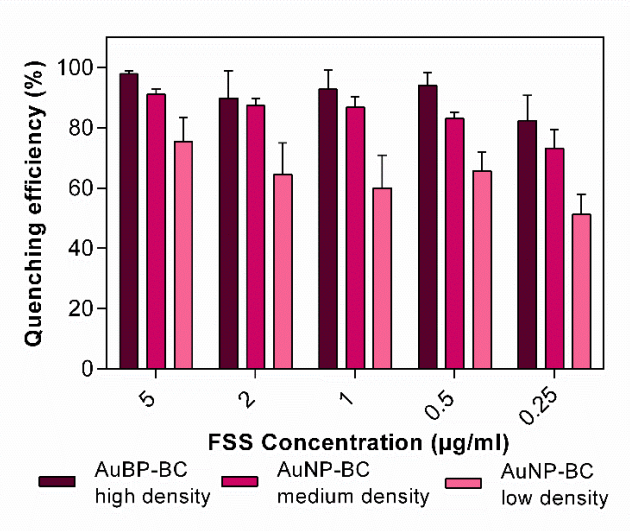

Figure 5-4. Evaluation of FSS quenching efficiency cast on nanopaper-based platform of AuNPs with different density.

The distribution of the estimated FSS quenching efficiency over different densities of AuNP-BCs is shown in Figure 5-5. The examined quenching efficiency of FSS on the high density of AuNP-BC revealed a narrower distribution, while a decrease in the density of AuNP-BC leads to a broader distribution. In fact, in FRET, the efficiency of energy transfer from donor to acceptor increases by the enhancement of acceptor molecules [28]. Due to the special design of the nanopaper platform employed as an acceptor, each excited FSS is simultaneously influenced by multiple AuNPs. This effect was remarkably diminished for the low density AuNP-BC, due to the large distance between nanoparticles. So, each FSS may be affected by the exceptionally less number of AuNPs; only the nearer ones to AuNP endure higher rate of energy transfer. As such, this effect is attributed as the main reason for the broader distribution of FSS quenching efficiency for AuNP-BC of lower density.

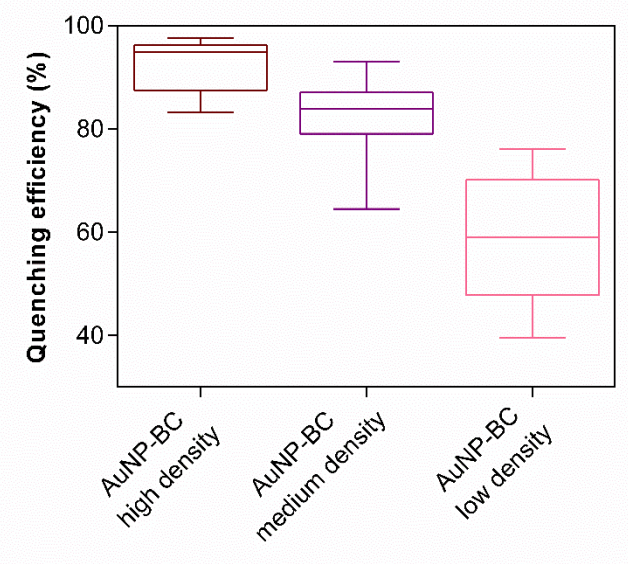

Figure 5-5. Distribution of the evaluated FSS quenching efficiency regarding to AuNP-BCs densities over different concentrations of FSS.

To verify if the quenching behavior of fluorophore can be affected by its structure, carboxylated quantum dot (QD), with an emission wavelength of 525 nm, was also employed. Despite its unique nano-spherical structure, its emission overlap with AuNP-BCs is similar to the emission spectra of FSS. Although the results are not presented here, our observations confirmed its quenching efficiency followed the same behavior as FSS.

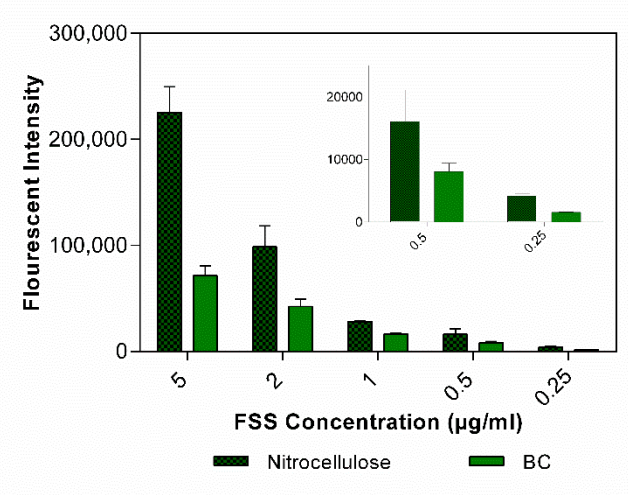

Figure 5-6. A comparison between FSS fluorescent intensity cast on the surface of nitrocellulose and BC. The graph insight is just a magnification of the last two concentrations. The measured

fluorescent intensities were the result of applying 5 µl of FSS with different concentration on the surface of BC or nitrocellulose.

It is worth mentioning that we also observed a significant difference in the photoluminescence intensity of FSS cast on the BC pieces (previously named as I_0) compared with the same amount spotted on nitrocellulose, as presented in Figure 5-6. The fluorescent emission spectra of bare nitrocellulose, excited at the wavelength of 460 nm (same excitation wavelength of FSS), revealed a peak at 505 nm, which may be related to impurities involved with cellulose [29]. At the same excitation condition, the drop casted FSS (in 5 µl/mg) on nitrocellulose displayed a photoluminescence 26.9-times higher than that of the nitrocellulose background. So, the high luminescence of FSS was not due to its background, however, the main reason for this phenomenon is still unclear. As compared in Figure 5-6, the obtained fluorescent intensity from the spotted FSS on the BC was notably less than the similar ones measured on the nitrocellulose. It may be attributed to the overlap between BC absorbance spectra and FSS emission spectra as presented in Figure 5-1B. Our findings also demonstrated that the QD exhibited higher fluorescent intensity when it was cast on nitrocellulose in comparison with BC. The significant reduction of the photoluminescence, it may restrict the application of BC as a nano-based platform to carry fluorescent molecules with similar emission spectra in bioassay.

5.5 Conclusion

In this work, we presented the potential of AuNP-BCs in quenching the emitted photons from fluorophores, such as FSS and QD in Fluorescence (Föster) resonance energy transfer (FRET) phenomena. It was found that the quenching efficiency is determined by the density of AuNPs embedded in BCs. By adjusting the precursor concentration, it was possible to successfully modulate the population density and distribution of AuNPs. Therefore, the developed nanostructure was assessed as a powerful solid-based quencher in FRET. Additionally, the broad absorbance spectra of AuNP-BC can have a large overlap with emission spectra of various fluorophores which can make it an appropriate substrate for the design of multiplex recognition FERT-based bioassays. Besides, the availability of functional groups, either provided by the BC or the AuNP, can offer a variety of biomolecule conjugation on this solid substrate. Owing to these properties, as well as its flexibility and biocompatibility, this platform can open new opportunities for nanopaper-based biosensors for application in the medical, environmental, and foodpackaging sectors. It can also be

used to improve approaches in the mobile-based detection which are of great interest in the future of biosensors.

5.6 Acknowledgments

The authors would like to thank the NSERC (Natural Science and Engineering Research Council of Canada), and ProAmpac, the industrial partner of 3SPack Chair for funding this project and financial support.

5.7 References

[1] J. Shi, F. Tian, J. Lyu, and M. Yang, "Nanoparticle based fluorescence resonance energy transfer (FRET) for biosensing applications," *Journal of Materials Chemistry B,* vol. 3, pp. 6989-7005, 2015.

[2] P. C. Ray, Z. Fan, R. A. Crouch, S. S. Sinha, and A. Pramanik, "Nanoscopic optical rulers beyond the FRET distance limit: fundamentals and applications," *Chemical Society Reviews,* vol. 43, pp. 6370-6404, 2014.

[3] K. E. Sapsford, L. Berti, and I. L. Medintz, "Materials for fluorescence resonance energy transfer analysis: beyond traditional donor–acceptor combinations," *Angewandte Chemie International Edition,* vol. 45, pp. 4562-4589, 2006.

[4] B. Hötzer, I. L. Medintz, and N. Hildebrandt, "Fluorescence in nanobiotechnology: sophisticated fluorophores for novel applications," *Small,* vol. 8, pp. 2297-2326, 2012.

[5] E. Morales-Narváez, B. Pérez-López, L. B. Pires, and A. Merkoçi, "Simple Förster resonance energy transfer evidence for the ultrahigh quantum dot quenching efficiency by graphene oxide compared to other carbon structures," *Carbon,* vol. 50, pp. 2987-2993, 2012.

[6] B. Dubertret, M. Calame, and A. J. Libchaber, "Single-mismatch detection using gold-quenched fluorescent oligonucleotides," *Nature biotechnology,* vol. 19, pp. 365-370, 2001.

[7] J. Griffin, A. K. Singh, D. Senapati, P. Rhodes, K. Mitchell, B. Robinson, *et al.*, "Size-and Distance-Dependent Nanoparticle Surface-Energy Transfer (NSET) Method for Selective

Sensing of Hepatitis C Virus RNA," *Chemistry–A European Journal,* vol. 15, pp. 342-351, 2009.

[8] E. Hutter and D. Maysinger, "Gold nanoparticles and quantum dots for bioimaging," *Microscopy research and technique,* vol. 74, pp. 592-604, 2011.

[9] K. Saha, S. S. Agasti, C. Kim, X. Li, and V. M. Rotello, "Gold nanoparticles in chemical and biological sensing," *Chemical reviews,* vol. 112, pp. 2739-2779, 2012.

[10] E. Dulkeith, A. Morteani, T. Niedereichholz, T. Klar, J. Feldmann, S. Levi, *et al.*, "Fluorescence quenching of dye molecules near gold nanoparticles: radiative and nonradiative effects," *Physical review letters,* vol. 89, p. 203002, 2002.

[11] Y.-P. Kim, Y.-H. Oh, E. Oh, S. Ko, M.-K. Han, and H.-S. Kim, "Energy Transfer-Based Multiplexed Assay of Proteases by Using Gold Nanoparticle and Quantum Dot Conjugates on a Surface," *Analytical Chemistry,* vol. 80, pp. 4634-4641, 2008/06/01 2008.

[12] C. Li, J. Zuo, Q. Li, Y. Chang, Y. Zhang, L. Tu, *et al.*, "One-step in situ solid-substrate-based whole blood immunoassay based on FRET between upconversion and gold nanoparticles," *Biosensors and Bioelectronics,* vol. 92, pp. 335-341, 2017.

[13] M. O. Noor and U. J. Krull, "Paper-based solid-phase multiplexed nucleic acid hybridization assay with tunable dynamic range using immobilized quantum dots as donors in fluorescence resonance energy transfer," *Analytical chemistry,* vol. 85, pp. 7502-7511, 2013.

[14] M. O. Noor, A. Shahmuradyan, and U. J. Krull, "Paper-based solid-phase nucleic acid hybridization assay using immobilized quantum dots as donors in fluorescence resonance energy transfer," *Analytical chemistry,* vol. 85, pp. 1860-1867, 2013.

[15] D. Zhang, D. Broyles, E. A. Hunt, E. Dikici, S. Daunert, and S. K. Deo, "A paper-based platform for detection of viral RNA," *Analyst,* vol. 142, pp. 815-823, 2017.

[16] X. Cai, Q. Yang, J. Ding, W. Ye, X. Li, and J. Xiao, "Paper-based FRET for the direct detection of collagen triple helix," *Journal of Materials Chemistry B,* vol. 4, pp. 7009-7013, 2016.

[17] S. K. Mahadeva, K. Walus, and B. Stoeber, "Paper as a platform for sensing applications and other devices: A review," *ACS applied materials & interfaces,* vol. 7, pp. 8345-8362, 2015.

[18] E. Nery and L. Kubota, "Sensing approaches on paper-based devices: a review," *Analytical and Bioanalytical Chemistry,* vol. 405, pp. 7573-7595, 2013/09/01 2013.

[19] E.-S. Kim, C.-K. Shim, J. W. Lee, J. W. Park, and K. Y. Choi, "Synergistic effect of orientation and lateral spacing of protein G on an on-chip immunoassay," *Analyst,* vol. 137, pp. 2421-2430, 2012.

[20] D. Klemm, B. Heublein, H.-P. Fink, and A. Bohn, "Cellulose: Fascinating Biopolymer and Sustainable Raw Material," *Angewandte Chemie International Edition,* vol. 44, pp. 3358-3393, 2005.

[21] R. J. Moon, A. Martini, J. Nairn, J. Simonsen, and J. Youngblood, "Cellulose nanomaterials review: structure, properties and nanocomposites," *Chemical Society Reviews,* vol. 40, pp. 3941-3994, 2011.

[22] E. Morales-Narváez, H. Golmohammadi, T. Naghdi, H. Yousefi, U. Kostiv, D. Horák, *et al.*, "Nanopaper as an Optical Sensing Platform," *ACS nano,* vol. 9, pp. 7296-7305, 2015.

[23] N. Pourreza, H. Golmohammadi, T. Naghdi, and H. Yousefi, "Green in-situ synthesized silver nanoparticles embedded in bacterial cellulose nanopaper as a bionanocomposite plasmonic sensor," *Biosensors and Bioelectronics,* vol. 74, pp. 353-359, 2015.

[24] B. Heli, E. Morales-Narvaez, H. Golmohammadi, A. Ajji, and A. Merkoci, "Modulation of population density and size of silver nanoparticles embedded in bacterial cellulose via ammonia exposure: visual detection of volatile compounds in a piece of plasmonic nanopaper," *Nanoscale,* vol. 8, pp. 7984-7991, 2016.

[25] A. J. Brown, "XLIII.—On an acetic ferment which forms cellulose," *Journal of the Chemical Society, Transactions,* vol. 49, pp. 432-439, 1886.

[26] T. Zhang, W. Wang, D. Zhang, X. Zhang, Y. Ma, Y. Zhou, *et al.*, "Biotemplated synthesis of gold nanoparticle–bacteria cellulose nanofiber nanocomposites and their application in biosensing," *Advanced Functional Materials,* vol. 20, pp. 1152-1160, 2010.

[27] X. Hu, T. Wang, X. Qu, and S. Dong, "In situ synthesis and characterization of multiwalled carbon nanotube/Au nanoparticle composite materials," *The Journal of Physical Chemistry B*, vol. 110, pp. 853-857, 2006.

[28] R. C. Somers, M. G. Bawendi, and D. G. Nocera, "CdSe nanocrystal based chem-/bio-sensors," *Chemical Society Reviews*, vol. 36, pp. 579-591, 2007.

[29] J. H. Zhu and D. G. Gray, "Fluorescence emission from mechanical pulp sheets II. Estimation of quantum yields," *Journal of Photochemistry and Photobiology A: Chemistry*, vol. 73, pp. 67-74, 1993.

CHAPTER 6 ARTICLE 3: TOWARD A NANOPAPER-BASED AND SOLID PHASE IMMUNOASSAY USING FRET FOR RAPID DETECTION OF BACTERIA

Bentolhoda Heli[1], Arben Merkoçi[2], Abdellah Ajji[1*]

[1] 3SPack, CREPEC, Département de génie chimique École Polytechnique de Montréal, Montréal, Québec, Canada.

[2] Nanobioelectronics and Biosensor GroupCatalan Institute of Nanoscience and Nanotechnology (ICN2) CSIC and BIST Campus UAB, Bellaterra, 08193 Barcelona, Spain

Submitted to: Biosensors & Bioelectronics

KEYWORDS: bacterial cellulose, nanopaper, gold nanoparticle, FRET method, immunosensor, pathogen detection, *E. coli*

6.1 Abstract

In this study, we propose a novel and sensitive FRET-based immunosensor for the detection of *E. coli* bacteria, developed on a nanopaper platform. The nanopaper platform was composed of carboxylated bacterial cellulose impregnated with gold nanoparticles (AuNPs). The as-synthesized platform was simultaneously exploited as the acceptor in FRET approach and, also as a substrate for the integration of biorecognition element. The anti-*E. coli* conjugated quantum dot (QD) (emitting at 525 nm and serving as the donor) was linked to the protein A/G, immobilized on the nanopaper platform through a covalent bond. Interestingly, once *E. coli* was captured by the anti-*E. coli*-QD, the energy transfer triggered due to the conformational change in the antibody structure and this, in turn, caused a reduction in the distance between the donor and acceptor. The limit of detection of *E. coli* was estimated to be around 10 CFU.mL^{-1} by the proposed immunosensor.

6.2 Introduction

During the last decades, the outbreak of foodborne diseases has seriously threatened people's lives worldwide and led to a considerable number of hospitalizations and even deaths [1, 2]. In fact, the incidence of foodborne infection is a result of ingesting food, which includes vegetables, and beverages, contaminated by foodborne pathogens. Generally, food sources can be contaminated with fatal pathogen during the processing and handling that takes place in delivering food from the farms to our table. However, precise monitoring and early recognition of pathogen can ensure the safety of our food and prevent the subsequence of foodborne pathogen that is widespread [3].

Various conventional methods, such as microbiological plate culturing and biochemical screening, have been used to detect bacteria quantitatively and qualitatively [4]. However, as they are expensive, have a long processing time, and require scientific expertise, their application has become restricted in the high-demand food industries [4]. So, to address the needs, it is crucial to develop a fast, highly selective and sensitive, low-priced, in-situ and user-friendly recognition device. Researchers all over the world are essaying to design the miniaturized tools that would improve the challenge of the foodborne pathogen detection, with the help of engineered nanomaterials and the science of nanotechnology [5, 6]. Nanoscale materials, with a size less than 100 nm are endowed with unique physical and chemical properties such as high surface area,

optical and electrical characteristics, which offer myriad opportunities about sensing technology [7, 8].

Among the various biosensing approaches and fabricated bioassays, fluorescence-based methods, such as the Förster (fluorescence) resonance energy transfer (FRET), have increasingly emerged as a promising approach due to their sensitivity, selectivity, and rapidness [9]. The feasibility of a FRET-based immunosensor has been studied in varieties of configurations for the detection of pathogen [10-12]. This phenomenon includes a non-radiative energy transfer between a pair of donor and acceptor molecules, with an extreme sensitivity to their distance [13]. The performance of FRET can be enhanced by maximizing the overlap of donor emission spectrum and absorbance spectra of the acceptor [14].

Owing to their narrow emission spectra, broad absorbance band, and high photostability, semiconductor quantum dots (QDs) have proven to be one of the effective donor candidates [15]. Particularly, their combination with size-tunable gold nanoparticles (AuNPs), with an efficient fluorescent quenching over a broad range of photoexcited QDs, enables them to be excellent donor-acceptor pairs for bioassay tools [16, 17].

Recently, exploiting the features of bacterial cellulose (BC) (such as crystalline nano-micro fibril structure, high mechanical strength, high porosity, surface area, and transparency) in combination with in-situ synthesized noble metal nanoparticles (gold and silver nanoparticles) has led to the development of improved plasmonic nanopaper [18]. Subsequently, its application as a successful optical sensor of either water-soluble species or volatile organic compounds (VOC) in dry state has been ascertained [18-20]. Moreover, in our previous effort, we studied this plasmonic nanopaper as a strong quencher, which absorbed up to 95% of the energy transfer from the high concentration of a photoexcited donor [21]. We also showed that the quenching efficiency is dependent on the density of the AuNP inside BC, as the quenching efficiency reduced with the decrease in the AuNP density.

To the best of our knowledge, there is no report of as-synthesized nanopaper applied in a FRET-based immunosensor yet. In this paper, we describe a novel, versatile, and sensitive immunosensor based on FERT, which utilizes gold nanoparticles embedded in carboxylated BC (AuNP-CBC) as nanopaper-based acceptor. As the Scheme 6-1 presents the operational concept of proposed immunosensor, the distinctive structure of the CBC and its abundant functional groups facilitated

the layer-by-layer assembly of gold nanoparticles and biomolecules. So, first, the protein A/G was covalently immobilized on the nanofiber surface of the AuNP-CBC. Second, the antibody conjugated QD (Ab-QD) (with emission wavelength of 525 nm) bonded with the protein A/G in a well-oriented configuration. The interaction of the analyte with the Ab-QD caused an alteration in the luminescence of the QD. This was due to the change of distance between the QD and the acceptor nanopaper, as the result of the conformational change induced in the antibody structure after its interaction with the analyte [22, 23]. The performance of this nanopaper-based immunosensor as a model was evaluated through the response gathered from the interaction of anti-HRP (HAb) and HRP, and at the end, it was finalized for the detection of *E. coli* as the representative of pathogenic bacteria.

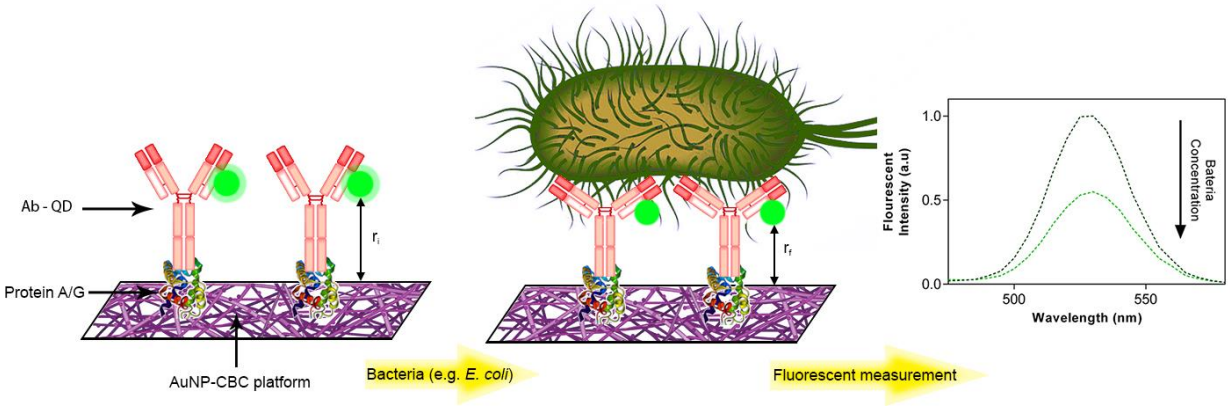

Scheme 6-1. The operational concept of proposed immunosensor. The carboxylated bacterial cellulose impregnated with AuNP (CBC-AuNP) is implemented as the solid platform to support the essential biorecognition elements, protein A/G and Ab-QD. Upon recognition of bacteria by the immunosensor there is a conformational change in the 3D structure of the Ab-QD that leads to the decrease of QD photoluminescence. This phenomenon is due to the reduction of effective distance between donor (QD) and acceptor (AuNP-CBC) from r_i to r_f. It should be noted that the scale of this scheme is irrelevant.

6.3 Experimental methods

6.3.1 Reagents and instruments

The nanopaper-based substrate, bacterial cellulose (BC), was obtained from Nanonovin Polymer Co. (Mazandaran, Iran). To oxidize BC and create carboxyl groups, sodium hypochlorite solution

(NaOCl), 2,2,6,6-Tetramethyl-1-piperidinyloxy 98% (TEMPO) and sodium bromide (NaBr) were purchased from Sigma-Aldrich Co. LLC (Oakville, Canada). The reagents such as 2-(N-Morpholino) ethanesulfonic acid (MES), the tablet of phosphate buffered saline (PBS), N-Ethyl-N′-(3-dimethylaminopropyl) carbodiimide hydrochloride (EDC), citric acid trisodium salt and gold (III) chloride trihydrate ($HAuCl_4 \cdot 3H_2O$) were provided from Sigma-Aldrich. The anti-peroxidase antibody produced in rabbit and horseradish peroxidase (HRP) (peroxidase from horseradish type VI) were acquired from the same supplier. TMB (3,3′,5,5′-Tetramethylbenzidine) solution substrate, used as HRP substrate for enzymatic reaction, was purchased from Thermo Fisher Scientific Inc (Ottawa, Ca). Also, Sulfo-NHS (N-hydroxysulfosuccinimide) and Pierce™ recombinant protein A/G were provided from Thermo Fisher Scientific Inc. Carboxyl Quantum dots (Qdot 525 ITK) was supplied from Invitrogen Co. (Carlsbad, Canada). Polyclonal antibody produced in rabbit against *E. coli* DH-5α without any BSA was purchased from Bioss Inc. (Ma, USA). The other reagents used in the experiments that are probably not mentioned here were obtained from Sigma-Aldrich.

Amicon ultra-0.5 mL centrifugal filters, MWCO 100 kD, was acquired from Millipore Corp. (Ontario, Canada). Samples were placed in the Costar 96 microplates (black and transparent, flat bottom) provided by Corning Inc. (Kennebunk, Me). Thermo-shaker incubator for micro tube and plate rack, used in antibody-QD conjugation and protein A/G immobilization was obtained from MBI (Montreal Biotech Inc., Canada). Measuring UV-Vis absorbance spectra and fluorophores emission spectra were carried out with Infinite 200 PRO (Tecan, Switzerland) microplate reader. Scanning electron microscopy (SEM) was performed by Hitachi's ultra-high resolution SU8200 FE-SEM operated at 1 kV (Hitachi High-Technology Cor., Japan).

6.3.2 Carboxylation of bacterial cellulose (CBC)

In general, the carboxyl functional groups are created on the nanofibrils of the BC by the TEMPO-oxidation procedure. As previously described [24], to obtain the carboxylated BC (CBC), 250 mg of dried BC was dispersed in 150 ml of Milli-Q water, which contained dissolved TEMPO (7.8 mg) and NaBr (78 mg). To start the oxidation, 11 wt % NaOCl with the ratio of 8:1 (mmol/ gr BC) was added to solution, and pH was adjusted to 10.5 by adding 0.1 M HCl. Since the pH of the solution decreased during the oxidation reaction, it was kept constant at 10.5 by adding 0.1 M NaOH. After an hour of gentle mixing at room temperature, the reaction was stopped by adding

ethanol to reach the pH of 7. The CBC was separated from the reaction solution and washed sufficiently with ethanol, and then with Milli-Q water. The obtained CBC was finally preserved in Milli-Q water.

To determine the content of carboxyl groups on the BC fibers, conductometric titration was performed on the as-oxidized BC [25]. 50 mg of dried and oxidized BC was dispersed in 50 ml of Milli-Q water. To protonate all carboxyl groups, 0.1 M HCl was added to the solution to reach pH of around 2.5. Then, the suspension was titrated with 0.01 M NaOH, and the changes in the conductivity of the solution were recorded to obtain the final pH of 11. The carboxyl group content was estimated by the obtained titration curve.

6.3.3 In-situ synthesis of AuNP within CBC (AuNP-CBC)

The CBC was impregnated with AuNPs in accordance with the Turkevich procedure [26]. 15 pieces of CBC (1×1 in^2) were soaked and mixed in 100 ml of $HAuCl_4$ solution with a concentration of 0.09 mM. The mixture was brought to boiling point, and citric acid trisodium solution (875 µl, 40 mM) was rapidly added to the container. Following 1 h of the same reaction condition, the gold ions were gradually reduced to AuNPs within the nanofibrils of the CBC. The formation of the AuNPs was indicated by the color change of the CBC from colorless to light purple. At that moment, the stirring of the mixture was continued without heating, to reach room temperature. Then, the synthesized AuNP-CBCs pieces were separated from the mixture and washed with plenty of Milli-Q water to remove all unreacted Au ions and free AuNPs. The obtained AuNP-CBC pieces were dried at room temperature by keeping them between pieces of filter paper to preserve them from wrinkle.

6.3.4 Protein A/G immobilization on the CBC and the AuNP-CBC

The protein A/G was covalently immobilized on the surface of the CBC and the AuNP-CBC through EDC/Sulfo-NHS chemistry. In short, the activated carboxyl groups on the surface of the nanofibrils were bound to the primary amines of the protein A/G. The immobilization procedure was as follows: EDC and Sulfo-NHS solution was freshly prepared by dissolving in 0.01 M MES pH 5. The respective nanopapers were cut in circular shape of 6 mm and placed in 96 wells microplate. Then, the nanopapers platforms were sequentially washed with water, 0.01 M PBS pH 7.4, and 0.01 M MES buffer pH 5 (each step was done for 20 min at room temperature and 650

rpm). Then, 40 µl of the fresh mixture of EDC and Sulfo-NHS, composed of 5 mM EDC and 4.6 mM Sulfo-NHS with the ratio of 1:2 (mole/mole), was added to the nanopapers platforms. The activation was completed in 20 min by incubation in a thermos-shaker at room temperature and 650 rpm.

As the ultimate purpose is to obtain the immobilized protein A/G on the AuNP-CBC, successive experiments were conducted to determine the efficient conditions of immobilization. These conditions were first evaluated on the surface of the CBC, and later induced into the AuNP-CBC. The strategy was as follows: 1) Investigating the effect of pH: 40 µl of 0.1 mg/ml protein A/G dispersed in 0.01 M MES with pH 4.1 and PBS with pH 7.4 was separately added to the activated CBC. 2) Determining the optimum amount of the protein A/G: 40 µl protein A/G with the concentrations of 0.3, 0.1, and 0.033 mg/ml (dispersed in the buffer selected from the earlier experiment) was immobilized on the surface of the activated CBC. The immobilization was accomplished through 2 h incubation in the thermo-shaker at room temperature and 650 rpm. Then, the unreacted protein A/G was removed and kept for a later Bradford assay analysis. After washing the resultant CBC immobilized with the protein A/G with MES and PBS buffer, the unreacted active carboxylates were blocked with 1% BSA in PBS pH 7.4 for 1 h at room temperature. The obtained nanopaper complex was stored at 4 °C for the following experiments.

6.3.5 Conjugation of antibody to quantum dot

Two different antibodies were explored in the experiment, anti-HRP (HAb) as a model antibody to evaluate the developed bioassay and anti-*E. coli* (EAb) as a model for the pathogen detection. The conjugation of carboxylated QD to antibody was performed by a previously described method [27]. At first, 10 µl of the fresh solution of EDC/Sulfo-NHS, as explained above, was mixed with 200 µl of 1.2 nM QD dispersed in 0.01 M MES buffer pH 5. After that, the activation of carboxyl groups of the QD was completed by incubating the mixture in the thermos-shaker for 30 min at room temperature and 650 rpm. The excess solution was eliminated through Amicon Ultra-0.5 ml centrifugal filters, cutoff 50 kDa for 7 min at 12,000 rpm. The resulting filtrate QD was diluted with 0.01 M MES pH 5 to reach 100 µl, and then mixed with 100 µl of HAb or EAb with the concentration 36 µg/ml. Next, it was incubated for 2h at 24 °C and 650 rpm. The free activated carboxyl groups were blocked by 20 µl of 1% BSA dissolved in PBS by the incubation of the solution for 30 min in the same condition. The obtained conjugate solution was filtered by Amicon

Ultra-0.5 ml, cutoff 100 kDa. Finally, the resultant Ab-QD conjugate was preserved at 4 °C. Its dilution (in 0.01 M PBS and 0.5% Tween 20 solution) would be according to the needs of the next steps.

6.3.6 Characterization of the immobilized protein A/G on nanopaper-based platform

The performance of nanopaper-based platforms integrated with the protein A/G were explored as follows: (i) The samples of CBC and the AuNP-CBC, immobilized with the protein A/G at different conditions, were incubated with 100 µl Ab with the concentration of 36 µg/ml. The immobilization was accomplished by overnight incubation at 4 °C and 650 rpm. Then, the excess solution was discarded, and the samples were washed three times with PBS. (ii) The 100 µl of the resultant HAb-QD (diluted 6 times) were incubated in the AuNP-CBC and CBC samples with the final immobilized protein A/G. The same condition of incubation as explained above was applied here. (iii) Finally, we pursued an optical test to verify the performance of the obtained nanopaper-biomolecules. Briefly, 20 µg of HRP in PBS buffer (10 mM, pH 7.4) was added to the obtained nanopapers and made to interact with antibodies for 1 h at room temperature and 650 rpm. Then, the uncaptured HRP was discarded by washing three times with PBS. The blank samples were considered to be the nanopaper immobilized with the protein A/G and HRP. Afterward, 120 µl of TMB, the substrate for the enzymatic reaction of HRP, was added to the resultant nanopapers. After 30 s, the reaction was stopped by adding 120 µl of 2 M HCl while the solution color changed from yellow to blue. The optical density of the produced color was then measured at 460 nm by TECAN spectroscopy device. Besides, the fluorescent intensity of those samples that contained the HAb-QD was estimated at 525 nm by exciting it at 350 nm before and after its interaction with HRP.

6.3.7 Pathogen recognition platform

The immunosensor platform for pathogen recognition proceeded, as explained before, by the immobilization of the protein A/G on the surface of AuNP-CBC. EAb-QD was diluted in PBS (0.01 M, pH 7.4, 0.5% Tween 20) to acquire the final concentration of 6 µg/ml and 0.2 nM for the EAb and the QD, respectively. Then, it was incubated overnight in the nanopaper immobilized protein A/G platform at 4 °C and 650 rpm. After eliminating the excess reactants and washing the final assembled platform, its initial fluorescent intensity (excited at 350 nm and emitted at 525 nm)

was recorded by the TECAN and named I_i. Following that, it was assessed for bacteria detection. Two strains of bacteria were investigated here, *Escherichia coli* (DH5α) as representative of pathogenic *E. coli* and *Staphylococcus aureus* (54-73) (*S. aureus*) as the control bacteria. The bacteria preparation steps are explained in detail in the supporting information. The serial dilutions of the bacteria, *E. coli* and *S. aureus*, were prepared in PBS from 10^8 to 10 CFU.ml^{-1}. 100 µl of the bacterial suspensions were allocated to the immunosensor platform and incubated for 1.5 h at 25 °C. Next, the unattached bacteria was discarded by washing. Lastly, the final fluorescent intensity (I_f) of the immunosensor was measured at the same excitation wavelength. The overall performance of the fabricated immunosensor, presented in terms of QD quenching efficiency, was evaluated by the following equation:

$$\varphi_F = 1 - \frac{I_f}{I_i}$$

The presented results in the following sections were obtained by means and standard deviation of three different samples which confirm the validity and reproducibility of the experiments.

6.4 Results and discussion

The utilized bacterial cellulose (BC), with the appearance similar to a hydrogel sheet, was produced by acetic acid bacteria (e.g., *Acetobacter xylinum*) through oxidative fermentation of a medium [28]. The synthesized BC has a high degree of cellulose purity with a 3D structure composed of the nanofibrils with the diameter around 50-60 nm, resulted from the glucan chains linked strongly together by hydrogen bonds [29]. This unique structure and features of BC facilitate the design of our proposed immunosensor by providing enough functional groups.

6.4.1 Carboxylation of bacterial cellulose (CBC)

First, inducing carboxyl groups by oxidization of the BC nanofibers through TEMPO/NaBr/NaClO in aqueous solution transformed it into a nanopaper-based platform, which is simply linked to the biomolecules. Basically, TEMPO-mediated oxidation selectivity treats the primary hydroxyl groups located at C6 of the cellulose molecule [24]. As-resulted carboxyl groups content on the CBC was estimated to be 0.5 mmol.g^{-1} BC through the conductivity titration curve. The induced carboxyl groups were assigned later for carboxyl-amine conjugation of protein on the surface of the CBC.

6.4.2 In-situ synthesis of AuNP within CBC

Second, by embedding the AuNP within the CBC, we obtained a nanopaper and solid-based platform with robust quenching behavior applicable to the FRET method. Through the Turkevich method, Au ions were reduced, capped by citrate ions and led to the in-situ synthesized AuNP-CBC. Due to the synthesis of AuNP, the color of CBC pieces was changed to purple which was detectable by naked eyes. Besides, as Figure 6-1.A shows electron microscopy imaging, AuNPs are uniformly distributed inside of the CBC nanofibrils. Moreover, the plasmonic properties of AuNP-CBC is illustrated by its UV-Vis absorbance spectra with a peak at 530 nm (Figure 6-1.B). The density of the AuNPs was adjusted by the concentration of the Au precursor, as we have previously demonstrated that the quenching behavior of a similar platform was dependent on it [21]. With respect to our funding, it is estimated to achieve a maximum quenching efficiency between 60%-70% through the obtained AuNP-CBC platform. Also, the evaluated carboxyl group content of AuNP-CBC (see experimental section) was 0.45 mmol.g^{-1}, which reduced slightly in comparison to those without AuNP. The carboxyl groups may be either hindered by the AuNPs or attributed to the formation of nanoparticles. Thus, the obtained nanopaper inherently took advantage of the CBC with its carboxyl groups, plasmonic properties of AuNP and its behavior of absorbing the energy transfer in the FRET method.

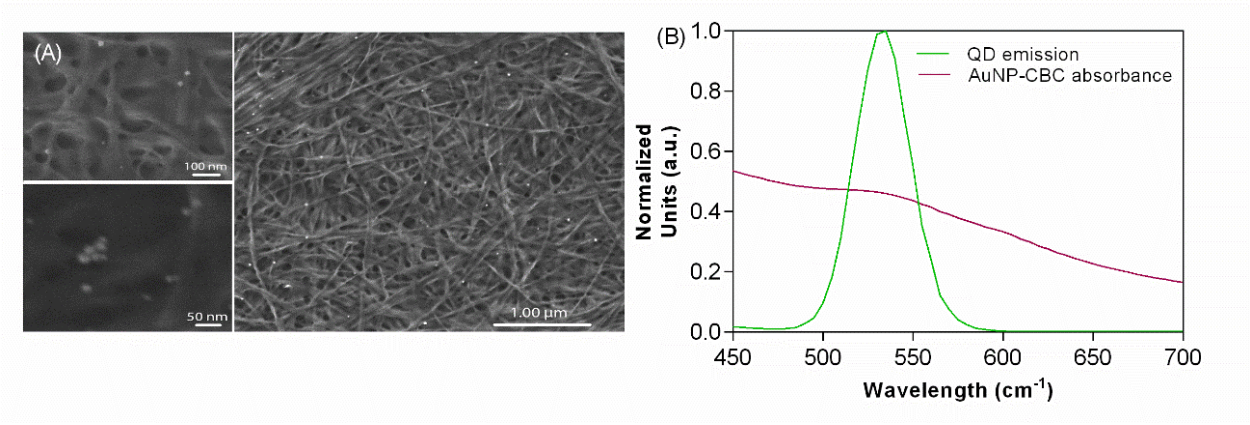

Figure 6-1. Characterization of the obtained AuNP-CBC, (A) scanning electron microscope (SEM) imaging from AuNP-CBC, (B) UV-Vis absorbance spectra of as-synthesized AuNP-CBC along with its overlap with emission spectra of QD (excited at 350 nm).

6.4.3 Protein A/G immobilization on the nanopaper platform and its characterization

Protein A/G (composed of the properties of protein A and protein G) is a recombinant protein that can bind strongly to the Fc region of an antibody, and therefore, a well-oriented antibody configuration can be obtained by its binding [30, 31]. Here, the protein A/G was immobilized on the surface of the bare CBC and AuNP-CBC through EDC/Sulfo-NHS chemistry by covalent binding between amino groups of the protein A/G and its activated carboxyl groups. The performance of the bound protein A/G was verified by its interaction with the model antibody (anti-HRP). Since the protein A/G plays a significant role in the orientation of the conjugated antibody, it would affect the final sensitivity of the immunosensor. Therefore, having the well-established antibody on the surface of the nanopaper is an essential step in the preparation of a highly efficient immunosensor. The suggested strategy would allow us to improve our understanding of the functionality of the bioassay platform. Previous studies have explored the direct correlation of properly immobilized protein A/G with the amount of bound antibodies that decisively influenced their interaction with the respective antigen [30, 32]. On the other hand, the number of captured analytes (e.g. HRP) can directly correspond to the respective antibodies. As a result, when the activity of HRP, which interacted with anti-HRP, is estimated by optical density, it would refer to the situation of the protein A/G that was immobilized by the particular conditions on the nanopaper platform.

First, the study of the effect of pH on immobilization of the protein A/G on the surface of the CBC, as presented in Figure 6-2A, showed the higher response of HRP captured by anti-HRP, corresponded to the protein A/G immobilized at pH of 4.1. Moreover, the Bradford assay analysis confirmed more amount of the immobilized protein A/G at this pH in comparison to the ones immobilized at pH of 7.4. As displayed in Table S6-1, the evaluated amount of the immobilized protein A/G is 3.96±0.04 and 2.62±0.01 µg for the reaction with pH at 4.1 (MES 0.01 M) and 7.4 (PBS 0.01 M), respectively. This pH of immobilization is very close to the isoelectric point (PI) of the protein A/G (4.65, supplier's data) which can impose a charge distribution on the amino group of the protein A/G, different from the other pH. This fact can control the orientation of the deposited protein A/G, which can significantly influence the antibody linkage with the protein A/G. Second, our experiments revealed the potential of the CBC to bind with the protein A/G (see Figure 6-2B).

However, the maximum amount of the protein A/G that bonded to the CBC was measured about 11.76±0.14 µg (presented in Table S6-1), the higher estimated performance of HRP was acquired for 4.29±0.05 µg of the immobilized protein A/G. It was also noted that if the immobilized protein A/G was reduced to 1.31±0.09 µg (67% less protein A/G in comparison with the previous amount), HRP activity decreased by 30%, which indicated a nonlinear correlation. These results may suggest the strong effect of hindrance. On the other hand, the increase in the number of the protein A/G on the CBC nanofibers caused the increase in the number of linked antibodies on the protein A/G. Due to this aggregation, the active sites of anti-HRP might be hindered, and therefore, it would be prevented from the appropriate accessibility for the attachment of HRP to the antibody. Given that the strategy of the protein A/G immobilization on the surface of the nanopaper affected its orientation and hindrance, its assessment for each individual platform was necessary to increase the sensitivity of the developed bioassay.

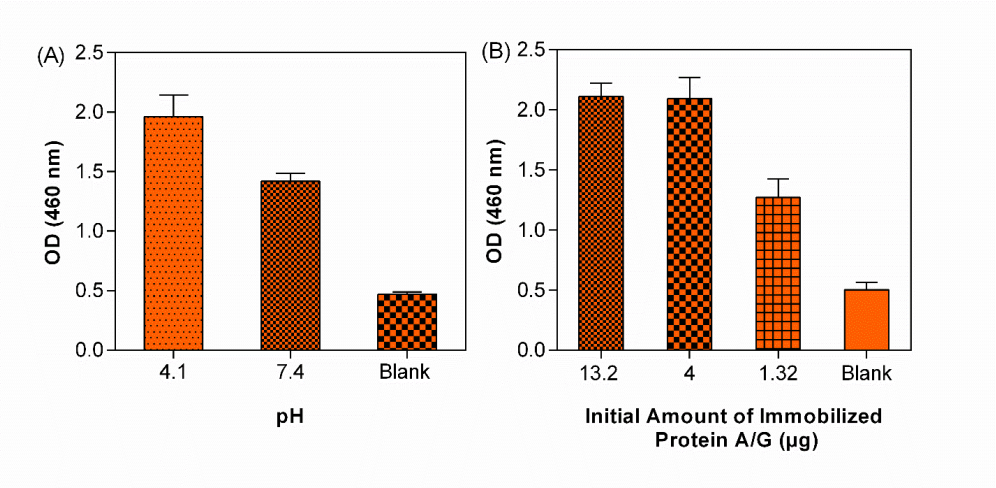

Figure 6-2. The optical density recorded at 460 nm as a result of the enzymatic reaction of HRP and TMB. It presents the situation of the protein A/G immobilized on the surface of CBC by the interaction between the amounts of HAb linked to protein A/G as well as captured HRP. (A) the effect of pH on the immobilization of protein A/G and, (B) the effect of the initial amount of protein A/G on its immobilization.

As-determined high efficient conditions of protein A/G immobilization on CBC were assigned thereafter for its immobilization to AuNP-CBC surface. The Bradford assay analysis indicated that 2.77±0.09 µg of the protein A/G was bonded to carboxylated AuNP-CBC (see Table S6-1). This result is in agreement with the outcome of conductimetry titration, as it previously revealed a

reduction in the content of carboxyl groups after synthesis of AuNPs. So, the decrease of available functional groups led to a reduction in immobilized protein A/G. However, as noted in Figure 6-3A, this decline in protein A/G did not considerably influence the response of the HAb-QD, and the HAb bonded to the protein A/G immobilized on AuNP-CBC in comparison to those bonded to CBC. It is worth mentioning that the negligible difference between the observed HRP optical density captured by the HAb-QD and that captured by the bare HAb (see Figure 6-3A) may be attributed to the presence of QD. According to the size of the conjugated QD (3.54±0.52 nm, shown in Figure S6-1) and its position in the antibody, it may insignificantly impact the ability of the antibody to bind to the antigen or link to protein A/G. Despite this trial effect, the overall performance of the developed bioassay for HRP recognition was estimated through the change of intensity of QD fluorescence. As Figure 6-3B presents, a quenching efficiency of 20% was assessed by the interaction of HRP and HAb-QD. It confirmed that the conformational change of HAb-QD resulted in the alteration of the distance between QD and AuNP-CBC. The change in the antibody structure is notably affected by the type and size of antigen; as binding to a larger antigen, such as bacteria, can induce more changes in the constant and variable domains of the antibody [22].

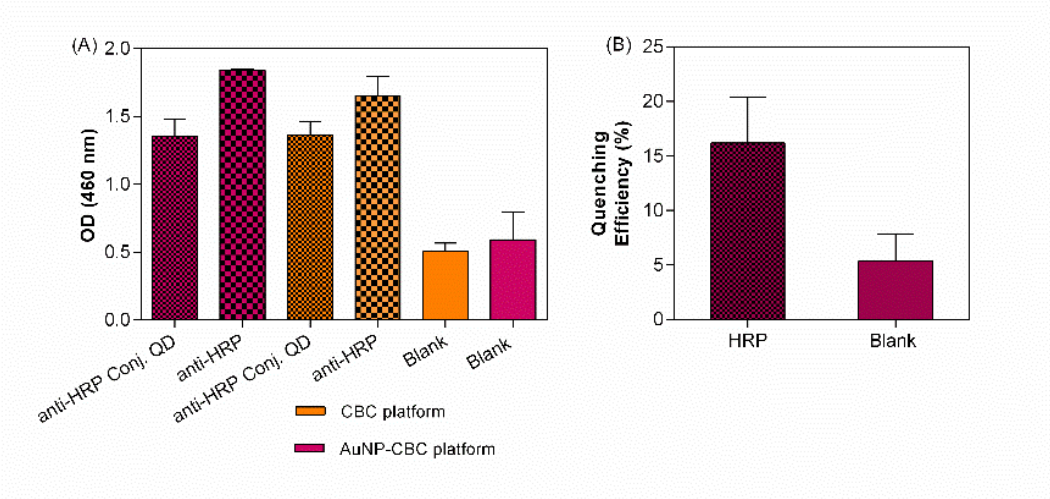

Figure 6-3. (A) Estimated optical density of HRP response attached to HAb and HAb-QD which are linked to protein A/G in two different platforms, AuNP-CBC and bare CBC. (B) Quenching efficiency evaluated by the capture of HRP to HAb-QD which is linked to protein A/G on the surface of AuNP-CBC.

6.4.4 Bacteria recognition

The configuration of the proposed immunosensor was thoroughly investigated and its efficiency was proved for the detection of HRP as a model analyte. In this step, the proficiency of the proposed FRET-based immunosensor was also examined for various concentrations of *E. coli* DH-5α, diluted from 10^8 to 10 CFU.mL^{-1} in a standard buffer. The response of this immunosensor was calculated by the alteration in the photoluminescence of the QD after the recognition of bacteria and thus, presented in terms of QD quenching efficiency (φ_F, by applying equation 1), as observed in Figure 6-4A. Moreover, the blank sample was examined by adding the buffer to the immunosensor platform that could reveal any deattachment of the antibody conjugated QD in these experimnetal conditions. Interestingly, the evaluated quenching efficiency showed a similar value of φ_F for both concentrations of 10^8 and 10^6 CFU.mL^{-1} that suggests the maximum capacity of this immunosensor for bacteria recognition. By lowering the concentration of bacteria from 10^4 to 10 CFU.mL^{-1}, the evaluated quenching efficiency reduced close to that of the blank solution. The limit of detection (LOD) was determined through the mean of the blank solution quenching efficiency plus three times that of its standard deviation. So, interestingly, the threshold of LOD was determined to be as low as 10 CFU/mL, confirming the sensitivity of this nanopaper and FRET-based immunosensor.

To evaluate the specificity and selectivity of the developed FRET-based immunosensor, *Staphylococcus aureus* (*S. aureus*) was selected as control bacteria. The estimated quenching efficiency for the highest concentration of *S. aureus* (10^8 and 10^6 CFU/mL) was within the range of the calculated LOD for *E. coli*. Meanwhile, by decreasing the concentration of *S. aureus* (from 10^4 to 10^2 CFU/mL), the respective quenching efficiencies declined under the LOD threshold. Despite the limited interaction of the immunosensor with the control bacteria, it can be employed for sensitive *E. coli* recognition.

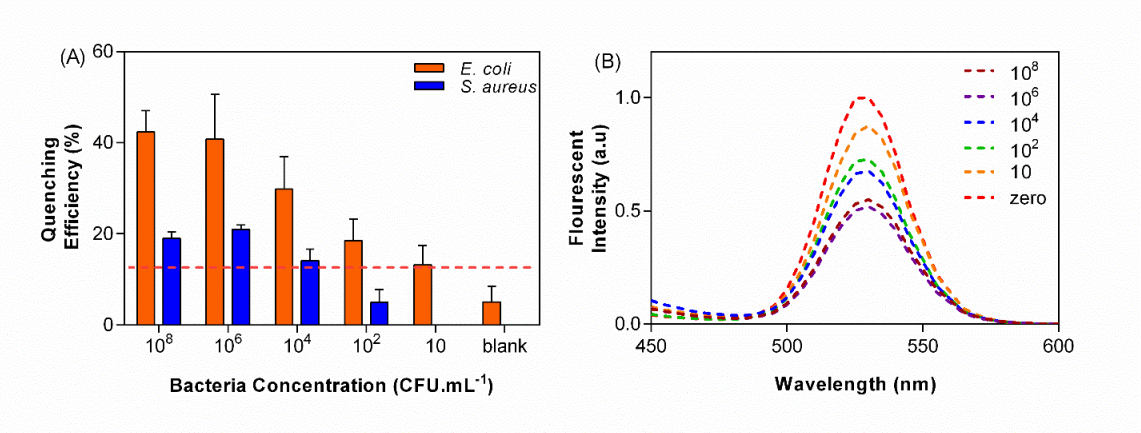

Figure 6-4. Performance of proposed immunosensor presented by (A) the quenching efficiency of QD corresponding to the concertation of *E. coli* (orange bars) and control bacteria *S. aureus* (blue bars) and (B) the change in fluorescent intensity QD after its response to *E. coli* detection.

Subsequently, this immunosensor was successfully developed by relying on the intrinsic characteristics of the antibody and its integration to the surface of AuNP-CBC. So, interestingly, any extra treatment was not required to define the response of the proposed immunosensor, which is a challenge in most of the developed bioassay-based FRET, and which may limit their application for on-site detection. Although this approach was proposed as a proof-of-concept for a novel solid nanopaper-based immunoassay, it exhibited appropriate sensitivity toward the recognition of pathogenic bacteria.

6.5 Conclusions

In this study, we developed a novel and versatile FRET-based immunosensor on a nanopaper platform for the detection of *E. coli*. The nanopaper (CBC) embedded with gold nanoparticles (AuNP-CBC) served as the acceptor and simultaneously carried out the immuno-recognition element as a solid platform. QD (emitting at 525 nm), conjugated to the antibody, served as a donor that bonded to the protein A/G immobilized on the surface of the AuNP-CBC with a certain orientation. Prior to evaluate the immunosensor for the detection of *E. coli*, the configuration was examined by binding anti-HRP, HAb-QD and its interaction with HRP as analyte. The photoluminescence of the QD endured a reduction once the anti-*E. coli* conjugated QD interacted with the respective bacteria, due to the decrease of the distance between the QD and the surface of the acceptor. Through this strategy, *E. coli* could be recognized within the range of 10^8 to 10

CFM.mL^{-1} with a LOD of about 10 CFM.mL^{-1}. This immunosensor identified the bacteria directly without employing a secondary antibody or any other biomolecule. This immunosensor was presented as proof of concept, and it has the potential to be improved for multiplex detection with respect to the unique features of AuNP-CBC and QDs. Additionally, the simplicity, selectivity, and specificity of the proposed immunosensor allow its potential use as a portable analytical device in medical, food and environmental industries.

6.6 Acknowledgments

The authors would like to thank the NSERC (Natural Science and Engineering Research Council of Canada), and ProAmpac, the industrial partner of 3SPack Chair for funding this project and financial support.

6.7 References

1. Lund, B. M.; O'Brien, S. J., The occurrence and prevention of foodborne disease in vulnerable people. *Foodborne Pathogens and Disease* 2011, *8* (9), 961-973.

2. Scallan, E.; Hoekstra, R. M.; Angulo, F. J.; Tauxe, R. V.; Widdowson, M.-A.; Roy, S. L.; Jones, J. L.; Griffin, P. M., Foodborne illness acquired in the United States—major pathogens. *Emerg Infect Dis* 2011, *17* (1).

3. Zhao, X.; Lin, C.-W.; Wang, J.; Oh, D. H., Advances in rapid detection methods for foodborne pathogens. *J. Microbiol. Biotechnol* 2014, *24* (3), 297-312.

4. Lazcka, O.; Del Campo, F. J.; Munoz, F. X., Pathogen detection: a perspective of traditional methods and biosensors. *Biosensors and bioelectronics* 2007, *22* (7), 1205-1217.

5. Kagan, C. R., At the Nexus of Food Security and Safety: Opportunities for Nanoscience and Nanotechnology. *ACS Nano* 2016, *10* (3), 2985-2986.

6. Chen, J.; Andler, S. M.; Goddard, J. M.; Nugen, S. R.; Rotello, V. M., Integrating recognition elements with nanomaterials for bacteria sensing. *Chemical Society Reviews* 2017.

7. Sutarlie, L.; Ow, S. Y.; Su, X., Nanomaterials-based biosensors for detection of microorganisms and microbial toxins. *Biotechnology Journal* 2016.

8. Vikesland, P. J.; Wigginton, K. R., Nanomaterial Enabled Biosensors for Pathogen Monitoring - A Review. *Environmental Science & Technology* 2010, *44* (10), 3656-3669.

9. Ray, P. C.; Fan, Z.; Crouch, R. A.; Sinha, S. S.; Pramanik, A., Nanoscopic optical rulers beyond the FRET distance limit: fundamentals and applications. *Chemical Society Reviews* 2014, *43* (17), 6370-6404.

10. Jin, B.; Wang, S.; Lin, M.; Jin, Y.; Zhang, S.; Cui, X.; Gong, Y.; Li, A.; Xu, F.; Lu, T. J., Upconversion nanoparticles based FRET aptasensor for rapid and ultrasenstive bacteria detection. *Biosensors and Bioelectronics* 2017, *90*, 525-533.

11. Morales-Narváez, E.; Hassan, A. R.; Merkoçi, A., Graphene Oxide as a Pathogen-Revealing Agent: Sensing with a Digital-Like Response. *Angewandte Chemie* 2013, *125* (51), 14024-14028.

12. Ko, S.; Grant, S. A., A novel FRET-based optical fiber biosensor for rapid detection of Salmonella typhimurium. *Biosensors and Bioelectronics* 2006, *21* (7), 1283-1290.

13. Chen, G.; Song, F.; Xiong, X.; Peng, X., Fluorescent nanosensors based on fluorescence resonance energy transfer (FRET). *Industrial & Engineering Chemistry Research* 2013, *52* (33), 11228-11245.

14. Hötzer, B.; Medintz, I. L.; Hildebrandt, N., Fluorescence in nanobiotechnology: sophisticated fluorophores for novel applications. *Small* 2012, *8* (15), 2297-2326.

15. Resch-Genger, U.; Grabolle, M.; Cavaliere-Jaricot, S.; Nitschke, R.; Nann, T., Quantum dots versus organic dyes as fluorescent labels. *Nat Meth* 2008, *5* (9), 763-775.

16. Pons, T.; Medintz, I. L.; Sapsford, K. E.; Higashiya, S.; Grimes, A. F.; English, D. S.; Mattoussi, H., On the quenching of semiconductor quantum dot photoluminescence by proximal gold nanoparticles. *Nano letters* 2007, *7* (10), 3157-3164.

17. Hildebrandt, N.; Spillmann, C. M.; Algar, W. R.; Pons, T.; Stewart, M. H.; Oh, E.; Susumu, K.; Díaz, S. A.; Delehanty, J. B.; Medintz, I. L., Energy Transfer with Semiconductor Quantum Dot Bioconjugates: A Versatile Platform for Biosensing, Energy Harvesting, and Other Developing Applications. *Chemical Reviews* 2017, *117* (2), 536-711.

18. Morales-Narváez, E.; Golmohammadi, H.; Naghdi, T.; Yousefi, H.; Kostiv, U.; Horák, D.; Pourreza, N.; Merkoçi, A., Nanopaper as an Optical Sensing Platform. *ACS nano* 2015, *9* (7), 7296-7305.

19. Heli, B.; Morales-Narvaez, E.; Golmohammadi, H.; Ajji, A.; Merkoci, A., Modulation of population density and size of silver nanoparticles embedded in bacterial cellulose via ammonia exposure: visual detection of volatile compounds in a piece of plasmonic nanopaper. *Nanoscale* 2016, *8* (15), 7984-7991.

20. Pourreza, N.; Golmohammadi, H.; Naghdi, T.; Yousefi, H., Green in-situ synthesized silver nanoparticles embedded in bacterial cellulose nanopaper as a bionanocomposite plasmonic sensor. *Biosensors and Bioelectronics* 2015, *74*, 353-359.

21. Heli, B.; Ajji, A., Nanopaper-based platform applicable in solid-state based FRET technique. *Biochimica et Biophysica Acta* 2017, submitted

22. Sela-Culang, I.; Alon, S.; Ofran, Y., A systematic comparison of free and bound antibodies reveals binding-related conformational changes. *The Journal of Immunology* 2012, *189* (10), 4890-4899.

23. Elgert, K. D., *Immunology: understanding the immune system*. John Wiley & Sons: 2009.

24. Saito, T.; Isogai, A., TEMPO-mediated oxidation of native cellulose. The effect of oxidation conditions on chemical and crystal structures of the water-insoluble fractions. *Biomacromolecules* 2004, *5* (5), 1983-1989.

25. da Silva Perez, D.; Montanari, S.; Vignon, M. R., TEMPO-mediated oxidation of cellulose III. *Biomacromolecules* 2003, *4* (5), 1417-1425.

26. Kimling, J.; Maier, M.; Okenve, B.; Kotaidis, V.; Ballot, H.; Plech, A., Turkevich method for gold nanoparticle synthesis revisited. *The Journal of Physical Chemistry B* 2006, *110* (32), 15700-15707.

27. Parolo, C.; de la Escosura-Muñiz, A.; Polo, E.; Grazú, V.; de la Fuente, J. s. M.; Merkoçi, A., Design, Preparation, and Evaluation of a Fixed-Orientation Antibody/Gold-Nanoparticle Conjugate as an Immunosensing Label. *ACS applied materials & interfaces* 2013, *5* (21), 10753-10759.

28. Iguchi, M.; Yamanaka, S.; Budhiono, A., Bacterial cellulose—a masterpiece of nature's arts. *Journal of Materials Science* 2000, *35* (2), 261-270.

29. Yamanaka, S.; Watanabe, K.; Kitamura, N.; Iguchi, M.; Mitsuhashi, S.; Nishi, Y.; Uryu, M., The structure and mechanical properties of sheets prepared from bacterial cellulose. *Journal of Materials Science* 1989, *24* (9), 3141-3145.

30. Kim, H.; Kang, D.-Y.; Goh, H.-J.; Oh, B.-K.; Singh, R. P.; Oh, S.-M.; Choi, J.-W., Analysis of direct immobilized recombinant protein G on a gold surface. *Ultramicroscopy* 2008, *108* (10), 1152-1156.

31. Makaraviciute, A.; Ramanaviciene, A., Site-directed antibody immobilization techniques for immunosensors. *Biosensors and Bioelectronics* 2013, *50*, 460-471.

32. Lee, J. M.; Park, H. K.; Jung, Y.; Kim, J. K.; Jung, S. O.; Chung, B. H., Direct immobilization of protein G variants with various numbers of cysteine residues on a gold surface. *Analytical chemistry* 2007, *79* (7), 2680-2687.

6.8 Supporting information

Toward a Nanopaper-Based and Solid Phase Immunoassay Using FRET For Rapid Detection of Bacteria

Bentolhoda Heli[1], Arben Merkoçi[2], Abdellah Ajji[1*]

[1] 3SPack, CREPEC, Département de génie chimique École Polytechnique de Montréal, Montréal, Québec, Canada.

[2] Nanobioelectronics and Biosensor GroupCatalan Institute of Nanoscience and Nanotechnology (ICN2) CSIC and BIST Campus UAB, Bellaterra, 08193 Barcelona, Spain

6.8.1 Bacteria growth and preparation

The bacterial dilutions were prepared freshly before the experiments. The strain of *Escherichia coli* (DH5α) and *Staphylococcus aureus* (54-73) were provided by the Laboratory of Microbiology, Université de Montréal (Québec, Canada). The bacteria strain was incubated in the growth media, Luria–Bertani (LB), and placed in an orbital shaker (New Brunswick) overnight at 37°C. So, the final concentration of 10^9 CFU.ml^{-1} was obtained. Then, the bacteria solution was washed and separated from growth media by three times centrifugation at 8000 rpm for 3 min and then resuspended in PBS 0.01 M pH 7.4. The bacterial samples with different concentrations of 10^8, 10^6, 10^4, 10^2 and 10 CFU.ml^{-1} were prepared by serial dilution of the stock suspension in PBS. The prepared dilutions were stored at 4°C before use.

Table S6-1. A comparison between the amount of immobilized protein A/G in different condition and various platforms. These amounts are estimated through the Bradford assay analysis.

	Protein A/G (µg) immobilized on		
	Initial amount	Immobilized amount	
No.	**CBC**		pH
1	4	2.62±0.01	7.4
	4	3.96±0.04	4.1
2	13.2	11.76±0.14	4.1
	4.4	4.29±0.05	4.1
	1.32	1.31±0.09	4.1
	AuNP-CBC		
3	4	2.77±0.09	4.1

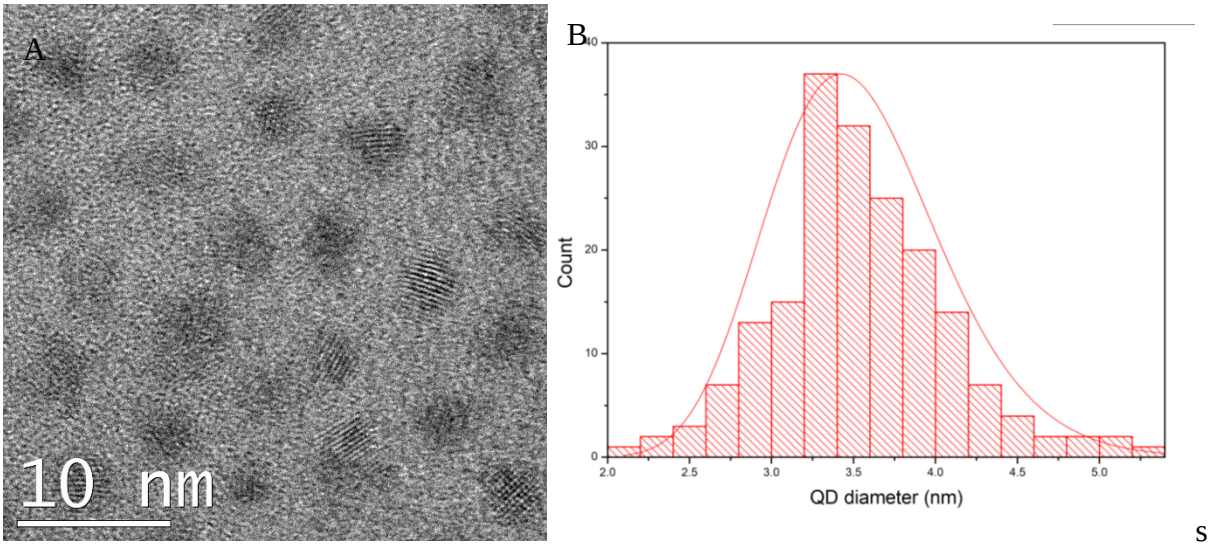

s

Figure S6-1. (A) TEM image of QD which was conjugated to antibody and (B) The size distribution of QD obtained by analyzing the diameter of 200 individual QD particles.

CHAPTER 7 GENERAL DISCUSSION

Ongoing research in the field of smart packaging, especially into the applicable biosensor, reflect the urgent demands for improvement of food safety [1, 3, 8, 129, 130]. Detection of both pathogenic bacteria and spoilage bacteria have been considered as one of the effective strategies to overcome the problems caused by the outbreak of pathogens [6, 13, 38, 93, 131-133]. Over recent decades, the stunning advances in the synthesis and engineering of nano-biomaterials, as well as discoveries and improvements of their marvelous properties, have accelerated and facilitated the fabrication of biosensors [10, 64]. As studied extensively in the literature, a wide variety of nanomaterials enabled the development of a bio-diagnostic assay for the microorganism, through direct or indirect detection [16, 134, 135]. Selectivity, sensitivity and ease of use are the three critical parameters that are appraised for the design of the appropriate biosensor. In this research, we sought the fabrication of a biosensor, which could satisfy the aforesaid parameters along with applicability in food packaging. Thus, it was necessary to establish a biosensor on a solid platform, which allows its application to smart packaging. In this regard, the common solid substrate in biosensing technology, such as glass and paper [89, 136], cannot fulfill the requisite criteria.

We found bacterial cellulose (BC) as a nano-based solid platform, which can successfully bond and support the varieties of nanoparticles and bio-molecules, owing to its versatile properties such as biocompatibility, abundant functional groups, ease of modification, optical and mechanical features, and nano-fibril structure (as reviewed in Chapter 2) [95, 112]. We observed that the nanocomposite composed of BC and nanoparticles could also offer fantastic features of both. As a proof-of-concept, we investigated the bacteria detection, indirectly and directly, by applying the BC as the platform.

In the first article, chapter 4, presents the first objective of the thesis, viz., the indirect recognition of microorganism, which refers to detecting a bacteria through its by-products that may be secreted or produced during its growth periods, such as toxins and gases. In this aspect, the volatile organic compounds (VOCs) have been widely explored as by-products of microorganism metabolites [116, 133]. The VOCs, called the fingerprint of microorganism, are strongly dependent on the type of microorganism and the environmental growth conditions[115]. Hence, we considered VOC from spoilage of meat and fish, as a model for proof-of-concept. Among various gases produced from spoilt meat and fish, ammonia has been assessed more for colorimetric detection, as it is very

reactive with basic dye and can cause a color change in the respective platform [123, 127]. In the published literature, two main challenges are attributed to this type of method. First, the selection of an appropriate solid substrate for fixation of dye, with low impact on its nature and stability. Paper, silica gel on glass slides and some polymers are among the most explored surfaces [121, 127, 137]. As such, the lack of enough porosity may impact the practical interaction of gases and sensor, leading to lower sensitivity. Second, mainly the colorimetric methods have accurately analyzed the color change with scanning and image analyzing of the platform, followed by mathematical algorithms that need a complicated computer programming [121, 127].

Despite the published literature, we explored the sensitivity of silver nanoparticles embedded in BC (AgNP-BC), due to plasmonic properties of noble metal nanoparticles (discussed in Chapter 2). Thus, implementation of BC as a solid surface offers plenty of advantages (listed below) that improve the detection system. 1) Its transparency allowed the use of a spectroscopy device for the accurate measurement of the modulation in the nanoparticles. Consequently, the changes were revealed in UV-vis absorbance spectra and the plasmonic peak of AgNP. 2) The high porosity, nanoporous structure, and high surface area of BC enhanced the contact of AgNP and the desired molecules of gases, besides simplifying their passing into the platform. 3) High mechanical properties guaranteed its sustainability and stability during usage. So, it is expected that the surface of the AgNP-BC is uniformly exposed to the analytes. Thus, as described in the article, we proved the sensitivity of the developed AgNP-BC by exploring a different concentration of ammonia. Further, its selectivity was evaluated by being exposed to the other organic vapor. Through the comparison of the results obtained, we confirmed that the developed AgNP-BC had a strong sensitivity to ammonia vapor. As observed, the color change of AgNP-BC was recognizable to the naked eye for higher concentration and longer exposure. Moreover, due to the presence of ammonia as an efficient and measurable element of fish and meat spoilage, this platform was assessed for spoilage detection, by being in contact with the produced gas. Successfully, we could recognize the spoilage through a colorimetric detection, as a result of AgNP-BC color change. As the TEM images revealed, the plasmonic absorbance of AgNP, as well as its color, were tuned as the result of AgNP etching, after exposure to ammonia or spoilage gases. Notably, this reaction occurred in the gas-solid phase, and hence prevents direct contact with the medium (spoilt fish or meat). Besides, as the AgNP-BC is composed of neither toxic components nor volatile chemicals, the samples were not affected by the evaporation and penetration of toxins. However, the

reproducibility of the plasmonic nano-paper, with similar plasmonic peak, remains a challenge for this study, because of its significant dependence on the size and population of AgNP. Nevertheless, the precise control of the effective parameter during the synthesizing reaction was a practical solution to overcome this issue. We also observed that highly populated AgNP-BC with higher absorbance peak and darker amber color, couldn't show a visual color change for detection, although it was measurable with UV-vis absorbance spectra.

In the second part of this thesis (Chapters 5 and 6), the bacteria was directly detected by the whole cells. In a similar way to the first part, we considered the integration of the final designed bioassay to the smart packaging. Hence, it was essential to solve two main challenges: 1) the applicability of the proposed biosensor platform in the food packaging and, 2) simplicity, sensitivity, and selectivity of the developed methods for pathogen detection. To answer the first challenge, we investigated the high-throughout immunosensor assembled on the solid surface. The selection of the appropriate solid surface was the first and essential step that could significantly influence the efficiency and flexibility of the developed immunosensor. Owing to the properties of BC as mentioned before, we also found it as a practical substrate here. Abundant hydroxyl groups of BC can transform to carboxyl groups through TEMPO chemical reaction; hence, it provides appropriate functional groups for crosslinking to the bioreceptor and transducer. To satisfy the second challenge, the biosensor was designed based on the Förster (fluorescence) resonance energy transfer (FRET) method. As discussed thoroughly in Chapter 2, this method results from a non-radiative energy transfer from a fluorophore donor to an acceptor molecule, that the efficiency of energy transfer highly relies on the pair distance. Due to the high efficiency of gold nanoparticles-quantum dot, this pair was chosen as the acceptor-donor pair. Unlike the reported solid-based FRET technique, where the donor is usually immobilized on the solid phase [89-91], we applied acceptor on the selected substrate, BC. Regarding literature, it is proven that the synthesized AuNP within the BC shows the plasmonic properties [112]. On the other hand, integration AuNP into BC didn't affect its plasmonic peak and UV-absorbance spectra. Thus, owing to this feature, the AuNP-BC can be a favorite candidate for a solid-based platform with the acceptor role for FRET. So, the tunable synthesized AuNP-BC were subjected to our investigation, to define the best condition of the proposed acceptor for such a technique that was studied in the second article (Chapter 5).

A single AuNP has been widely explored as an acceptor in the solution phase, with a combination of various fluoroprobes [51, 75]. It is known as a strong quencher, with a remarkable increase in

the efficiency of energy transfer and distance between the acceptor-donner pair, which is beyond the traditional FRET distance [138]. We took these facts into account and in our second article, we illustrated the bulk behavior of AuNP embedded in the transparent BC, for absorbing the energy from a donor.

As described in article 2, three different population densities of AuNP-BCs were embedded into the BC, by the adjustment of Au precursor concentration. To estimate the energy transfer from fluorophores to the developed acceptor substrate (AuNP-BC), the fluorescent intensity of the various concentrations of dissolved fluorescein saline salt (FSS) was recorded, while it was spotted on the surface of AuNP-BC samples. It should be noted that FSS with an emission spectrum at 515 nm showed a considerable overlap with absorbance spectra of AuNP-BCs. Evaluating the quenching efficiency of FSS directly corresponds to the percentage of energy transfer absorbed by the acceptor after excitation at 460 nm. We were successful in demonstrating that the quenching efficiency was increased by the enhancement of the density of AuNP-BC as the determinative parameter. The high density of AuNP-BC could quench the FSS with different concentrations higher than 95%. The quenching efficiency decrease with a decrease in the density of AuNP-BC, while it was not affected by the concentration of FSS. In fact, the increase in the number of acceptor molecules caused an increase in the energy transfer and therefore in the quenching efficiency. Besides, the overlap of FSS emission intensity with absorbance spectra was maximised, since the higher density of AuNP-BC presented the higher plasmonic peak. The obtained results suggested the effect of density of AuNP-BC on the quenching efficiency, with negligible dependency on the concentration of fluorophore.

It is worth mentioning that a comparison between the photoluminescence of the spotted fluorophores on the nitrocellulose and bacterial cellulose revealed a remarkable difference: the FSS and QD on nitrocellulose showed a higher fluorescent intensity than those spotted on BC. Although this observation might seem controversial, it indicated to us that the BC is more suitable if it served as a support for the acceptor molecule.

Further, we observed that AgNP-BC could behave as a strong quencher. However, its application as an acceptor platform is restricted due to two main reasons: 1) the antibacterial activity of Ag that can affect the detection mechanism. 2) our efforts for transformation of BC to carboxylated

BC (CBC) and the integration of CBC with Ag didn't provide an acceptable platform to meet all our demands.

The outcome of the second article was a guide for the proper development of the solid surface, and therefore the assembly of the immunosensor. The fabrication of the immunosensor was discussed in detail in the third article (Chapter 6), based on the FRET method. The antibody that served as the bioelement to capture the antigen was conjugated to QD as the donor. In order to improve the high-efficiency immunosensor, there were some scientific challenges, thus addressing them conducted us to the high-throughout platform.

The main challenge was to find the appropriate analytical methods that could confirm the results of the experiments. Generally, quantitative analysis using the precise instruments (such as SEM, TEM or AFM) is not practically applicable for imaging of biomolecules, e.g., antibody and protein A/G. In this case, qualitative analysis (such as those are conducted with optical measurement) with relying on specific protocols could provide more reliable results for evaluation and comparison. Here, an antibody against horseradish peroxidase (HRP) (anti-HRP) was exploited for the primary experiments of conjugation and evaluation of the immunosensor platform, as HRP contributes in a catalytic reaction to convert a chromogenic substrate into a colored one [139]. Consequently, the intensity of the produced color is directly dependent on the number of HRP captured by the anti-HRP. Besides, the Bradford assay and Polyacrylamide gel electrophoresis (PAGE-gel) are two other common methods in biochemistry for qualitative analysis of proteins amount.

As such, the experimental conditions were firstly investigated for anti-HRP-QD conjugation. As mentioned before, in Chapter 2, the conjugation was followed by covalent binding between the carboxyl groups of QD and primary amino groups on anti-HRP through EDC/Sulfo-NHS crosslinker. By accomplishing some primary experiments, we found that the ratios of EDC/ Sulfo-NHS to active the carboxyl groups and pH of reaction were among the important parameters which could affect the activity of the resultant anti-HRP conjugated QD, because the pH of reaction may lead to blockage of the active site of antibodies by conjugated QD and also an excess amount of EDC/Sulfo-NHS may cause precipitation of biomolecules. Although some protocols have been recommended in the literature for the optimized conjugation, they have to be evaluated according to the type of applied antibody [21]. Hence, the activity of resulting anti-HRP-QD conjugates were estimated by comparison of their interaction with HRP followed by measuring the optical density

of captured HRP. As observed, the conjugation reaction at pH 5 was more effective than pH 7.4, due to the higher optical density. Besides, the PAGE-gel was used to predict the location of QD on the surface of the antibody. However, the results obtained from the differentiation of antibody conjugated QD fragments in the gel revealed the conjugation of QD to the heavy chain of an antibody; this concept remains an intriguing subject for future work. The EDC/Sulfo-NHS chemistry does not cause any deformation of antibody structure upon conjugation to QD. Random conjugation was also adjusted by controlling the pH of the reaction, as illustrated through capturing the HRP.

Likewise, the immobilization of protein A/G on the surface of the platform was another challenge of this part of the study that was accomplished by EDC/Sulfo-NHS chemistry, to bond the carboxyl groups of AuNP-CBC to amino groups of protein A/G. As mentioned in the literature review, the protein A/G allows the antibody conjugated QD to be placed in the oriented form, while the active sites are free to interact with the analyte. Thus, various parameters were investigated to assess the proper link between protein A/G and the surface of the immunosensor, as presented in the third article in Chapter 6. Similarly, a qualitative experiment such as the Bradford assay was also performed, to evaluate the amount of protein A/G immobilized on the surface. Further evaluations were assayed, when the antibody and antibody conjugated QD linked to the protein A/G. As before, the optical density obtained from the enzymatic reaction of the captured HRP revealed the efficiency of the assembled platforms.

The established results provided enough evidence for the development of the immunosensor for bacteria detection. The FRET-based method was designed with respect to the huge conformational change of antibody structure, after capturing the bacteria. This issue was the biggest challenge for this project. The researchers have proved the occurrence of the conformational change in the 3D structure of IgG. While it varied with the type and size of antigens, as bigger antigens (e.g., bacteria) induced more conformational change after interaction with the antibody [140]. However, the lack of an accurate measurement of the changes can be an obstacle for the widespread use of this method; we confirmed that this event was adequate to detect bacteria due to the decrease in the distance between the donor (QD) and acceptor (AuNP-CBC). Therefore, considering the intrinsic property of the antibody is one of the most notable advantages of this method for the direct detection of bacteria, without any extra treatments. On the other hand, a secondary antibody marked

with the fluorophores is not essential. However, the reproducibility of this method may be restricted for the other type of antigen, so further studies would be needed.

Through this way, the maximum quenching efficiency obtained for the detection of bacteria in high concentration was estimated around 45%, while the ideal platform would be the “on and off” state. It means that once the immunosensor recognizes the bacteria, the QDs photoluminescence quenches completely.

Another big challenge of this study was the selection of the antibody that was the most significant element of the immunosensor with direct influence on its efficacy. As presented in the article, we have used a non-pathogenic type of *E. coli* DH-5α as the model for bacteria detection. Due to this feature, the abundance of an appropriate type of antibody for this bacteria was very limited that wasn’t provided by popular suppliers. On the contrary, the various antibodies of the pathogenic *E. coli* (e.g., *E. coli* O175) are widely available, as well as their conjugated form to different biomarkers. So this caused an obstacle, restricted further examinations of the immunosensor. For examples, we applied the polyclonal anti- *E. coli* DH-5α while its substitution with a monoclonal antibody could improve the sensitivity of detection. Implementing the antibodies with different biomarkers (such as Cyc 5 or Alexa flour) might also advance the immunosensor and it could improve our understanding of the conformational change.

Although the proposed platform was successfully recognized bacteria as a proof-of-concept, there are some concerns about the applicability of the developed immunosensor to food packaging. 1) The bacteria samples interacted with the antibody of the immunosensor platform while they suspended in the PBS buffer. Thus, the direct contact of the immunosensor with dispersed bacteria on the contaminated food remains a challenge. 2) The toxicity of QD and AuNP and, the probability of their direct contact with the food products is another issue that may limit its application [141, 142]. 3) The activity of the antibody may change, with a change in environmental conditions such as pH and temperature, so these parameters may affect the stability, sensitivity, and sustainability of the immunosensor. 4) Reproducibility of the immunosensor has to be verified according to the type of bacteria with the specific design.

We envisage that these drawbacks can be addressed in the near future, by improving the biorecognition elements, as well as the characteristics and functionalities of nanoparticles.

CHAPTER 8 CONCLUSIONS AND RECOMMENDATIONS

8.1 Summary and Conclusions

This research investigated the development of a bioassay for bacteria detection and the possibility of its integration into the food packaging sector. This work emphasized the importance of advancing the novel nanocomposite and reappraising the inherent properties of biomolecules like an antibody, for the fabrication of efficient biosensors that ameliorate social health, by taking into account the versatile, sensitive, selective, friendly, in-situ and rapid detection. Regarding our results, the main conclusion derived from this research is that bacteria can be recognized by its whole cell or by-products upon, interacting with the surface of the solid-based bioassay platform. Thus any secondary biomarker or reaction was not needed to improve the diagnosis. In this chapter, we present the primary outcomes achieved from this thesis, with respect to the three major publications. They are summarised as follows:

The first part of the thesis was dedicated to examining a proof-of-concept for the indirect detection of bacteria, through the produced gases. In this case, the functionality of bacterial cellulose embedded with silver nanoparticles was explored, as an optical platform for visual detection. By considering spoilage of meat and fish as the result of bacterial growth and the fact that ammonia is one of the major components produced during spoilage, the proposed method was examined by exposure to different concentrations of ammonia and next it was assayed for the detection of spoilage. The results clearly revealed the sensitivity of the proposed platform to the various concentrations of ammonia, in different durations of exposure. The important outcomes of this section are summarised below:

1) Due to the interaction of ammonia vapor with AgNP embedded in the bacterial cellulose, they become partially or completely etched. Consequently, the reduction in the size and density of nanoparticles was shown by TEM images.
2) As the result of the nanoparticles etching, the color of AgNP-BC changed from dark amber to light amber, recognizable visually. Further changes in the color of plasmonic nanopaper were accurately recorded by the change in the UV-vis absorbance spectra of AgNP-BC

3) The plasmonic nanopaper also illustrated a high sensitivity upon exposure to the gases produced from the spoilage of food, which was a mixture of ammonia with other components, whereby its initial amber color changed to gray or taupe.

The second part of this research focuses on the direct detection of bacteria through its whole cell, by developing a solid phase and FRET-based approach. This part consists of two articles. In the first section, we investigated the establishment of the solid substrate, which could also function in the FRET method. Our results demonstrated that by in situ synthesis of gold nanoparticles within bacterial cellulose, it is possible to achieve a promising platform which meets the demands for the assembly of the immunosensor. The density of synthesized AuNP was successfully adjusted by the control of gold precursor solution, and the obtained platform showed that plasmonic spectra relied on the density of nanoparticles. We also found that the density of AuNP was an effective parameter in the quenching efficiency of fluorophores. The other relevant results derived from this part are:

1) The high populatio density AuNP-BC strongly quenched the fluorophore with high concentration, while the quenching efficiency was reduced with the reduction in the density of gold nanoparticles.
2) We observed that the quenching efficiency was not significantly affected by either the concentration fluorophore or its structure and type.
3) The drop casted fluorophore on the surface of nitrocellulose revealed a higher photoluminescence, compared to the one on the BC surface.

The second part of this section and final part of the thesis are devoted to a proof-of-concept for bacteria detection by developing an immunosensor. Results generated from the previous section were applied to the design of a promising platform that served as the acceptor and for carrying the biorecognition elements. We investigated the functionality of the surface of the immunosensor, upon immobilization of the protein A/G, by employing the anti-HRP and HRP as the model antigen. Our results illustrated that the optical density estimated from the captured HRP could provide a qualitative evaluation of biorecognition elements. Other main results are highlighted below:

1) The immunosensor was designed based on the inherent feature of an antibody which is the conformational change of the 3D structure after binding to antigen. So, the

conjugation of the antibody to the donor molecule (QD) led to the detection of bacteria upon interacting with the antibody.

2) The functionality of the immunosensor, relying on the intrinsic feature of the antibody, is more reliable for a large antigen such as bacteria.
3) The proposed immunosensor showed high sensitivity and selectivity for *E. coli*, with the limit of detection of 10 CFM.mL^{-1}.

8.2 Original contribution and novelty

The key novelty of this research lies in the employment of bacterial cellulose as a nano-based platform. The significant and versatile features of BC such as optical transparency, mechanical strength, nano-fibers structure, flexibility and abundant functional groups, make this novel biopolymer a marvelous substrate to create a new generation of optical biosensor. Importantly, the coupling of BC with advantageous nanomaterials (e.g., plasmonic nanoparticles) leads to the emergence of multifunctional nanocomposites. As such, we have studied the outstanding characteristics of BC embedded with plasmonic nanoparticles (Ag and Au) for the fabrication of simple, versatile and amenable biosensors for bacteria detection. So far, there has been no report of the advance of the optical and solid-based biosensor through the implementation of either BC or its composite. The most important and novel points of this research are as follows:

1) Development of colorimetric detection of ammonia vapor and spoilage food through plasmonic properties of AgNP embedded within BC.
2) Transformating BC to a quencher surface through in situ synthesis of AuNP. The density of AuNP modulated the functionality of AuNP-BC to accept the energy transfer from the fluorophores.
3) Designing the solid-based FRET biosensor for bacteria detection. Taking advantage of the inherent properties of the antibody after interaction with antigen, it led to the one-step detection. No additional or secondary step was not needed to reveal the presence of bacteria.

Taking all these aspects into consideration, it is envisaged that the opportunities offered by nanocellulose will revolutionize the biosensor technology, especially those fabricated based on glass, paper, and plastic. Further advances would be expeditious, due to their compatibility with recent mobile phone-based sensing approach.

8.3 Recommendations

The following topics are recommended for future study:

- The decoration of the plasmonic nanoparticles embedded into BC, with the specific chemical functions to improve the sensitivity of the nanocomposite for other types of volatile organic compounds.
- Due to the dependency of plasmonic properties of metal nanoparticles on their size and shape (e.g., nanorod, nanoplate), the in-situ synthesis of nanoparticles with different shapes may reveal new properties in optical sensing.
- Defining the Föster distance while the AuNP-BC serves as an acceptor, by immobilization of DNA with different lengths conjugated to various fluorophores.
- Transforming the hydroxyl groups of the nanopaper to specific carbohydrate groups such as mannose, for direct detection of *E. coli* associated with auto-fluorescent of bacteria.
- Designing of a biosensor for bacteria detection through the employment of AgNP, so that it would be possible to take advantage of the optical properties and antibacterial features in one platform.
- Implementing the dyes (especially those that are common in colorimetric detection of VOC) insight of BC through covalent binding or physical absorption. It is expected to ensure more sensitive detection devices, compared to those using silica gel on the glass.
- Applying the aptamer as a biorecognition element, as it can overcome the drawbacks of antibodies.
- In-situ synthesizing of the metal oxide nanoparticles (e.g., zinc oxide, silica oxide, and titanium oxide) within BC and characterizing their properties for antibacterial activity, oxygen scavenging, and electrochemical features as well as their application in food packaging.

LIST OF REFERENCES

[1] M. Ghaani, C. A. Cozzolino, G. Castelli, and S. Farris, "An overview of the intelligent packaging technologies in the food sector," *Trends in Food Science & Technology,* vol. 51, pp. 1-11, 2016.

[2] T. Janjarasskul and P. Suppakul, "Active and intelligent packaging: the indication of quality and safety," *Critical reviews in food science and nutrition,* pp. 00-00, 2016.

[3] S. P. Oliver, B. M. Jayarao, and R. A. Almeida, "Foodborne pathogens in milk and the dairy farm environment: food safety and public health implications," *Foodbourne Pathogens & Disease,* vol. 2, pp. 115-129, 2005.

[4] R. L. Scharff, "Health-Related Costs From Foodborne Illness in the United States," *Georgetown University: Washington, DC,* 2010.

[5] E. Scallan, R. M. Hoekstra, F. J. Angulo, R. V. Tauxe, M.-A. Widdowson, S. L. Roy, *et al.*, "Foodborne illness acquired in the United States—major pathogens," *Emerg Infect Dis,* vol. 17, 2011.

[6] X. Zhao, C.-W. Lin, J. Wang, and D. H. Oh, "Advances in rapid detection methods for foodborne pathogens," *J. Microbiol. Biotechnol,* vol. 24, pp. 297-312, 2014.

[7] A. Singh, S. Poshtiban, and S. Evoy, "Recent advances in bacteriophage based biosensors for food-borne pathogen detection," *Sensors,* vol. 13, pp. 1763-1786, 2013.

[8] B. Pérez-López and A. Merkoçi, "Nanomaterials based biosensors for food analysis applications," *Trends in Food Science & Technology,* vol. 22, pp. 625-639, 2011.

[9] L. Sutarlie, S. Y. Ow, and X. Su, "Nanomaterials-based biosensors for detection of microorganisms and microbial toxins," *Biotechnology Journal,* 2016.

[10] P. J. Vikesland and K. R. Wigginton, "Nanomaterial Enabled Biosensors for Pathogen Monitoring - A Review," *Environmental Science & Technology,* vol. 44, pp. 3656-3669, 2010/05/15 2010.

[11] Y. Wang and T. V. Duncan, "Nanoscale sensors for assuring the safety of food products," *Current Opinion in Biotechnology,* vol. 44, pp. 74-86, 4// 2017.

[12] T. V. Duncan, "Applications of nanotechnology in food packaging and food safety: barrier materials, antimicrobials and sensors," *Journal of colloid and interface science,* vol. 363, pp. 1-24, 2011.

[13] O. Lazcka, F. J. Del Campo, and F. X. Munoz, "Pathogen detection: a perspective of traditional methods and biosensors," *Biosensors and bioelectronics,* vol. 22, pp. 1205-1217, 2007.

[14] J. Chen, S. M. Andler, J. M. Goddard, S. R. Nugen, and V. M. Rotello, "Integrating recognition elements with nanomaterials for bacteria sensing," *Chemical Society Reviews,* 2017.

[15] K. El-Boubbou, C. Gruden, and X. Huang, "Magnetic Glyco-nanoparticles: A Unique Tool for Rapid Pathogen Detection, Decontamination, and Strain Differentiation," *Journal of the American Chemical Society,* vol. 129, pp. 13392-13393, 2007/11/01 2007.

[16] B. Byrne, E. Stack, N. Gilmartin, and R. O'Kennedy, "Antibody-based sensors: principles, problems and potential for detection of pathogens and associated toxins," *Sensors,* vol. 9, pp. 4407-4445, 2009.

[17] S. Rosati, Y. Yang, A. Barendregt, and A. J. R. Heck, "Detailed mass analysis of structural heterogeneity in monoclonal antibodies using native mass spectrometry," *Nat. Protocols,* vol. 9, pp. 967-976, 04//print 2014.

[18] N. G. Welch, J. A. Scoble, B. W. Muir, and P. J. Pigram, "Orientation and characterization of immobilized antibodies for improved immunoassays," *Biointerphases,* vol. 12, p. 02D301, 2017.

[19] G. T. Hermanson, "Chapter 2 - Functional Targets for Bioconjugation," in *Bioconjugate Techniques (Third edition)*, ed Boston: Academic Press, 2013, pp. 127-228.

[20] G. T. Hermanson, "Chapter 4 - Zero-Length Crosslinkers," in *Bioconjugate Techniques (Third edition)*, ed Boston: Academic Press, 2013, pp. 259-273.

[21] G. T. Hermanson, "Chapter 20 - Antibody Modification and Conjugation," in *Bioconjugate Techniques (Third edition)*, ed Boston: Academic Press, 2013, pp. 867-920.

[22] L. C. Shriver-Lake, B. Donner, R. Edelstein, K. Breslin, S. K. Bhatia, and F. S. Ligler, "Antibody immobilization using heterobifunctional crosslinkers," *Biosensors and Bioelectronics,* vol. 12, pp. 1101-1106, 1997.

[23] C. Parolo, A. de la Escosura-Muñiz, E. Polo, V. Grazú, J. s. M. de la Fuente, and A. Merkoçi, "Design, Preparation, and Evaluation of a Fixed-Orientation Antibody/Gold-Nanoparticle Conjugate as an Immunosensing Label," *ACS applied materials & interfaces,* vol. 5, pp. 10753-10759, 2013.

[24] Y. Sun, H. Du, C. Feng, and Y. Lan, "Oriented immobilization of antibody through carbodiimide reaction and controlling electric field," *Journal of Solid State Electrochemistry,* vol. 19, pp. 3035-3043, October 01 2015.

[25] https://www.thermofisher.com/ca/en/.

[26] Y. Xing, Q. Chaudry, C. Shen, K. Y. Kong, H. E. Zhau, L. W. Chung, *et al.*, "Bioconjugated quantum dots for multiplexed and quantitative immunohistochemistry," *Nature Protocols,* vol. 2, pp. 1152-1165, 2007.

[27] A. Kausaite-Minkstimiene, A. Ramanaviciene, J. Kirlyte, and A. Ramanavicius, "Comparative study of random and oriented antibody immobilization techniques on the binding capacity of immunosensor," *Analytical chemistry,* vol. 82, pp. 6401-6408, 2010.

[28] A. Makaraviciute and A. Ramanaviciene, "Site-directed antibody immobilization techniques for immunosensors," *Biosensors and Bioelectronics,* vol. 50, pp. 460-471, 2013.

[29] J. YoungáJeong and B. HyunáChung, "Recent advances in immobilization methods of antibodies on solid supports," *Analyst,* vol. 133, pp. 697-701, 2008.

[30] S. R. Ahmed, A. T. Lutes, and T. A. Barbari, "Specific capture of target proteins by oriented antibodies bound to tyrosinase-immobilized Protein A on a polyallylamine affinity membrane surface," *Journal of Membrane Science,* vol. 282, pp. 311-321, 10/5/ 2006.

[31] Y. M. Bae, B.-K. Oh, W. Lee, W. H. Lee, and J.-W. Choi, "Study on orientation of immunoglobulin G on protein G layer," *Biosensors and Bioelectronics,* vol. 21, pp. 103-110, 2005.

[32] E.-S. Kim, C.-K. Shim, J. W. Lee, J. W. Park, and K. Y. Choi, "Synergistic effect of orientation and lateral spacing of protein G on an on-chip immunoassay," *Analyst,* vol. 137, pp. 2421-2430, 2012.

[33] A. H. Talasaz, M. Nemat-Gorgani, Y. Liu, P. Ståhl, R. W. Dutton, M. Ronaghi, *et al.*, "Prediction of protein orientation upon immobilization on biological and nonbiological surfaces," *Proceedings of the National Academy of Sciences,* vol. 103, pp. 14773-14778, 2006.

[34] B. N. Johnson and R. Mutharasan, "pH Effect on Protein G Orientation on Gold Surfaces and Characterization of Adsorption Thermodynamics," *Langmuir,* vol. 28, pp. 6928-6934, 2012/05/01 2012.

[35] S. K. Vashist, C. K. Dixit, B. D. MacCraith, and R. O'Kennedy, "Effect of antibody immobilization strategies on the analytical performance of a surface plasmon resonance-based immunoassay," *Analyst,* vol. 136, pp. 4431-4436, 2011.

[36] Y. Ryu, Z. Jin, M. S. Kang, and H.-S. Kim, "Increase in the detection sensitivity of a lateral flow assay for a cardiac marker by oriented immobilization of antibody," *BioChip Journal,* vol. 5, p. 193, September 20 2011.

[37] G. Shen, C. Cai, K. Wang, and J. Lu, "Improvement of antibody immobilization using hyperbranched polymer and protein A," *Analytical Biochemistry,* vol. 409, pp. 22-27, 2011/02/01/ 2011.

[38] S. M. Yoo and S. Y. Lee, "Optical biosensors for the detection of pathogenic microorganisms," *Trends in biotechnology,* vol. 34, pp. 7-25, 2016.

[39] J. R. Lakowicz, *Principles of fluorescence spectroscopy*: Springer, 2009.

[40] M. Sauer, J. Hofkens, and J. Enderlein, "Basic Principles of Fluorescence Spectroscopy," in *Handbook of Fluorescence Spectroscopy and Imaging*, ed: Wiley-VCH Verlag GmbH & Co. KGaA, 2011, pp. 1-30.

[41] S. Sarasanandarajah, J. Kunnil, E. Chacko, B. V. Bronk, and L. Reinisch, "Reversible changes in fluorescence of bacterial endospores found in aerosols due to hydration/drying," *Journal of aerosol science,* vol. 36, pp. 689-699, 2005.

[42] M. Sohn, D. S. Himmelsbach, F. E. Barton, and P. J. Fedorka-Cray, "Fluorescence spectroscopy for rapid detection and classification of bacterial pathogens," *Applied spectroscopy,* vol. 63, pp. 1251-1255, 2009.

[43] H. E. Giana, L. Silveira, R. A. Zângaro, and M. T. T. Pacheco, "Rapid identification of bacterial species by fluorescence spectroscopy and classification through principal components analysis," *Journal of Fluorescence*, vol. 13, pp. 489-493, 2003.

[44] U. Resch-Genger, M. Grabolle, S. Cavaliere-Jaricot, R. Nitschke, and T. Nann, "Quantum dots versus organic dyes as fluorescent labels," *Nat Meth*, vol. 5, pp. 763-775, 09//print 2008.

[45] G. Chen, F. Song, X. Xiong, and X. Peng, "Fluorescent nanosensors based on fluorescence resonance energy transfer (FRET)," *Industrial & Engineering Chemistry Research*, vol. 52, pp. 11228-11245, 2013.

[46] B. Hötzer, I. L. Medintz, and N. Hildebrandt, "Fluorescence in nanobiotechnology: sophisticated fluorophores for novel applications," *Small*, vol. 8, pp. 2297-2326, 2012.

[47] K. E. Sapsford, L. Berti, and I. L. Medintz, "Materials for fluorescence resonance energy transfer analysis: beyond traditional donor–acceptor combinations," *Angewandte Chemie International Edition*, vol. 45, pp. 4562-4589, 2006.

[48] P. C. Ray, Z. Fan, R. A. Crouch, S. S. Sinha, and A. Pramanik, "Nanoscopic optical rulers beyond the FRET distance limit: fundamentals and applications," *Chemical Society Reviews*, vol. 43, pp. 6370-6404, 2014.

[49] J. Shi, F. Tian, J. Lyu, and M. Yang, "Nanoparticle based fluorescence resonance energy transfer (FRET) for biosensing applications," *Journal of Materials Chemistry B*, vol. 3, pp. 6989-7005, 2015.

[50] Q. Zeng, Y. Zhang, X. Liu, L. Tu, X. Kong, and H. Zhang, "Multiple homogeneous immunoassays based on a quantum dots–gold nanorods FRET nanoplatform," *Chemical Communications*, vol. 48, pp. 1781-1783, 2012.

[51] E. Dulkeith, M. Ringler, T. A. Klar, J. Feldmann, A. Muñoz Javier, and W. J. Parak, "Gold Nanoparticles Quench Fluorescence by Phase Induced Radiative Rate Suppression," *Nano Letters*, vol. 5, pp. 585-589, 2005/04/01 2005.

[52] E. Hutter and D. Maysinger, "Gold nanoparticles and quantum dots for bioimaging," *Microscopy research and technique*, vol. 74, pp. 592-604, 2011.

[53] Y.-P. Kim, Y.-H. Oh, E. Oh, S. Ko, M.-K. Han, and H.-S. Kim, "Energy Transfer-Based Multiplexed Assay of Proteases by Using Gold Nanoparticle and Quantum Dot Conjugates on a Surface," *Analytical Chemistry,* vol. 80, pp. 4634-4641, 2008/06/01 2008.

[54] M. Li, Q. Wang, X. Shi, L. A. Hornak, and N. Wu, "Detection of Mercury(II) by Quantum Dot/DNA/Gold Nanoparticle Ensemble Based Nanosensor Via Nanometal Surface Energy Transfer," *Analytical Chemistry,* vol. 83, pp. 7061-7065, 2011/09/15 2011.

[55] A. D. Quach, G. Crivat, M. A. Tarr, and Z. Rosenzweig, "Gold nanoparticle− quantum dot− polystyrene microspheres as fluorescence resonance energy transfer probes for bioassays," *Journal of the American Chemical Society,* vol. 133, pp. 2028-2030, 2011.

[56] K. Saha, S. S. Agasti, C. Kim, X. Li, and V. M. Rotello, "Gold Nanoparticles in Chemical and Biological Sensing," *Chemical Reviews,* vol. 112, pp. 2739-2779, 2012/05/09 2012.

[57] W. R. Algar, K. Susumu, J. B. Delehanty, and I. L. Medintz, "Semiconductor quantum dots in bioanalysis: crossing the valley of death," ed: ACS Publications, 2011.

[58] F. A. Esteve-Turrillas and A. Abad-Fuentes, "Applications of quantum dots as probes in immunosensing of small-sized analytes," *Biosensors and Bioelectronics,* vol. 41, pp. 12-29, 2013.

[59] H. Li, W. Y. Shih, and W.-H. Shih, "Synthesis and characterization of aqueous carboxyl-capped CdS quantum dots for bioapplications," *Industrial & Engineering Chemistry Research,* vol. 46, pp. 2013-2019, 2007.

[60] L. Yang and Y. Li, "Quantum dots as fluorescent labels for quantitative detection of Salmonella typhimurium in chicken carcass wash water," *Journal of Food Protection®,* vol. 68, pp. 1241-1245, 2005.

[61] M. Varshney, L. Yang, X.-L. Su, and Y. Li, "Magnetic nanoparticle-antibody conjugates for the separation of Escherichia coli O157: H7 in ground beef," *Journal of Food Protection®,* vol. 68, pp. 1804-1811, 2005.

[62] Y. Liu, R. Brandon, M. Cate, X. Peng, R. Stony, and M. Johnson, "Detection of pathogens using luminescent CdSe/ZnS dendron nanocrystals and a porous membrane immunofilter," *Analytical chemistry,* vol. 79, pp. 8796-8802, 2007.

[63] H. Wang, Y. Li, and M. Slavik, "Rapid detection of Listeria monocytogenes using quantum dots and nanobeads-based optical biosensor," *Journal of Rapid Methods & Automation in Microbiology,* vol. 15, pp. 67-76, 2007.

[64] A. Vinayaka and M. Thakur, "Focus on quantum dots as potential fluorescent probes for monitoring food toxicants and foodborne pathogens," *Analytical and bioanalytical chemistry,* vol. 397, pp. 1445-1455, 2010.

[65] E. Morales-Narváez, A. R. Hassan, and A. Merkoçi, "Graphene Oxide as a Pathogen-Revealing Agent: Sensing with a Digital-Like Response," *Angewandte Chemie,* vol. 125, pp. 14024-14028, 2013.

[66] N. Duan, S. Wu, S. Dai, T. Miao, J. Chen, and Z. Wang, "Simultaneous detection of pathogenic bacteria using an aptamer based biosensor and dual fluorescence resonance energy transfer from quantum dots to carbon nanoparticles," *Microchimica Acta,* vol. 182, pp. 917-923, April 01 2015.

[67] B.-B. Wang, Q. Wang, Y.-G. Jin, M.-H. Ma, and Z.-X. Cai, "Two-color quantum dots-based fluorescence resonance energy transfer for rapid and sensitive detection of Salmonella on eggshells," *Journal of Photochemistry and Photobiology A: Chemistry,* vol. 299, pp. 131-137, 2015.

[68] J. N. Anker, W. P. Hall, O. Lyandres, N. C. Shah, J. Zhao, and R. P. Van Duyne, "Biosensing with plasmonic nanosensors," *Nature materials,* vol. 7, pp. 442-453, 2008.

[69] K. M. Mayer and J. H. Hafner, "Localized surface plasmon resonance sensors," *Chemical reviews,* vol. 111, pp. 3828-3857, 2011.

[70] A. J. Haes and R. P. Van Duyne, "A Nanoscale Optical Biosensor: Sensitivity and Selectivity of an Approach Based on the Localized Surface Plasmon Resonance Spectroscopy of Triangular Silver Nanoparticles," *Journal of the American Chemical Society,* vol. 124, pp. 10596-10604, 2002/09/01 2002.

[71] C. Cobley, S. Skrabalak, D. Campbell, and Y. Xia, "Shape-Controlled Synthesis of Silver Nanoparticles for Plasmonic and Sensing Applications," *Plasmonics,* vol. 4, pp. 171-179, 2009/06/01 2009.

[72] https://nanocomposix.com.

[73] B. Sepúlveda, P. C. Angelomé, L. M. Lechuga, and L. M. Liz-Marzán, "LSPR-based nanobiosensors," *Nano Today,* vol. 4, pp. 244-251, 2009.

[74] J. Griffin, A. K. Singh, D. Senapati, P. Rhodes, K. Mitchell, B. Robinson, *et al.*, "Size-and Distance-Dependent Nanoparticle Surface-Energy Transfer (NSET) Method for Selective Sensing of Hepatitis C Virus RNA," *Chemistry–A European Journal,* vol. 15, pp. 342-351, 2009.

[75] E. Dulkeith, A. Morteani, T. Niedereichholz, T. Klar, J. Feldmann, S. Levi, *et al.*, "Fluorescence quenching of dye molecules near gold nanoparticles: radiative and nonradiative effects," *Physical review letters,* vol. 89, p. 203002, 2002.

[76] T. Pons, I. L. Medintz, K. E. Sapsford, S. Higashiya, A. F. Grimes, D. S. English, *et al.*, "On the quenching of semiconductor quantum dot photoluminescence by proximal gold nanoparticles," *Nano letters,* vol. 7, pp. 3157-3164, 2007.

[77] L. Dyadyusha, H. Yin, S. Jaiswal, T. Brown, J. Baumberg, F. Booy, *et al.*, "Quenching of CdSe quantum dot emission, a new approach for biosensing," *Chemical Communications,* pp. 3201-3203, 2005.

[78] X. Li, J. Qian, L. Jiang, and S. He, "Fluorescence quenching of quantum dots by gold nanorods and its application to DNA detection," *Applied Physics Letters,* vol. 94, p. 063111, 2009.

[79] G.-X. Liang, H.-C. Pan, Y. Li, L.-P. Jiang, J.-R. Zhang, and J.-J. Zhu, "Near infrared sensing based on fluorescence resonance energy transfer between Mn:CdTe quantum dots and Au nanorods," *Biosensors and Bioelectronics,* vol. 24, pp. 3693-3697, 2009/08/15/ 2009.

[80] D. Huang, C. Niu, M. Ruan, X. Wang, G. Zeng, and C. Deng, "Highly Sensitive Strategy for Hg2+ Detection in Environmental Water Samples Using Long Lifetime Fluorescence Quantum Dots and Gold Nanoparticles," *Environmental Science & Technology,* vol. 47, pp. 4392-4398, 2013/05/07 2013.

[81] X. Leng, D. Huang, C. Niu, X. Wang, G. Zeng, and Q. Niu, "Time-gated fluorescence sensor for silver ions using Mn: CdS/ZnS quantum dots/DNA/gold nanoparticle complexes," *Analytical Methods,* vol. 6, pp. 6265-6270, 2014.

[82] K. L. Brenneman, S. Poduri, M. A. Stroscio, and M. Dutta, "Optical detection of lead (II) ions using DNA-based nanosensor," *IEEE Sensors Journal,* vol. 13, pp. 1783-1786, 2013.

[83] N. Hildebrandt, C. M. Spillmann, W. R. Algar, T. Pons, M. H. Stewart, E. Oh, *et al.*, "Energy Transfer with Semiconductor Quantum Dot Bioconjugates: A Versatile Platform for Biosensing, Energy Harvesting, and Other Developing Applications," *Chemical Reviews,* vol. 117, pp. 536-711, 2017/01/25 2017.

[84] C. Wang and J. Irudayaraj, "Gold nanorod probes for the detection of multiple pathogens," *Small,* vol. 4, pp. 2204-2208, 2008.

[85] S. Wang, A. K. Singh, D. Senapati, A. Neely, H. Yu, and P. C. Ray, "Rapid Colorimetric Identification and Targeted Photothermal Lysis of Salmonella Bacteria by Using Bioconjugated Oval-Shaped Gold Nanoparticles," *Chemistry-A European Journal,* vol. 16, pp. 5600-5606, 2010.

[86] A. K. Singh, D. Senapati, S. Wang, J. Griffin, A. Neely, P. Candice, *et al.*, "Gold Nanorod Based Selective Identification of Escherichia coli Bacteria Using Two-Photon Rayleigh Scattering Spectroscopy," *ACS Nano,* vol. 3, pp. 1906-1912, 2009/07/28 2009.

[87] C.-z. Li, K. Vandenberg, S. Prabhulkar, X. Zhu, L. Schneper, K. Methee, *et al.*, "Paper based point-of-care testing disc for multiplex whole cell bacteria analysis," *Biosensors and Bioelectronics,* vol. 26, pp. 4342-4348, 2011/07/15/ 2011.

[88] G. V. Naik, V. M. Shalaev, and A. Boltasseva, "Alternative plasmonic materials: beyond gold and silver," *Advanced Materials,* vol. 25, pp. 3264-3294, 2013.

[89] C. Li, J. Zuo, Q. Li, Y. Chang, Y. Zhang, L. Tu, *et al.*, "One-step in situ solid-substrate-based whole blood immunoassay based on FRET between upconversion and gold nanoparticles," *Biosensors and Bioelectronics,* vol. 92, pp. 335-341, 2017.

[90] M. O. Noor and U. J. Krull, "Paper-based solid-phase multiplexed nucleic acid hybridization assay with tunable dynamic range using immobilized quantum dots as donors in fluorescence resonance energy transfer," *Analytical chemistry,* vol. 85, pp. 7502-7511, 2013.

[91] M. O. Noor, A. Shahmuradyan, and U. J. Krull, "Paper-based solid-phase nucleic acid hybridization assay using immobilized quantum dots as donors in fluorescence resonance energy transfer," *Analytical chemistry,* vol. 85, pp. 1860-1867, 2013.

[92] Y. Shi, J. Wu, Y. Sun, Y. Zhang, Z. Wen, H. Dai, *et al.*, "A graphene oxide based biosensor for microcystins detection by fluorescence resonance energy transfer," *Biosensors and Bioelectronics,* vol. 38, pp. 31-36, 2012/10/01/ 2012.

[93] J. H. Jung, D. S. Cheon, F. Liu, K. B. Lee, and T. S. Seo, "A graphene oxide based immuno-biosensor for pathogen detection," *Angewandte Chemie International Edition,* vol. 49, pp. 5708-5711, 2010.

[94] M. D. Sonawane and S. B. Nimse, "Surface modification chemistries of materials used in diagnostic platforms with biomolecules," *Journal of Chemistry,* vol. 2016, 2016.

[95] H. Golmohammadi, E. Morales-Narváez, T. Naghdi, and A. Merkoçi, "Nanocellulose in Sensing and Biosensing," *Chemistry of Materials,* vol. 29, pp. 5426-5446, 2017/07/11 2017.

[96] D. Klemm, B. Heublein, H.-P. Fink, and A. Bohn, "Cellulose: Fascinating Biopolymer and Sustainable Raw Material," *Angewandte Chemie International Edition,* vol. 44, pp. 3358-3393, 2005.

[97] E. W. Nery and L. T. Kubota, "Sensing approaches on paper-based devices: a review," *Analytical and bioanalytical chemistry,* vol. 405, pp. 7573-7595, 2013.

[98] N. Lin and A. Dufresne, "Nanocellulose in biomedicine: Current status and future prospect," *European Polymer Journal,* vol. 59, pp. 302-325, 2014/10/01/ 2014.

[99] S. Doughan, U. Uddayasankar, A. Peri, and U. J. Krull, "A paper-based multiplexed resonance energy transfer nucleic acid hybridization assay using a single form of upconversion nanoparticle as donor and three quantum dots as acceptors," *Analytica Chimica Acta,* vol. 962, pp. 88-96, 2017.

[100] R. J. Moon, A. Martini, J. Nairn, J. Simonsen, and J. Youngblood, "Cellulose nanomaterials review: structure, properties and nanocomposites," *Chemical Society Reviews,* vol. 40, pp. 3941-3994, 2011.

[101] H. Wei, K. Rodriguez, S. Renneckar, and P. J. Vikesland, "Environmental science and engineering applications of nanocellulose-based nanocomposites," *Environmental Science: Nano,* vol. 1, pp. 302-316, 2014.

[102] S. J. Eichhorn, A. Dufresne, M. Aranguren, N. E. Marcovich, J. R. Capadona, S. J. Rowan, *et al.*, "Review: current international research into cellulose nanofibres and nanocomposites," *Journal of Materials Science,* vol. 45, p. 1, September 24 2009.

[103] Z. Fang, H. Zhu, Y. Yuan, D. Ha, S. Zhu, C. Preston, *et al.*, "Novel Nanostructured Paper with Ultrahigh Transparency and Ultrahigh Haze for Solar Cells," *Nano Letters,* vol. 14, pp. 765-773, 2014/02/12 2014.

[104] X. Cai, Q. Yang, J. Ding, W. Ye, X. Li, and J. Xiao, "Paper-based FRET for the direct detection of collagen triple helix," *Journal of Materials Chemistry B,* vol. 4, pp. 7009-7013, 2016.

[105] H. Zhu, Z. Fang, C. Preston, Y. Li, and L. Hu, "Transparent paper: fabrications, properties, and device applications," *Energy & Environmental Science,* vol. 7, pp. 269-287, 2014.

[106] S. Farjana, F. Toomadj, P. Lundgren, A. Sanz-Velasco, O. Naboka, and P. Enoksson, "Conductivity-dependent strain response of carbon nanotube treated bacterial nanocellulose," *Journal of Sensors,* vol. 2013, 2013.

[107] W. Wang, T.-J. Zhang, D.-W. Zhang, H.-Y. Li, Y.-R. Ma, L.-M. Qi, *et al.*, "Amperometric hydrogen peroxide biosensor based on the immobilization of heme proteins on gold nanoparticles–bacteria cellulose nanofibers nanocomposite," *Talanta,* vol. 84, pp. 71-77, 2011.

[108] Z. Shi, S. Zang, F. Jiang, L. Huang, D. Lu, Y. Ma, *et al.*, "In situ nano-assembly of bacterial cellulose–polyaniline composites," *Rsc Advances,* vol. 2, pp. 1040-1046, 2012.

[109] P. A. Marques, H. I. Nogueira, R. J. Pinto, C. P. Neto, and T. Trindade, "Silver-bacterial cellulosic sponges as active SERS substrates," *Journal of Raman Spectroscopy,* vol. 39, pp. 439-443, 2008.

[110] M. Park, H. Chang, D. H. Jeong, and J. Hyun, "Spatial deformation of nanocellulose hydrogel enhances SERS," *BioChip Journal,* vol. 7, pp. 234-241, September 01 2013.

[111] H. Wei, K. Rodriguez, S. Renneckar, W. Leng, and P. J. Vikesland, "Preparation and evaluation of nanocellulose–gold nanoparticle nanocomposites for SERS applications," *Analyst,* vol. 140, pp. 5640-5649, 2015.

[112] E. Morales-Narváez, H. Golmohammadi, T. Naghdi, H. Yousefi, U. Kostiv, D. Horák, *et al.*, "Nanopaper as an Optical Sensing Platform," *ACS nano,* vol. 9, pp. 7296-7305, 2015.

[113] N. Pourreza, H. Golmohammadi, T. Naghdi, and H. Yousefi, "Green in-situ synthesized silver nanoparticles embedded in bacterial cellulose nanopaper as a bionanocomposite plasmonic sensor," *Biosensors and Bioelectronics,* vol. 74, pp. 353-359, 2015.

[114] Y. S. Huh, A. J. Chung, and D. Erickson, "Surface enhanced Raman spectroscopy and its application to molecular and cellular analysis," *Microfluidics and nanofluidics,* vol. 6, p. 285, 2009.

[115] J. Zhu, H. D. Bean, Y.-M. Kuo, and J. E. Hill, "Fast detection of volatile organic compounds from bacterial cultures by secondary electrospray ionization-mass spectrometry," *Journal of clinical microbiology,* vol. 48, pp. 4426-4431, 2010.

[116] E. Tait, J. D. Perry, S. P. Stanforth, and J. R. Dean, "Identification of Volatile Organic Compounds Produced by Bacteria Using HS-SPME-GC–MS," *Journal of Chromatographic Science,* vol. 52, pp. 363-373, 2014.

[117] A. Korpi, J. Järnberg, and A.-L. Pasanen, "Microbial volatile organic compounds," *Critical reviews in toxicology,* vol. 39, pp. 139-193, 2009.

[118] C. D. Cox and J. Parker, "Use of 2-aminoacetophenone production in identification of Pseudomonas aeruginosa," *Journal of Clinical Microbiology,* vol. 9, pp. 479-484, 1979.

[119] D. Wang, X. Ding, and P. N. Rather, "Indole Can Act as an Extracellular Signal inEscherichia coli," *Journal of Bacteriology,* vol. 183, pp. 4210-4216, 2001.

[120] J. N. Labows, K. J. McGINLEY, G. Webster, and J. Leyden, "Headspace analysis of volatile metabolites of Pseudomonas aeruginosa and related species by gas chromatography-mass spectrometry," *Journal of Clinical Microbiology,* vol. 12, pp. 521-526, 1980.

[121] M. C. Janzen, J. B. Ponder, D. P. Bailey, C. K. Ingison, and K. S. Suslick, "Colorimetric sensor arrays for volatile organic compounds," *Analytical chemistry,* vol. 78, pp. 3591-3600, 2006.

[122] J. R. Carey, K. S. Suslick, K. I. Hulkower, J. A. Imlay, K. R. Imlay, C. K. Ingison, *et al.*, "Rapid identification of bacteria with a disposable colorimetric sensing array," *Journal of the American Chemical Society,* vol. 133, pp. 7571-7576, 2011.

[123] T. H. Wu and P. J. Bechtel, "Ammonia, dimethylamine, trimethylamine, and trimethylamine oxide from raw and processed fish by-products," *Journal of Aquatic Food Product Technology,* vol. 17, pp. 27-38, 2008.

[124] D. Dave and A. E. Ghaly, "Meat spoilage mechanisms and preservation techniques: a critical review," *American Journal of Agricultural and Biological Sciences,* vol. 6, pp. 486-510, 2011.

[125] M. Etienne, "Volatile amines as criteria for chemical quality assessment," 2005.

[126] A. Casaburi, P. Piombino, G.-J. Nychas, F. Villani, and D. Ercolini, "Bacterial populations and the volatilome associated to meat spoilage," *Food Microbiology,* vol. 45, pp. 83-102, 2015/02/01/ 2015.

[127] M. K. Morsy, K. Zór, N. Kostesha, T. S. Alstrøm, A. Heiskanen, H. El-Tanahi, *et al.*, "Development and validation of a colorimetric sensor array for fish spoilage monitoring," *Food Control,* vol. 60, pp. 346-352, 2016/02/01/ 2016.

[128] X. Huang, J. Xin, and J. Zhao, "A novel technique for rapid evaluation of fish freshness using colorimetric sensor array," *Journal of Food Engineering,* vol. 105, pp. 632-637, 2011/08/01/ 2011.

[129] C. R. Kagan, "At the nexus of food security and safety: opportunities for nanoscience and nanotechnology," ed: ACS Publications, 2016.

[130] B. M. Lund and S. J. O'Brien, "The occurrence and prevention of foodborne disease in vulnerable people," *Foodborne Pathogens and Disease,* vol. 8, pp. 961-973, 2011.

[131] L. Gram and P. Dalgaard, "Fish spoilage bacteria – problems and solutions," *Current Opinion in Biotechnology,* vol. 13, pp. 262-266, 6/1/ 2002.

[132] L. Prester, "Biogenic amines in fish, fish products and shellfish: a review," *Food Additives & Contaminants: Part A,* vol. 28, pp. 1547-1560, 2011.

[133] Y. Xu, W. Cheung, C. L. Winder, and R. Goodacre, "VOC-based metabolic profiling for food spoilage detection with the application to detecting Salmonella typhimurium-contaminated pork," *Analytical and Bioanalytical Chemistry,* vol. 397, pp. 2439-2449, July 01 2010.

[134] B. Jin, S. Wang, M. Lin, Y. Jin, S. Zhang, X. Cui, *et al.*, "Upconversion nanoparticles based FRET aptasensor for rapid and ultrasenstive bacteria detection," *Biosensors and Bioelectronics,* vol. 90, pp. 525-533, 2017/04/15/ 2017.

[135] G. Naja, P. Bouvrette, S. Hrapovic, and J. H. T. Luong, "Raman-based detection of bacteria using silver nanoparticles conjugated with antibodies," *Analyst,* vol. 132, pp. 679-686, 2007.

[136] E. Nery and L. Kubota, "Sensing approaches on paper-based devices: a review," *Analytical and Bioanalytical Chemistry,* vol. 405, pp. 7573-7595, 2013/09/01 2013.

[137] A. Pacquit, J. Frisby, D. Diamond, K. T. Lau, A. Farrell, B. Quilty, *et al.*, "Development of a smart packaging for the monitoring of fish spoilage," *Food Chemistry,* vol. 102, pp. 466-470, 2007/01/01/ 2007.

[138] B. Dubertret, M. Calame, and A. J. Libchaber, "Single-mismatch detection using gold-quenched fluorescent oligonucleotides," *Nature biotechnology,* vol. 19, pp. 365-370, 2001.

[139] C. Verlander, "Detection of horseradish peroxidase by colorimetry," *Nonisotopic DNA Probe Techniques,* pp. 185-201, 1992.

[140] I. Sela-Culang, S. Alon, and Y. Ofran, "A systematic comparison of free and bound antibodies reveals binding-related conformational changes," *The Journal of Immunology,* vol. 189, pp. 4890-4899, 2012.

[141] T. S. Hauck, R. E. Anderson, H. C. Fischer, S. Newbigging, and W. C. W. Chan, "In vivo Quantum-Dot Toxicity Assessment," *Small,* vol. 6, pp. 138-144, 2010.

[142] A. M. Alkilany and C. J. Murphy, "Toxicity and cellular uptake of gold nanoparticles: what we have learned so far?," *Journal of Nanoparticle Research,* vol. 12, pp. 2313-2333, September 01 2010.